MONTHLY NOTICES

OF THE

ROYAL ASTRONOMICAL SOCIETY

Vol. 112 No. 4 1952

Published and Sold by the

ROYAL ASTRONOMICAL SOCIETY
BURLINGTON HOUSE
LONDON, W. 1

Price Thirteen Shillings and Sixpence

NOTICE TO AUTHORS

1. *Communications.*—Papers must be communicated to the Society by a Fellow. They should be accompanied by a summary at the *beginning* of the paper conveying briefly the content of the paper, and drawing attention to important new information and to the main conclusions. The summary should be intelligible in itself, without reference to the paper, to a reader with some knowledge of the subject; it should not normally exceed 200 words in length. **Authors are requested to submit MSS. in duplicate. These should be typed using double spacing and leaving a margin of not less than one inch on the left-hand side. Corrections to the MSS. should be made in the text and not in the margin.** Unless a paper reaches the Secretaries more than seven days before a Council meeting it will not normally be considered at that meeting. By Council decision, MSS. of accepted papers are retained by the Society for one year after publication; unless their return is then requested by the author, they are destroyed.

2. *Presentation.*—Authors are allowed considerable latitude, but they are requested to follow the general style and arrangement of *Monthly Notices*. References to literature should be given in the standard form, including a date, for printing either as footnotes or in a numbered list at the end of the paper. Each reference should give the **name and initials** of the author cited, irrespective of the occurrence of the name in the text (some latitude being permissible, however, in the case of an author referring to his own work). The following examples indicate the style of reference appropriate for a paper and a book, respectively :—

A. Corlin, *Zs. f. Astrophys.*, **15**, 239, 1938.
H. Jeffreys, *Theory of Probability*, 2nd edn., section 5.45, p. 258, Oxford, 1948.

3. *Notation.*—For technical astronomical terms, authors should conform closely to the recommendations of Commission 3 of the International Astronomical Union (*Trans. I.A.U.*, Vol. VI, p. 345, 1938). Council has decided to adopt the I.A.U. 4-letter abbreviations for constellations where contraction is desirable (Vol. IV, p. 221, 1932). In general matters, authors should follow the recommendations in *Symbols, Signs and Abbreviations* (London : Royal Society, 1951) except where these conflict with I.A.U. practice.

4. *Diagrams.*—**These should be designed to appear upright on the page, drawn about twice the size required in print and prepared for direct photographic reproduction except for the lettering, which should be inserted in pencil. Legends should be given in the manuscript indicating where in the text the figure should appear.** Blocks are retained by the Society for 10 years; unless the author requires them before the end of this period they are then destroyed.

5. *Tables.*—**These should be arranged so that they can be printed upright on the page.**

6. *Proofs.*—Costs of alterations exceeding 5 per cent of composition must be borne by the author. Fellows are warned that such costs have risen sharply in recent years, and it is in their own and the Society's interests to seek the maximum conciseness and simplification of symbols and equations consistent with clarity.

7. *Revised Manuscripts.*—When papers are submitted in revised form it is especially requested that they be accompanied by the original MS.

Reading of Papers at Meetings

8. When submitting papers authors are requested to indicate whether they will be willing and able to read the paper at the next or some subsequent meeting, and approximately how long they would like to be allotted for speaking.

9. Postcards giving the programme of each meeting are issued some days before the meeting concerned. Fellows wishing to receive such cards whether for Ordinary Meetings or for the Geophysical Discussions or both should notify the Assistant Secretary.

MONTHLY NOTICES

OF THE

ROYAL ASTRONOMICAL SOCIETY

Vol. 112 No. 4

MEETING OF 1952 MARCH 14

Professor H. Dingle, President, in the Chair

The election by the Council of the following Fellows was duly confirmed:—

Raymond Fallaw, 3 Jesmond Park West, Newcastle-on-Tyne, 2 (proposed by G. R. Goldsbrough); and

Norman Charles Hanslip, Cherry Cottage, Kingsdown, Box, Wiltshire (proposed by K. A. Hirsch).

The election by the Council of the following Junior Members was duly confirmed:—

Brian Miles, Newington, West Lane, Freshfield, Formby, Liverpool (proposed by W. H. Ramsey); and

Brien George Tunmore, B.Sc., 15 Melrose Road, Shirley, Southampton (proposed by E. W. Mason).

Eighty-four presents were announced as having been received since the last meeting, including:—

A. C. B. Lovell and J. A. Clegg, *Radio Astronomy* (presented by the authors); and

P. Rousseau, *Mars—Terre Mystérieuse* (presented by C. A. Swindin).

The President announced that Dr E. Hubble would deliver the George Darwin Lecture at the Ordinary Meeting on 1952 October 10.

MEETING OF 1952 APRIL 9

Professor H. Dingle, President, in the Chair

The President announced that the death had taken place of Dr Bernard Lyot, an Associate of the Society. He paid a brief tribute to his memory, the Fellows standing.

The election by the Council of the following Fellows was duly confirmed:—

Joseph M. Chamberlain, Hayden Planetarium, Central Park West, New York, U.S.A. (proposed by Catherine E. Barry);

David Rowland Davies, M.Sc., Ph.D., 104 Furness Avenue, Dore, Sheffield (proposed by R. R. S. Cox);

Heinrich Karl Johannes Eichhorn, D.Phil., University Observatory, Glasgow, W.2 (proposed by W. M. Smart);

Kenneth Heuer, Hayden Planetarium, Central Park West, New York, U.S.A. (proposed by Catherine E. Barry);

Alan Jeffrey, 62 Dalmally Road, Addiscombe, Surrey (proposed by J. G. Porter);

*Edward Kendrick, B.Sc., 247 King's Road, Chorlton, Manchester, 21 (proposed by S. W. R. Mottram);

Duncan Macnaughton, M.A., LL.B., F.R.S.E., W.S., 22 Young Street, Edinburgh, 2 (proposed by Lord Cooper);

Desmond Johns Memory, 11 Ponsonsby Road, Milehouse, Plymouth (proposed by V. C. A. Ferraro); and

Alwyn Rudolph Robbins, B.Sc., M.A., 58 Five Mile Drive, Oxford (proposed by J. de Graaff-Hunter).

The President announced that the Council had elected the following Associates of the Society:—

Dr Gerald M. Clemence, U.S. Naval Observatory, Washington, D.C., U.S.A.; and

Professor Otto Heckmann, The Observatory, Hamburg, Germany.

Eighty-seven presents were announced as having been received since the last meeting, including:—

A. Bečvář, *Atlas Coeli, Volume II* (presented by Prague Observatory);

E. C. Bullard, *The origin of the Earth's magnetic field* (presented by the author);

H. Spencer Jones, *Life on other worlds* (presented by the author);

E. A. Milne, *Modern cosmology and the Christian idea of God* (presented by G. J. Whitrow);

E. O. Tancock, *Starting astronomy* (presented by G. J. Whitrow);

Lowell Observatory Report No. 9: Project for the study of planetary atmospheres (presented by the Observatory);

Hamburg Observatory: *Bergedorfer Spektral-Durchmusterung Band IV* (presented by the Observatory); and

Zweiter Katalog der Astronomischen Gesellschaft, Bände 1, 2, 3 and 4 (presented by the Hamburg Observatory).

* Transferred from Junior Membership.

OSCILLATIONS OF A STAR IN ITS OWN MAGNETIC FIELD: AN ILLUSTRATIVE PROBLEM

V. C. A. Ferraro and D. J. Memory

(Received 1952 January 10)

Summary

The free oscillations of a highly idealized star in its own magnetic field are considered for the case when the magnetic field, instead of being assumed uniform, after Schwarzschild, increases radially inwards from the surface. It is shown that, in Schwarzschild's discussion, the identification of the uniform magnetic field with the value of the star's magnetic field near its centre is incorrect. As a consequence, for a star such as HD 125 248 possessing a magnetic field whose surface value is of the order 7 000 gauss, the periods of the lowest modes of (free) vibrations are of the order of two years and not of the order of several days. It is suggested that a variable stellar magnetic field may be explained as due to forced oscillations in a pulsating magnetic star, but that a detailed investigation must take into account gravity variations as well as the increase of magnetic field with depth.

1. *Introduction.*—In 1947, H. W. Babcock discovered that some stars, notably HD 125 248, possessed magnetic fields which reversed their polarity. One of the suggestions made to account for this variation is that it is caused by the oscillations of the star in its own magnetic field. This suggestion was first made to one of us (V.C.A.F.) by S. K. Runcorn in 1948 (**1**, p. 62) and since then M. Schwarzschild (**2**) has investigated this problem in some detail for a highly idealized star, the magnetic field of which was assumed to be uniform throughout. Schwarzschild states (*loc. cit.*, p. 148) that "in rough comparisons with observations no serious discrepancies are found" and Babcock appears to favour this mechanism as a probable explanation of the variability of stellar magnetic fields (**3**).

The case considered by Schwarzschild is essentially that of free oscillations of a star in its own magnetic field, assumed uniform, neglecting gravity variations. Assuming that the calculated periods of the two normal modes of vibration examined by him are comparable with that of about $9\frac{1}{4}$ days found by Babcock for the variable HD 125 248, Schwarzschild deduced the value of the uniform field to be of the order of one million gauss. This value appears to be excessive, and Schwarzschild's conclusion of "no serious discrepancies" with observations difficult to reconcile with it. For, even if the field increases with depth as in Cowling's model of the solar magnetic field (**4**), the *effective* value of this magnetic field over its volume must be considerably less than its value at the centre.

In this paper we consider this point in some detail by taking account of the increase with depth of the stellar magnetic field, though, as in Schwarzschild's work, we consider the case of an idealized model star. We suppose, firstly, that the magnetic field of the star is due to a central magnetic *pole*. Although such a field is highly artificial, and moreover has the disadvantage of not possessing a definite axis, it has the advantage of increasing with depth at a rate comparable with Cowling's model of the solar magnetic field (**4**). Further, apart from the greater mathematical difficulties encountered in considering the permanent field

of the star to be due to, say, a central magnetic dipole, there seemed to be little advantage to be gained by considering such a case.

Our method of solution differs essentially from Schwarzschild's: by using spherical harmonic analysis we are able to find readily the periods of the normal modes of vibration for each spherical harmonic. We find that for a star with a surface magnetic field of the order found by Babcock and of the same mass and radius as Sirius A, the periods of the fundamental modes of vibration for the first two harmonics are of the order of a few *years* instead of several *days* as found by Schwarzschild.

The reason for this discrepancy is that the oscillations are most pronounced in the outer layers of the model star, where the magnetic field is not much greater than its value at the surface. The long periods found here for the free oscillations suggest that the variability of stellar magnetic fields is not due to free oscillations; such oscillations are suggestive of long-period cycles, such as the 11-year solar cycle, rather than the rapid variations of stellar magnetic fields. This result was to be expected; for, as was shown by Alfvén (**5**) in his theory of sunspots, disturbances of a general solar magnetic field (of the order of a thousand gauss) generated in the deep interior of the Sun would travel to the surface in a time of the order of tens of years. A similar conclusion appears to have been reached by Grotrian (**6**).

There remains the possibility that the variability of stellar magnetic fields can be accounted for by *forced* oscillations, the exciting mechanism being the mechanical vibration of the star itself. Whether this is likely to be the case, however, can only be settled by an investigation of a more refined stellar model in which, in addition to electromagnetic forces, gravitational and other forces are also taken into account.

2. *The idealized problem.*—We follow Schwarzschild in considering a highly simplified stellar model. We take no account of gravitational forces in the star, which we assume to be a highly conducting incompressible fluid sphere of radius a and density ρ, subject to a uniform pressure P over its surface.* The conductivity of the fluid is taken as infinite, the effect of a finite conductivity being negligible. Only the case of small oscillations about the equilibrium configuration of the star will be considered.

3. *The idealized permanent magnetic field of the star.*—We shall assume that this is due to a central magnetic pole of strength m. In numerical illustrations of the problem we shall assume m to correspond to a surface value of the mean field of the star of the order of 7000 gauss (**3**). The radius and mass M of the star are assumed to be the same as for Sirius A, that is, we take $a = 1{\cdot}58 R_\odot$ and $M = 0{\cdot}88 M_\odot$. This gives $m = 8{\cdot}3 \times 10^{25}$ e.m.u. The oscillations of the star will be supposed to be the same in all planes through some fixed diameter of the star, which we define as the "axis" of the star.

4. *The electromagnetic field equations.*—Neglecting displacement currents, the relevant equations in electromagnetic units are

$$\operatorname{curl} \mathbf{E} = -\partial \mathbf{H}/\partial t, \tag{1}$$

$$\operatorname{curl} \mathbf{H} = 4\pi \mathbf{j}, \tag{2}$$

$$\operatorname{div} \mathbf{H} = 0, \tag{3}$$

$$\operatorname{div} \mathbf{E} = 4\pi \nu, \tag{4}$$

$$\mathbf{j} = \sigma(\mathbf{E} + \mathbf{v} \wedge \mathbf{H}), \tag{5}$$

* These, in effect, amount to Schwarzschild's assumptions.

where **E** and **H** are the electric and magnetic field intensities, **j** is the electric current density, ν the space charge density and σ and **v** the electrical conductivity and velocity of the fluid. Since we assume that $\sigma = \infty$, it follows from (5) that

$$\mathbf{E} = -\mathbf{v} \wedge \mathbf{H}. \tag{6}$$

Again, as we suppose that the vibrations take place in meridian planes through the axis of the star, the only non-vanishing resolute of the electric field is the azimuthal one, which is, moreover, the same in all meridian planes. Hence, $\operatorname{div} \mathbf{E} = 0$ so that $\nu = 0$ also.

Outside the sphere, $\mathbf{j} = 0$, and the field equations are the same as (1) to (4) with $\mathbf{j} = 0$ in (2).

5. *Equations of small oscillations.*—The equations of continuity and motion of the incompressible fluid are respectively

$$\operatorname{div} \mathbf{v} = 0, \tag{7}$$

$$\rho(D\mathbf{v}/Dt) = \mathbf{j} \wedge \mathbf{H} - \operatorname{grad} p, \tag{8}$$

where ρ is the mass density and p is the pressure. Using (2), (8) may be written

$$\rho(D\mathbf{v}/Dt) = (1/4\pi)(\operatorname{curl} \mathbf{H}) \wedge \mathbf{H} - \operatorname{grad} p. \tag{9}$$

Substituting (6) in (1), this becomes

$$\partial \mathbf{H}/\partial t = \operatorname{curl} (\mathbf{v} \wedge \mathbf{H}), \tag{10}$$

which expresses the fact that the magnetic lines of force move with the fluid.

To form the equations of small oscillations, we write

$$\mathbf{H} = \mathbf{H}_0 + \mathbf{h}, \qquad p = P + p', \tag{11}$$

where $\mathbf{H}_0$ is the permanent field; neglecting squares and products of quantities of the first order, **v**, **h** and p', (9) then becomes

$$\rho(\partial \mathbf{v}/\partial t) = (1/4\pi)(\operatorname{curl} \mathbf{h}) \wedge \mathbf{H}_0 - \operatorname{grad} p' \tag{12}$$

approximately, and (10) becomes approximately

$$\partial \mathbf{h}/\partial t + (\mathbf{v} \,.\, \operatorname{grad}) \mathbf{H}_0 = (\mathbf{H}_0 \,.\, \operatorname{grad}) \mathbf{v}. \tag{13}$$

Finally, we eliminate p' from (12) by operating with curl; we find

$$4\pi\rho\{\partial(\operatorname{curl} \mathbf{v})/\partial t\} = \operatorname{curl}\{(\operatorname{curl} \mathbf{h}) \wedge \mathbf{H}_0\}. \tag{14}$$

Further, since $\operatorname{div} \mathbf{H}_0 = 0$, we have, from (3),

$$\operatorname{div} \mathbf{h} = 0. \tag{15}$$

Then (7), (13), (14) and (15) are the relevant equations to determine the small oscillations.

6. *Solution of the equations in spherical polar coordinates.*—Since the oscillations take place in planes through the axis of the sphere and are the same in all such planes, we take this axis to be the axis $\theta = 0$ of a system of spherical polar coordinates (r, θ, ϕ), the origin of coordinates being at the centre of the sphere.

Since $\operatorname{div} \mathbf{v} = 0$, $\operatorname{div} \mathbf{H}_0 = 0$, $\operatorname{div} \mathbf{h} = 0$, and there is axial symmetry about $\theta = 0$, we may express **v**, $\mathbf{H}_0$ and **h** in terms of appropriate Stokes' "stream-functions", ψ, U, u, respectively. At any time the family of curves $\psi =$ constant will then be the stream lines of the motion, and the family of curves $U =$ constant, $u =$ constant, will respectively give the equations of the lines of force of the permanent field and of the field of the currents induced by the motion of the fluid in the permanent field.

Denoting by suffixes r and θ the resolutes of vectors in the directions of r and θ increasing, the velocity and magnetic field resolutes are given by

$$\left.\begin{aligned} v_r &= -\frac{1}{r^2\sin\theta}\frac{\partial\psi}{\partial\theta}, & v_\theta &= \frac{1}{r\sin\theta}\frac{\partial\psi}{\partial r}, \\ (H_0)_r &= -\frac{1}{r^2\sin\theta}\frac{\partial U}{\partial\theta}, & (H_0)_\theta &= \frac{1}{r\sin\theta}\frac{\partial U}{\partial r}, \\ h_r &= -\frac{1}{r^2\sin\theta}\frac{\partial u}{\partial\theta}, & h_\theta &= \frac{1}{r\sin\theta}\frac{\partial u}{\partial r}. \end{aligned}\right\} \tag{16}$$

Let $\mu=\cos\theta$ and let Δ denote the operator

$$\Delta=\frac{\partial^2}{\partial r^2}+\frac{1-\mu^2}{r^2}\frac{\partial^2}{\partial\mu^2}, \tag{17a}$$

and D denote the operator

$$D=\Delta/(r^2\sin^2\theta); \tag{17b}$$

then (13) and (14) may be expressed in the form

$$\frac{\partial u}{\partial t}=\frac{1}{r^2\sin\theta}\frac{\partial(U,\psi)}{\partial(\theta,r)}, \tag{18}$$

$$4\pi\rho D\left(\frac{\partial\psi}{\partial t}\right)=\frac{1}{r^2\sin\theta}\frac{\partial(U,Du)}{\partial(\theta,r)}, \tag{19}$$

and these are the equations to determine ψ and u; here $\partial(U,\psi)/\partial(\theta,r)$ is the Jacobian of U and ψ with respect to θ, r.

In the case of a permanent field due to a central magnetic pole of strength m,

$$U=-m\cos\theta$$

(Section 3), and equations (18) and (19) reduce to

$$\frac{\partial u}{\partial t}=\frac{m}{r^2}\frac{\partial\psi}{\partial r}, \tag{20}$$

$$4\pi\rho\Delta\left(\frac{\partial\psi}{\partial t}\right)=m\frac{\partial}{\partial r}\left(\frac{1}{r^2}\Delta u\right). \tag{21}$$

Assuming harmonic vibrations with the periodic time $2\pi/\lambda$, these equations become respectively

$$\mathrm{i}\lambda u=\frac{m}{r^2}\frac{\partial\psi}{\partial r}, \tag{22a}$$

$$4\pi\mathrm{i}\rho\lambda\Delta\psi=m\frac{\partial}{\partial r}\left(\frac{\Delta u}{r^2}\right). \tag{22b}$$

These equations show that the phases of the functions u and ψ, and, hence, of the induced magnetic field $\mathbf{h}$ and velocity $\mathbf{v}$, differ by a quarter period. Eliminating u between (22*a*) and (22*b*), we obtain finally the following differential equation for ψ:

$$-4\pi\rho\lambda^2\Delta\psi=m^2\frac{\partial}{\partial r}\left\{\frac{1}{r^2}\Delta\left(\frac{1}{r^2}\frac{\partial\psi}{\partial r}\right)\right\}. \tag{23}$$

We can express this equation in non-dimensional form by writing

$$r=\eta x, \qquad \eta^6=m^2/4\pi\rho\lambda^2; \tag{24}$$

(23) then becomes

$$\Delta_1\psi=-\frac{\partial}{\partial x}\left\{\frac{1}{x^2}\Delta_1\left(\frac{1}{x^2}\frac{\partial\psi}{\partial x}\right)\right\}, \tag{25}$$

where

$$\Delta_1 = \frac{\partial^2}{\partial x^2} + \frac{1-\mu^2}{x^2}\frac{\partial^2}{\partial \mu^2}. \tag{26}$$

To solve (25) we write

$$\psi = \sum_n (1-\mu^2)^{1/2} F_n(x) P_n^1(\mu), \tag{27}$$

where $F_n(x)$ is a function of x to be determined, and P_n^1 is the associated Legendre function of degree n and order 1. Substitution of (26) in (25) leads to the following fourth-order differential equation for F_n,

$$x^3 F_n^{iv} - 8x^2 F_n^{iii} + ((26-l)x + x^2) F_n^{ii} - (36-6l) F_n^{i} - l x^5 F_n = 0, \tag{28}$$

where affixes denote derivatives and $l = n(n+1)$.

7. *Solution of the equation for F_n in series.*—Equation (27) can be solved in a series of the form

$$F_n = \sum_0^\infty a_k x^{\alpha+k}; \tag{29}$$

substituting in (27) the indicial equation is found to be

$$\alpha^4 - 14\alpha^3 + (61 - n^2 - n)\alpha^2 + (7n^2 + 7n - 84)\alpha = 0,$$

the roots of which are

$$0, \quad 3-n, \quad n+4, \quad 7. \tag{30}$$

It is found that the series proceeds by powers of x^6, so that (28) may be written

$$F_n = \sum_0^\infty A_k x^{\alpha+6k}, \tag{31}$$

where the As are determined from the recurrence relation

$$\frac{A_k}{A_{k-1}} = -\frac{(6k+\alpha-n-7)(6k+\alpha+n-6)}{(6k+\alpha)(6k+\alpha-7)(6k+\alpha+n-3)(6k+\alpha-n-4)}.$$

8. *Discussion of the four solutions F_n*

Case (i): $\alpha = 0$.—Here the series (30) is finite at the origin and

$$\frac{A_k}{A_{k-1}} = -\frac{(6k-n-7)(6k+n-6)}{6k(6k-7)(6k+n-3)(6k-n-4)}.$$

If n is of the form $6k-7$, the series terminates; if n is not of the form $6k-4$, the series converges absolutely and uniformly for all values of x. If n is of the form $6k-4$, some of the coefficients are infinite and a second solution must be obtained. This, however contains a logarithmic singularity at the origin and so must be rejected since ψ is finite there.

For other values of n, from the first of equations (16) we see that $v_r = O(r^{-2})$ as $r \to 0$, so the velocity is not finite there. Hence, this solution of (28) must be rejected.

Case (ii): $\alpha = 3-n$.—Here

$$\frac{A_k}{A_{k-1}} = -\frac{(6k-2n-4)(6k-3)}{6k(6k+3-n)(6k-n-4)(6k-2n-1)},$$

and so, unless the values of n make some of the factors in the denominator vanish, the series is absolutely and uniformly convergent for all $|x| > 0$. The solution is not finite at the origin if $n > 3$, and if $n = 2$, the solution possesses a logarithmic singularity at the origin. If $n = 1$, the series terminates and the solution reduces

to x^2. In this case the velocity is finite at the origin but the electric and magnetic fields are not, by (16). Hence, this solution must also be rejected.

Case (iii): $\alpha = n+4$.—Here

$$\frac{A_k}{A_{k-1}} = -\frac{(6k-3)(6k+2n-2)}{6k(6k+n+4)(6k+n-3)(6k+2n+1)}, \tag{32}$$

and the series is uniformly and absolutely convergent for all values of x. Moreover, all variables are finite or zero at the origin and so this gives a possible solution for F_n; we shall denote this solution by $F_n^{(1)}$.

Case (iv): $\alpha = 7$.—Here

$$\frac{A_k}{A_{k-1}} = -\frac{(6k-n)(6k+n+1)}{6k(6k+7)(6k+n+4)(6k-n+3)}, \tag{33}$$

and the series is absolutely and uniformly convergent for all values of x, except when n is of the form $6k$, where k is an integer, when the series terminates. If n is of the form $6k+3$ some of the coefficients become infinite and a second solution must be sought. This will not be investigated here, since we shall restrict our discussion to the first two harmonics ($n = 1, 2$). The field variables are all finite or zero at the origin and so this case also provides a solution; we shall denote it by $F_n^{(2)}$.

The required solution of (27) is thus of the form

$$F_n = AF_n^{(1)} + BF_n^{(2)}, \tag{34}$$

where A and B are arbitrary constants.

Each of the four solutions discussed above are integral functions of order 3 and in fact two normal integrals have been found which are $O(x^{-1}e^{\pm 1x^3/3})$ at infinity. To this must be added a term $O(x^{n+1})$.

For certain special values of x, all but the function $F_n^{(1)}$ terminate, and in each case the highest power of x in the polynomial is $n+1$. Thus, at infinity, we have $F_n = O(x^{n+1})$ in these special cases.

9. *The magnetic field associated with the oscillations.*—For points *within* the sphere, the stream function of the magnetic field is given by (22) and (26), namely (omitting the time factor),

$$u = -\mathrm{i}(4\pi\rho)^{1/2}\Sigma F_n'(x)(1-\mu^2)P_n^1(\mu), \qquad \mu = \cos\theta, \tag{35}$$

where accents denote derivatives with respect to x.

To find the magnetic field *outside* the sphere, we have to find solutions of the equations

$$\operatorname{curl}\mathbf{H} = 0, \qquad \operatorname{div}\mathbf{H} = 0 \tag{36}$$

(neglecting displacement currents).

Since the field outside will only differ slightly from the field of the central magnetic pole, we write as before

$$\mathbf{H} = \mathbf{H}_0 + \mathbf{h}'; \tag{37}$$

writing u' for the stream function of the induced field $\mathbf{h}'$, we have from (36) that

$$\Delta_1 u' = 0, \tag{38}$$

where Δ_1 is given by (26).

Boundary conditions.—Let the value of x at the surface of the sphere be denoted by x_1, so that, by (24),

$$a = \eta x_1. \tag{39}$$

To satisfy the continuity of the radial resolute of the magnetic field at the surface, the solution of (38) must involve the Legendre functions P_n^1 and must vanish at infinity. Such a solution is

$$u' = \Sigma B_n x^{-n}(1-\mu^2)P_n^1, \tag{40}$$

where the B_ns are constants to be determined. Continuity of the magnetic field resolutes at the surface $x = x_1$ then gives the two conditions

$$\left.\begin{aligned} x_1^{n-2}F_n'(x_1) &= iB_n(4\pi\rho)^{-1/2}, \\ nB_n x_1^{2-n} &= i\{(4\pi\rho)^{1/2}(x_1F_n''(x_1) - 2F_n'(x_1)\}. \end{aligned}\right\} \tag{41}$$

Elimination of B_n gives

$$(2-n)F_n'(x_1) = x_1F_n''(x_1), \tag{42}$$

and

$$u' = -i(4\pi\rho)^{1/2}\Sigma x_1^{n-2}x^{-n}F_n'(x_1)(1-\mu^2)P_n^1. \tag{43}$$

10. *The electric field associated with the oscillations.*—The electric field within the sphere is given by (6), or since **v** is small, approximately by

$$\mathbf{E} = -\mathbf{v}\wedge\mathbf{H}_0;$$

thus **E** is wholly azimuthal and its intensity E is given by

$$E = -(i\lambda/\eta)(4\pi\rho)^{1/2}\Sigma F_n(x)x^{-3}P_n'. \tag{44}$$

Outside the sphere the electric field satisfies the equations

$$\operatorname{curl}\mathbf{E} = -\partial\mathbf{H}/\partial t, \quad \text{or} \quad \operatorname{curl}\mathbf{E} = -\partial\mathbf{h}'/\partial t,$$

by (37). Using the stream function u' for the field $\mathbf{h}'$ given by (43), and the fact that **E** is continuous at the surface of the sphere, we find

$$E = (i\lambda/\eta x)u'(1-\mu^2)^{-1/2}, \tag{45}$$

where u' is given by (43).

11. *The variations of pressure in the sphere.*—This is most readily derived from the equation of motion (12), viz.,

$$\rho(\partial\mathbf{v}/\partial t) = (1/4\pi)(\operatorname{curl}\mathbf{h})\wedge\mathbf{H}_0 - \operatorname{grad}p.$$

Considering the transverse resolute of this equation in a meridian plane, we find that p' is of the form

$$p' = -(i\rho\lambda/\eta)\Sigma G_n(r)P_n(\cos\theta), \tag{46}$$

where the G functions, expressed in terms of $x(=r/\lambda)$, are given by

$$G_n(x) = F_n'(x) + x^{-2}\mathscr{D}(x^{-2}F_n(x)), \tag{47}$$

and $\mathscr{D}$ denotes the operator

$$\mathscr{D} = \frac{\partial^2}{\partial x^2} - l^2x^{-2} \tag{48}$$

and accents derivatives with respect to x. We shall denote by $G_n^{(1)}$ and $G_n^{(2)}$ the G functions corresponding to $F_n^{(1)}$ and $F_n^{(2)}$ respectively. Let

$$F_n^{(1)} = x^{n+4}\sum_0^\infty A_k x^{6k}, \quad F_n^{(2)} = x^{7}\sum_0^\infty A_k^1 x^{6k}, \tag{49}$$

where $A_0 = A_0^1 = 1$, and A_k and A_k^1 are given by (31) and (32). Then we find that

$$G_n^{(1)} = \sum_0^\infty \frac{lA_k}{6k+n+3}x^{n+3+6k}, \quad G_n^{(2)} = 7(4\cdot3-l) + \sum_0^\infty \frac{l}{6k+6}A_k^1 x^{6k+6}, \tag{50}$$

where $l=n(n+1)$. The series are absolutely and uniformly convergent for all values of x.

12. *The periods of the normal modes of vibrations.*—At the boundary of the sphere $Dp/Dt=0$, and to the first order this equation implies that

$$p'=0, \tag{51}$$

since $p' \propto e^{i\lambda t}$, and $p=P+p'$.

From (34) and (47) we have

$$G_n(x)=AG_n^{(1)}+BG_n^{(2)},$$

where A and B are the same arbitrary constants entering in (34). The condition (51) then requires, by (46), that

$$G_n(x_1)=0,$$

or

$$AG_n^{(1)}(x_1)+BG_n^{(2)}(x_1)=0. \tag{52}$$

Again, (42) gives

$$(2-n)\{A(dF_n^{(1)}/dx)+B(dF_n^{(2)}/dx)\}_{x=x_1}=x_1\{A(d^2F_n^{(1)}/dx^2)+B(d^2F_n^{(2)}/dx^2)\}_{x=x_1}. \tag{53}$$

Elimination of the ratio B/A between (52) and (53) gives the period equation for the normal modes of vibration; we write this in the form

$$G_n^{(2)}H_n^{(1)}=G_n^{(1)}H_n^{(2)}, \tag{54}$$

where

$$\begin{aligned} H_n^{(1)}&=(2-n)\,dF_n^{(1)}/dx-x_1(d^2F_n^{(1)}/dx^2),\\ H_n^{(2)}&=(2-n)\,dF_n^{(2)}/dx-x_1(d^2F_n^{(2)}/dx^2). \end{aligned} \tag{55}$$

It is easily verified that*

$$\left.\begin{aligned} H_n^{(1)}&=\sum_0^\infty(6k+n+4)(6k+2n+1)A_kx^{6k+n+3},\\ H_n^{(2)}&=\sum_0^\infty(6k+n+4)(6k+7)A_k{}^1x^{6k+6}. \end{aligned}\right\} \tag{56}$$

Equation (54) determines the value of x_1 and hence by (24) and (39) the period $2\pi/\lambda$ of the oscillations for the normal modes. We find

$$\lambda=\frac{m}{a^3}\left(\frac{x_1^6}{4\pi\rho}\right)^{1/2}, \tag{57}$$

which may be expressed in the terms of the surface value of the permanent magnetic field $H_s(=m/a^2)$ in the form

$$\lambda=\frac{H_s}{a}\left(\frac{x_1^6}{4\pi\rho}\right)^{1/2}. \tag{58}$$

This corresponds to equation (12) of Schwarzschild's paper (**2**, p. 151).

13. *Numerical solution of the problem for the first and second harmonics.*—We have only attempted the numerical computations of the functions $F_n^{(1)}$ and $F_n^{(2)}$ for the most important cases, namely the first and second harmonics. This has been done for the range of values of x given by $0\leqslant x\leqslant 3$ and the graphs of the four functions $F_1^{(1)}$, $F_2^{(1)}$, $F_1^{(2)}$, $F_2^{(2)}$ are shown respectively in Figs. 1 and 2. The periods of the oscillations are given by the roots of equations (54) and (58). The eigenvalues of x_1 are approximately $x_1=1{\cdot}63$, $2{\cdot}35$, $2{\cdot}80$, ... for the first

* It can be shown that $H_1^{(2)}=5\,.\,6^{7/6}\Gamma\left(\frac{13}{6}\right)x^{11/2}J_{1/6}\left(\frac{x^3}{3}\right)$.

harmonic, $n=1$, and $x_1=1{\cdot}68$, $2{\cdot}35$, $2{\cdot}79$, ... for the second harmonic, $n=2$. Taking $H_s=7\,000$ gauss for the maximum value of the surface field, in accordance with the findings of Babcock (**3**), for the star HD 125 248, and taking also the

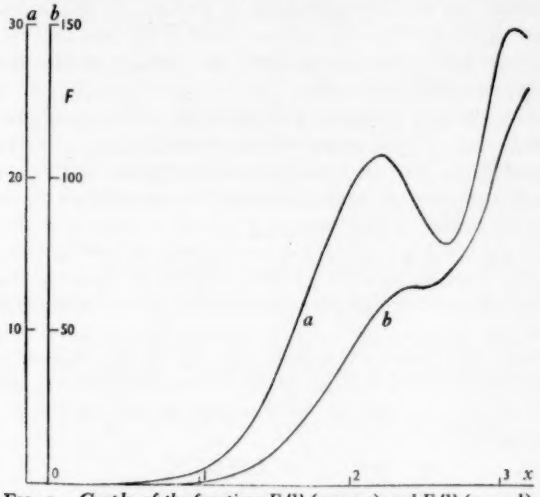

FIG. 1.—*Graphs of the functions* $F_1^{(1)}$ *(curve a) and* $F_2^{(1)}$ *(curve b).*

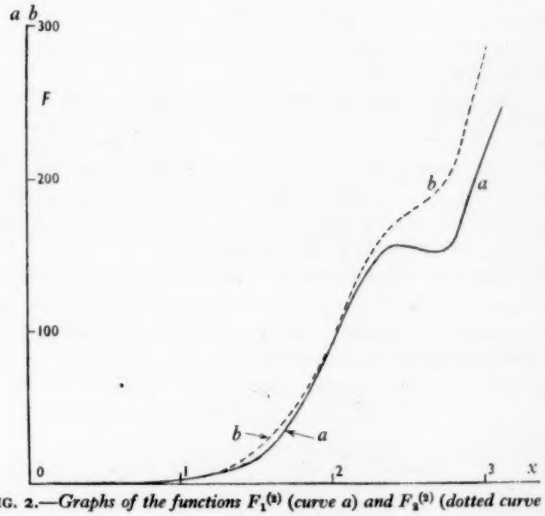

FIG. 2.—*Graphs of the functions* $F_1^{(2)}$ *(curve a) and* $F_2^{(2)}$ *(dotted curve b).*

radius and density of the sphere to be of the same order of magnitude as for Sirius A, viz. $a=1{\cdot}58R_\odot=1{\cdot}09\times10^{11}$ cm, $\rho=0{\cdot}93$, we find

$$\lambda=1{\cdot}88\times10^{-8}x_1^3. \tag{59}$$

The period $2\pi/\lambda$ of the fundamental mode of vibration of the first harmonic $n=1$, corresponding to $x=1{\cdot}63$, is found to be, by (59), equal to 894 days and the period of the fundamental mode for the second harmonic differs little from this.

The periods of the higher modes for the first two harmonics are somewhat shorter, but it is clear that it is only for very high harmonics that the periods may be shortened to the order of a few days. Thus, our result conflicts with Schwarzschild's conclusion; as we have explained in Section 1, this is because he has chosen a rather high value for the uniform field of the star and to the fact that the oscillations are most pronounced near the surface of the star where the magnetic field is considerably smaller.

The field of the central magnetic pole down to a distance of about one-tenth of the radius from the centre appears to decrease with depth at a rate comparable with that computed for the solar magnetic field by Cowling (**4**), and it seems unlikely that a shorter period can be obtained by some other choice of a model permanent magnetic field of the star.

Although we have not investigated the possible existence of complex roots of the equation (54), it seems unlikely on physical grounds that the oscillations are unstable; for the action of the magnetic field would be to damp large oscillations if such were set up.

14. *The velocity and velocity stream function for the first normal mode and first harmonic.*—The surface of the sphere corresponds to $x = x_1 = 1{\cdot}63$, approximately, in this case; from (27), (49) and (52) we find that the stream function is given by (omitting the time-factor)

$$\psi = Cx^5(1 - kx^2)\sin^2\theta, \tag{60}$$

approximately, where C is an arbitrary constant and

$$k = 0{\cdot}0415 \tag{61}$$

very nearly. The radial and transverse resolutes of velocity, given by (16), are thus approximately (omitting the time-factor)

$$v_r = 2C\eta^{-2}x^3(1 - kx^2)\cos\theta, \qquad v_\theta = Cx^3\eta^{-2}(5 - 7kx^2)\sin\theta. \tag{62}$$

Thus v_r vanishes on the equatorial plane $\theta = \pi/2$, and the stream lines $\psi =$ constant are symmetrical with respect to this plane and with respect to the axis $\theta = 0$; they are shown in Fig. 3. It will be seen that they tend to avoid the central region of the sphere where the magnetic field is large. This is also seen from the fact that the velocity resolutes vary very nearly as the cube of the distance from the centre, so that near the centre these are very small compared with their surface values.

If u_1 denotes the (radial) velocity at the poles of the sphere, these may be written in the form (omitting the time-factor)

$$\left.\begin{aligned} v_r &= -u_1 \frac{x^2(1 - kx^2)}{x_1^3(1 - kx_1^2)}\cos\theta, \\ v_\theta &= \frac{u_1}{2}\left(\frac{5 - 7kx^2}{1 - kx_1^3}\right)\frac{x^3}{x_1^3}\sin\theta, \end{aligned}\right\} \tag{63}$$

and

$$C = \frac{u_1\eta^2}{2x_1^3(1 - kx_1^2)}.$$

15. *The magnetic field of the induced currents inside the sphere (fundamental mode of the first harmonic).*—The equations (22*a*) and (60) give at once

$$u = -5\,\mathrm{Ci}\,(4\pi\rho)^{1/2}(x^2 - k_1{}^1x^4 - k_2{}^1x^6)\sin^2\theta, \tag{64}$$

where

$$k_1{}^1 = 0{\cdot}0581, \quad k_2{}^1 = 0{\cdot}0166, \tag{65}$$

approximately, and we have omitted, as usual, the time-factor.

The resolutes of the variable magnetic field induced by the vibrations are given by (16) ; we find (omitting the time-factor)

$$\left.\begin{aligned} h_r &= -10\,Ci\,(4\pi\rho)^{1/2}\eta^{-2}(1-k_1{}^1x^2-k_2{}^1x^6)\cos\theta, \\ h_\theta &= -10\,Ci\,(4\pi\rho)^{1/2}\eta^{-2}(1-2k_1{}^1x^2-4k_2{}^1x^6)\sin\theta. \end{aligned}\right\} \tag{66}$$

We first note that the presence of the imaginary factor i in (66) implies that the phases of the magnetic field and velocity differ by a quarter period so that the maxima of one correspond to the minima of the other. Also, since for $x<1{\cdot}63\ldots$, $k^1x^2\ll 1$ we see that, except near the surface, the induced magnetic field is very nearly uniform. This result, at first surprising, implies that the current flowing within the sphere must be concentrated near the surface of the sphere. This is easily verified, for the current density, **j**, is given by (2), viz.

$$\mathbf{j}=(1/4\pi)\,\mathrm{curl}\,\mathbf{H}=(1/4\pi)\,\mathrm{curl}\,\mathbf{h},$$

and is wholly azimuthal ; its magnitude is given by

$$j=10\,C(4\pi\rho)^{1/2}\eta^{-3}x(5k_1{}^1+27k_2{}^1x^4)\sin\theta, \tag{67}$$

approximately. The current I_r flowing in a sphere centre O and radius $r=\lambda x$ is

$$I_r=\int_0^2 d\theta\int_0^x \frac{50\,C\,(4\pi\rho)^{1/2}}{\eta^3}x^2\left(1+\frac{27k_2{}^1}{5k_1{}^1}x^4\right)\sin\theta dx,$$

so that

$$I_r\propto x^3\left(1+\frac{81}{35}\frac{k_2{}^1}{k_1{}^1}x^4\right)\div x^3(1+0{\cdot}66x^4).$$

Ten equal steps of current therefore flow in shells bounded by spheres of radii

0·66, 0·76, 0·82, 0·86, 0·89, 0·92, 0·95, 0·97, 0·99, 1·00,

these being expressed in terms of the radius of the sphere as unit. Thus, nearly 80 per cent of the current flows in a shell below the surface whose thickness is one-quarter of the radius.

The magnetic field intensity h at the pole of the sphere may be expressed, by (62) and (66), in terms of the velocity at the pole, u_1. We find

$$h=5(4\pi\rho)^{1/2}u_1/x_1{}^3, \tag{68}$$

and so h varies directly as the velocity.

The magnetic lines of force $u=$ constant for this mode of vibration are shown in Fig. 4. It will be seen that they are very nearly parallel except near the surface.

16. *The velocity stream function for the fundamental mode of the second harmonic.*—In this case the boundary of the sphere corresponds to $x=1{\cdot}68$ approximately, and the stream function ψ is approximately given by

$$\psi=Cx^6(1-k_1x)(1-\mu^2)\,P_2{}^1, \tag{69}$$

where C is a constant,

$$k_1=+0{\cdot}278 \tag{70}$$

approximately, and we have omitted the time-factor.

The stream lines $\psi=$ constant are shown in Fig. 5 and it will be seen that in this case also the stream lines tend to avoid the central region of the sphere where the magnetic field is large.

17. *The magnetic field inside the sphere for the fundamental mode of the second harmonic.*—In this case we find that approximately (omitting the time-factor)

$$u=-6\,Ci\,(4\pi\rho)^{1/2}(x^3-k_1{}^1x^4)\sin^2\theta\cos\theta, \tag{71}$$

where, approximately,

$$k_1^1 = 0{\cdot}0324. \tag{72}$$

The magnetic lines of force u = constant are shown in Fig. 6.

18. *Discussion.*—In Section 13 we showed that the period of the fundamental modes of free vibration of the sphere for the first two harmonics is of the order of 900 days or say $2\frac{1}{2}$ years. This is so much longer than the period of $9\frac{1}{4}$ days found by Babcock for HD 125 248 that it seems to preclude the possibility of explaining the variations of the magnetic field of the star as free vibrations in its own magnetic field.

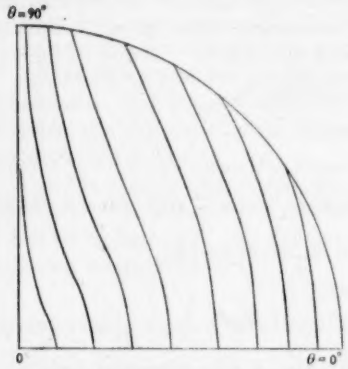

FIG. 3.—*Stream lines for the fundamental mode of the first harmonic, n=1. (Only one quadrant of the meridian plane is shown, the stream lines being symmetrical with respect to θ=0 and θ=π/2.)*

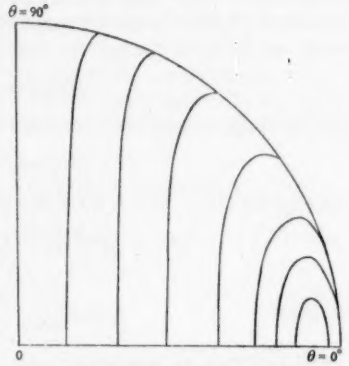

FIG. 4.—*Magnetic lines of force for the additional field in the fundamental mode of the first harmonic vibration. (Only one quadrant in a meridian plane is shown.)*

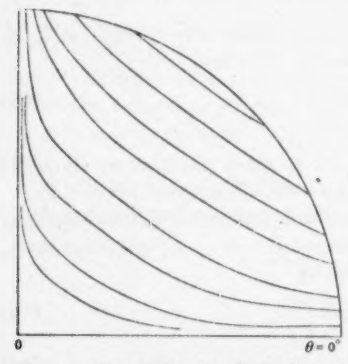

FIG. 5.—*Stream lines for the fundamental mode of the second harmonic vibration. (Only one quadrant in a meridian plane is shown.)*

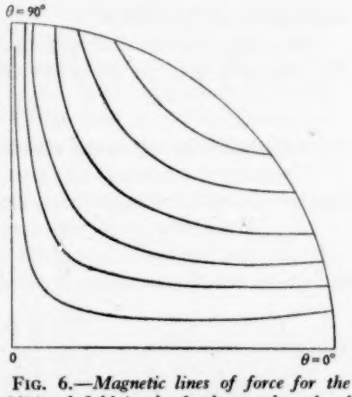

FIG. 6.—*Magnetic lines of force for the additional field in the fundamental mode of the second harmonic vibration. (Only one quadrant in a meridian plane is shown.)*

This conclusion may be looked at from another angle, namely, by calculating from (68) the magnitude of the amplitude of the magnetic field variations at the pole from the observed radial velocity of the star, which Babcock (3) gives as of the order of 3 to 10 km/s. Taking $u_1 = 10$ km/s and $\rho = 0{\cdot}93$, as in Section 13, we find that the amplitude of oscillation of the magnetic field is of the order of $3{\cdot}9 \times 10^6$ gauss,

or about *one thousand times* the value of the observed surface value of the star. In order to obtain a field *comparable* with the surface value of a few thousand gauss, the radial velocity of the sphere must be of the order of a few cm/s.

Whilst free oscillations of the star seem unlikely to provide an explanation of the variability of the magnetic field, there remains the possibility that these variations may be due to forced magnetic oscillations excited by the star's *mechanical* vibrations. Because of the highly specialized model of the star it is difficult to arrive at any definite conclusions. Nevertheless, a brief discussion of the forced oscillations of the sphere is not altogether devoid of interest.

In our special model of the star, let us suppose that the forced vibrations are excited by a variable pressure at the surface varying harmonically with time and with a period $2\pi/\lambda_0$, say, and let us suppose further that the amplitude of the pressure variation in colatitude θ is equal to $p_0 \cos\theta$, where p_0/P is small, and P is the uniform pressure (*cf.* Section 2) over the surface of the star.

The solution of the problem then proceeds as above, except that only the first harmonic is excited and (52) is to be replaced by

$$G_1(x_1) = p_0,$$

where

$$x_1^3 = \lambda_0 a(4\pi\rho)^{1/2}/H_s. \tag{73}$$

We then find from (52) and (53), for $n = 1$, that

$$A = \frac{p_0 H_1^{(2)}}{G_1^{(1)} H_1^{(2)} - H_1^{(1)} G_1^{(2)}}, \qquad B = -\frac{p_0 H_1^{(1)}}{G_1^{(1)} H_1^{(2)} - H_1^{(1)} G_1^{(2)}};$$

thus the amplitude of the oscillations is finite so long as we do not have resonance.

Since for large values of x, $F' = O(F/x)$, it follows that (68) must obtain in this case also, provided that x_1 corresponds to a period of the order of $9\frac{1}{4}$ days. Putting $2\pi/\lambda_0 = 9\frac{1}{4}$ days $= 9{\cdot}55 \times 10^5$ s, we find $\lambda_0 = 7{\cdot}86 \times 10^{-6}$ which is considerably larger than the values given by (59). Putting this value of λ_0 in (73) and taking also as before $\rho = 0{\cdot}93$, $a = 1{\cdot}09 \times 10^5$ cm and $H_s = 7\,000$ gauss, we find $x_1 = 7{\cdot}48$; so that if $u_1 = 10$ km/s, we infer from (68) that h is of the order of $4{\cdot}1 \times 10^4$ gauss, which is still somewhat larger than the observed surface field. This could be reduced to a comparable surface value of the field by taking $u_1 = 3$ km/s.

In view of the crudeness of the model adopted here, this result does not altogether preclude the possibility that the variable stellar magnetic field may be explained in terms of forced oscillations of a star in its own magnetic field, not excluding the possibility of resonance. Only a complete discussion which takes into account gravitational forces and compressibility and allows for the large observed amplitudes of the magnetic field, however, can decide whether an explanation along these lines is, in fact, possible.

University College of the South-West,
Exeter :
1951 *January* 9.

References

(1) V. C. A. Ferraro, *Magrétisme solaire et cosmique*, Observatoire Royal de Belgique, 1950.
(2) M. Schwarzschild, *Annales d'Astrophysique*, **12**, 148, 1949.
(3) H. W. Babcock, *Nature*, **166**, 249, 1950.
(4) T. G. Cowling, *M.N.*, **105**, 166, 1945.
(5) H. Alfvén, *M.N.*, **105**, 382, 1945.
(6) W. Grotrian, *Naturwiss.*, **37**, 163, 1950.

THE UNSTEADY ACCRETION PROBLEM

K. N. Dodd

(Communicated by W. H. McCrea)

(Received 1952 February 1)

Summary

A method is given for examining the behaviour of the Bondi–Hoyle–Lyttleton mechanism of accretion in the unsteady state. The results are given of a numerical investigation carried out on the Manchester University Electronic Computer, to find the rate of accretion by a star after entering a cloud of interstellar material and to examine the effect on the accretion rate of the variation of density at the edge of the cloud. The value obtained for the rate of accretion in a case similar to that considered by Bondi and Hoyle shows satisfactory agreement with their estimate and the results confirm that the more rapid the change of density, the less is the accretion rate, as suggested by Bondi and Hoyle.

1. *Introduction.*—The theory of accretion by stars according to the mechanism originally investigated by Hoyle and Lyttleton* has been elaborated by Bondi and Hoyle.† The possible importance of this process in regard to problems of stellar evolution is now widely appreciated. In the mechanism proposed by Bondi and Hoyle, it is supposed that a column of interstellar material is formed behind a moving star, which is maintained by an inflow of material from the surrounding space, caused by the gravitational attraction of the star. The particles of material in the column eventually either fall in towards the star and are captured by it, or else escape from the gravitational field of the star. A consideration of the "steady state", in which a star is moving through a cloud of interstellar material of uniform density, does not give a unique solution for the motion. Bondi and Hoyle therefore conclude that the amount of material captured by a star must depend on the perturbations previously suffered by the star and its column of interstellar material. They then obtain an approximate solution in the case of a star moving from empty space into a cloud of uniform density; the density of interstellar material being discontinuous across the surface of the cloud.

In the present paper a method is suggested which may be used when the density is not discontinuous at the edge of the cloud. The method may also be used when the density within the cloud varies with time. A case similar to that considered by Bondi and Hoyle and also one other case have been examined using this method. Considerable computation was required and this was performed on the Manchester University Electronic Computer.

The Manchester University Electronic Computer has been constructed by Ferranti Ltd. and is the only engineered electronic machine in operation in this country. It is a development of the experimental machine built in the Department

* F. Hoyle and R. A. Lyttleton, *Proc. Camb. Phil. Soc.*, **35**, 405–415, 1939; **36**, 424–437, 1940.
† H. Bondi and F. Hoyle, *M.N.*, **104**, 273–282, 1944.

of Electrical Engineering at Manchester University by T. Kilburn and F. C. Williams. Also the Manchester University Electronic Computer is the only machine in the country with an auxiliary magnetic storage system, which is essential for large problems.

2. *The Bondi–Hoyle mechanism.*—Consider a star moving in a straight line with uniform velocity through a cloud of interstellar material. We may suppose the star to be at rest at a point O and the material to be moving in a direction $O\xi$ with velocity $c(>0)$, when undisturbed by the star. According to the Bondi–Hoyle mechanism, a column of material forms round the axis $O\xi(\xi>0)$, which is sufficiently small in cross-section for the velocity of the particles to be considered uniform over any cross-section. Let $\mathfrak{V}(\xi,\tau)$ be the velocity of a particle (on $O\xi$ at a distance ξ from O) in the direction $O\xi$ at time τ, $\mathfrak{M}(\xi,\tau)$ be the mass of material per unit length of column at a distance ξ from O at time τ, $\mathfrak{A}(\xi,\tau)$ be the mass of material entering the column per unit length of column per unit time at a distance ξ from O at time τ.

Then these quantities satisfy the following equations in the unsteady state:

$$\frac{\partial \mathfrak{M}}{\partial \tau} = \mathfrak{A} - \frac{\partial(\mathfrak{M}\mathfrak{V})}{\partial \xi}, \tag{2.1}$$

$$\mathfrak{M}\mathfrak{V}\frac{\partial \mathfrak{V}}{\partial \xi} + \mathfrak{M}\frac{\partial \mathfrak{V}}{\partial \tau} = \mathfrak{A}(c-\mathfrak{V}) - \frac{\mu \mathfrak{M}}{\xi^2}, \tag{2.2}$$

where μ = mass of star $\times$ constant of gravitation.

In the steady state, in which $\mathfrak{M}$, $\mathfrak{V}$ and $\mathfrak{A}$ are independent of τ, and when the star is moving through material which has a uniform density ρ, except where disturbed by the star, there is a point $\xi=\beta$ such that

$$\mathfrak{V} \gtrless 0 \quad \text{according as} \quad \xi \gtrless \beta,$$

so that all material entering the column at points nearer to O than $\xi=\beta$ will eventually fall in and be captured by the star. In the steady state

$$\mathfrak{A} = \frac{2\pi\mu\rho}{c},$$

which is independent of ξ, so the mass of material captured by the star per unit time is

$$\frac{2\pi\mu\rho}{c}\beta.$$

The determination of β is therefore of considerable importance as it determines the rate at which material is captured by the star. Unfortunately, β cannot be determined from the steady state. It can only be found by examining the unsteady state preceding the steady state. Bondi and Hoyle, however, give reasons for inferring that

$$\frac{\mu}{c^2} < \beta < \frac{2\mu}{c^2}.$$

It may be noted here that a steady state (defined as a state in which $\mathfrak{M}$, $\mathfrak{V}$ and $\mathfrak{A}$ are all independent of τ) cannot exist unless ρ is independent of τ. But if ρ becomes independent of τ, it does not follow that a steady state will occur immediately. However, the system will immediately start tending towards such a steady state.

3. *The proposed method.*—Let us concentrate attention on a particle of material in the column. Its position at any time will be $\xi=X(\tau)$, say. Let the

values of $\mathfrak{V}$, $\mathfrak{A}$ and $\mathfrak{M}$ in the neighbourhood of the particle be V, A and M respectively. Now $\mathfrak{V}(\xi,\tau)$ is the velocity of a particle at point ξ at time τ. So

$$\mathfrak{V}(X(\tau),\tau)=V(\tau)=\frac{dX}{d\tau}, \tag{3.1}$$

and

$$\frac{dV}{d\tau}=\frac{\partial\mathfrak{V}}{\partial\xi}\frac{dX}{d\tau}+\frac{\partial\mathfrak{V}}{\partial\tau};$$

which from (3.1)

$$=\frac{\partial\mathfrak{V}}{\partial\xi}\mathfrak{V}+\frac{\partial\mathfrak{V}}{\partial\tau}. \tag{3.2}$$

Substituting (3.2) in (2.2) we obtain

$$\frac{dV}{dt}=\frac{A}{M}(c-V)-\frac{\mu}{X^2}. \tag{3.3}$$

We also have

$$M(\tau)=\mathfrak{M}(X(\tau),\tau),$$

so

$$\frac{dM}{d\tau}=\frac{\partial\mathfrak{M}}{\partial\xi}\frac{dX}{d\tau}+\frac{\partial\mathfrak{M}}{\partial\tau}$$

$$=\frac{\partial\mathfrak{M}}{\partial\xi}\mathfrak{V}+\frac{\partial\mathfrak{M}}{\partial\tau}. \tag{3.4}$$

Writing (2.1) as

$$\frac{\partial\mathfrak{M}}{\partial\tau}+\frac{\partial\mathfrak{M}}{\partial\xi}\mathfrak{V}=\mathfrak{A}-\mathfrak{M}\frac{\partial\mathfrak{V}}{\partial\xi},$$

and substituting for the left-hand side from (3.4) we have

$$\frac{dM}{d\tau}=A-M\left(\frac{\partial\mathfrak{V}}{\partial\xi}\right)_{\xi=X}. \tag{3.5}$$

Let us suppose equations (3.1), (3.3) and (3.5) to be solved, giving X, V and M as functions of τ starting from the boundary condition $\xi=\xi_1$ when $\tau=\tau_0$. Then the function X would represent the path of the particle as shown by ξ_1MBK in Fig. 1. In this case (as shown in the diagram) the particle starts to move away from the star but then returns and falls into it. If a somewhat larger value of ξ had been taken in the boundary condition, say $\xi=\xi_2$ then the path would have been as ξ_2AI, indicating that the particle escapes from the star. If the density ρ is constant so that $\mathfrak{A}$ also is constant, then the system must eventually become steady and there is a value ξ_3 of ξ at $\tau=\tau_0$ such that the particle neither falls into the star nor escapes from it, but follows a path ξ_3J and comes to rest at $\xi=\xi_4$. This value ξ_4 is what we denoted by β above.

In general, the method may be looked upon as a way of determining the alteration in β caused by a change from one constant value of ρ to another. It is not necessary that the change be instantaneous; the value of ρ between the two constant values may be any function of time.

4. *The numerical solution.*—The object of the numerical investigation was to obtain the value of β in the case of a star entering a cloud with a discontinuous change of density at its edge, and also to examine the effect on β of a slower change in ρ.

On account of the gradient on the right-hand side of (3.5), it is not possible to solve (3.1), (3.3) and (3.5) for a single particle. It is necessary to solve for a number of paths simultaneously. It is a property of the equations (parabolic equations) that disturbances are propagated along the paths ξ_1BK, etc. and not from one path to another.

The star is supposed to enter a cloud from empty space at a time $\tau = 0$. The value of $\mathfrak{A}$ is supposed to increase either instantaneously or else linearly with time from zero to its final value which is reached at $\tau = \mu t_e/c^3$, after which $\mathfrak{A}$ remains constant. (The factor μ/c^3 is to make t_e a dimensionless constant.) The surface of the cloud is taken to be of such a shape that $\mathfrak{A}$ is a function of τ only. It is at this point that the problem here considered differs from that of Bondi and Hoyle. They considered the cloud to have a plane boundary when at a great distance from the star. As the star approaches the cloud, the boundary becomes distorted and they take this into account. In this problem, on the other hand, the surface

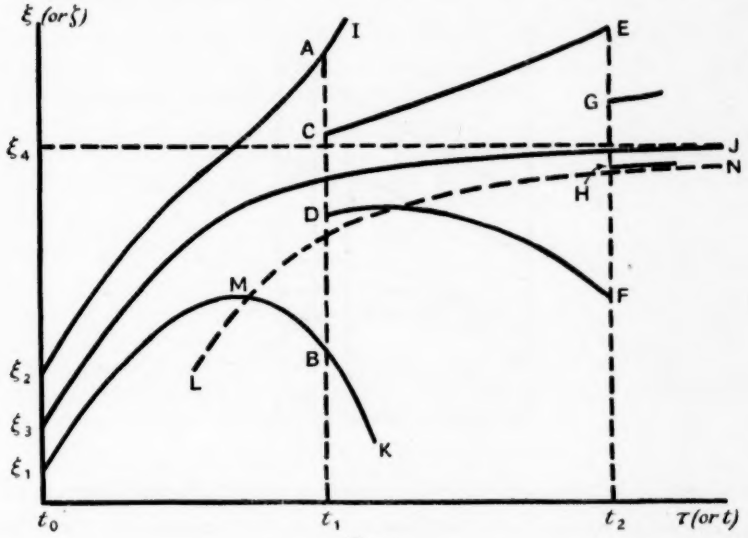

FIG. 1.

of the cloud (and in general the surfaces of constant density), when at a great distance from the star, is supposed to be such that as the star approaches, the surface will become distorted and will fall on to the axis Oξ in such a way that all points on it hit the axis at the same instant. This makes $\mathfrak{A}$ a function of τ only and independent of ξ. The surfaces of constant density in the undisturbed cloud will be surfaces of revolution with the path of the star as axis, and the surfaces will present a concave side towards the star. In view of the difference between this problem and that of Bondi and Hoyle, it is not justifiable to expect that the values of β will be the same in the two cases.

The general method given in this paper could be applied to a cloud with a plane boundary, but this would make $\mathfrak{A}$ a function of τ as well as of ξ. The extra information that would have to have been stored in the electronic machine would have considerably reduced the rate of computation. For this reason it was decided to use the simpler case for the purpose of obtaining a result.

The equations may first be made dimensionless by the transformation

$$X=8(\mu/c^2)x; \quad \xi=8(\mu/c^2)\zeta, \quad \tau=(\mu/c^3)t, \quad M=1024(\mu\bar{A}/c^3)m,$$

$$\mathfrak{V}=4c\mathfrak{v}; \quad V=4cv, \quad A=\bar{A}a,$$

where $\bar{A}$ here indicates the final value attained by A. The equations (3.1), (3.3) and (3.5) become

$$\frac{dx}{dt}=\frac{v}{2}, \tag{4.1}$$

$$\frac{dv}{dt}=\frac{1}{4}\left(\frac{a(1-4v)}{1024m}-\frac{1}{64x^2}\right), \tag{4.2}$$

$$\frac{dm}{dt}=\frac{a}{1024}-\frac{m}{2}\left(\frac{\partial\mathfrak{v}}{\partial\zeta}\right)_{\zeta=x}. \tag{4.3}$$

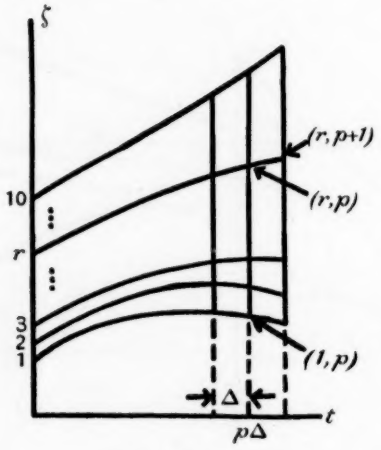

FIG. 2.

The numerical factors in the transformation were necessitated by the decision to use an electronic calculating machine. In any machine there are limits between which numbers must lie. In the machine used the limits were

$$-\tfrac{1}{2}\leqslant N<\tfrac{1}{2}.$$

Scale factors must therefore be inserted to ensure that the variables all lie in this range. The equations involve a single parameter a. In the equations, the derivatives with respect to t indicate ratios of small changes which, in the distance–time diagram (Fig. 1), are taken *in the direction of the path.*

The solution of the problem was obtained by building up a network formed by ten particle paths and the lines $t=$ constant as in Fig. 2. Denoting the paths by the integers 1 to 10 and taking equal intervals Δ in t, we may attach a number pair (r,p) to each point of the network, where r is the number of the path on which the point lies and p indicates that the point is on $t=p\Delta$. The values of the variables at any point of the network will be denoted by the appropriate symbol with the number pair of the point as a suffix.

Since only about three significant figures were required in β, it was not thought worth while to use more than second-order approximations for the derivatives in equations (4.1) to (4.3). Thus in (4.1), $(dx/dt)_{r,p}$ was represented by

$$(x_{r,p+1}-x_{r,p-1})/2\Delta,$$

and similarly for $(dm/dt)_{r,p}$ in (4.3). As a formula of this sort for $(dv/dt)_{r,p}$ would have caused oscillation in the solutions, it was decided to use

$$v_{r,p+1}-v_{r,p}=\frac{\Delta}{2}\left\{\left(\frac{dv}{dt}\right)_{r,p+1}+\left(\frac{dv}{dt}\right)_{r,p}\right\}.$$

For $(\partial\mathfrak{v}/\partial\zeta)_{r,p}$ in (4.3) the approximation

$$(v_{r+1,p}-v_{r-1,p})/(x_{r+1,p}-x_{r-1,p})$$

was used except at the edges of the network ($r=1$ and 10) where the third-order approximation of the type

$$(-11v_{1,p}+18v_{2,p}-9v_{3,p}+2v_{4,p})/(-11x_{1,p}+18x_{2,p}-9x_{3,p}+2x_{4,p})$$

was used.

The equations (4.1) to (4.3) then give the formulae:

$$x_{r,p+1}=x_{r,p-1}+\Delta v_{r,p}, \tag{4.4}$$

$$m_{r,p+1}=m_{r,p-1}+\frac{a_p\Delta}{512}-\Delta m_{r,p}\frac{(v_{r+1,p}-v_{r-1,p})}{(x_{r+1,p}-x_{r-1,p})}, \tag{4.5}$$

$$v_{r,p+1}=\left(\frac{v_{r,p}}{4}+\frac{\Delta a_p(\frac{1}{4}-v_{r,p})}{8\,192m_{r,p}}+\frac{\Delta a_{p+1}}{32\,768m_{r,p+1}}-\frac{\Delta}{2\,048x_{r,p}^2}-\frac{\Delta}{2\,048x_{r,p+1}^2}\right)$$

$$\text{divided by}\quad\left(\tfrac{1}{4}+\frac{\Delta a_{p+1}}{8\,192m_{r,p+1}}\right), \tag{4.6}$$

with the appropriate change in the last term of (4.5) when $r=1$ or 10.

The initial conditions were as follows: The initial values of x were taken at equal intervals so that

$$x_{r,0}=\epsilon+r(\delta x), \qquad r=1,2,\ldots,10.$$

ϵ and δx being suitably chosen constants. There is no material in the column initially, so

$$m_{r,0}=0,$$

and the initial velocity is c*, so

$$v_{r,0}=\tfrac{1}{4} \quad\text{and}\quad a_0=0.$$

The first-order approximations for the variables at $t=\Delta$ were taken:

$$x_{r,1}=\epsilon+r(\delta x)+\tfrac{1}{8}\Delta,$$

$$m_{r,1}=\Delta^2/2\,048t_c,$$

$$v_{r,1}=\tfrac{1}{4}-\frac{\Delta}{1\,024x_{r,1}^2},$$

$$a_1=\Delta/t_c.$$

* This is because all the material has a velocity component c along $O\xi$ when it hits $O\xi$; a result which is a consequence of the equations of motion of the particles of material in the gravitational field of the star.

These formulae are for the case where a increases linearly from zero at $t=0$ to unity at $t=t_e$ and then remains constant. In the case of an instantaneous increase in the value of a from zero to unity, the last three formulae are changed to

$$m_{r,1}=\Delta/1024,$$

$$v_{r,1}=\tfrac{1}{4}-\frac{\Delta}{768x_{r,1}^2},$$

$$a_1=1.$$

By using the above formulae the network can be built up. The best way to determine the value of β is to find, for various values of t, the value of x (which we shall refer to as η) at which $v=0$. This can be determined by an interpolation between the points of the network on the lines $t=$constant. If the results are plotted, a curve is obtained like LMN in Fig. 1. This curve passes through all the maxima of the paths and so tends to $\zeta=\beta/8(\mu/c^2)$.

It was found that as soon as the maximum of a path had been passed, the path rapidly fell away towards the t axis. In machine computation this meant that the velocity grew (negatively) so rapidly that there was a danger of it going out of the number range. To avoid this, arrangements were made at certain intervals of t to interpolate between the paths and to continue the integration with ten new paths. Thus, in Fig. 1, suppose that the integration had been performed up to $t=t_1$, so that the network was $\xi_1\xi_2$AB. At this point a new set of paths would be formed by selecting five of the original paths and forming five new ones by mid-point interpolation between the old paths. These ten new paths would intersect AB between C and D, say. The next part of the network would be like CDFE. At $t=t_2$ a further ten paths would be formed and the integration would continue from GH.

Considering the points on AB, the changes in v and x from one point to another are small until the velocity goes negative. After this, the changes become large. These large changes reduce the accuracy of the interpolation between paths. For this reason it was found wise to choose the disposition of CD with respect to AB so that at D, v was just slightly positive.

The instructions to cause the machine to carry out the calculations had to be punched in a certain code on to paper tape. The tape was about 24 feet long. These instructions were put into the machine by means of a tape reader. The value of t_e was specified on the tape and so each different value of t_e involved a slight alteration of the tape. The values of ϵ, δx (used in forming $x_{r,0}$) and Δ were specified by the setting of switches on the machine. When these switches had been set, the machine was caused to form the initial conditions and to integrate up to $t=1$ and then stop. The values of the variables at the points on $t=1$ could then be printed out on paper if desired or they could be examined by means of a matrix of dots which appeared on the screen of a cathode ray tube. It was then necessary to tell the machine, by the manipulation of switches, whether to carry on the integration or whether first to form ten new paths. In the latter case, the disposition of the new paths with respect to the old ones had to be specified, again by switches. The machine would then integrate up to $t=2$, when the decisions would be taken again as at $t=1$, after an examination of the variables. To avoid the risk of errors due to a unit of the machine not functioning properly, it was arranged for each part of the calculation to be repeated until two consecutive results agreed. This could be tested by the machine itself. Only

when agreement was reached, would the next part of the calculation be attempted. Integrations were tried with $\Delta = \frac{1}{8}$ and $\Delta = \frac{1}{16}$ and as these agreed to the desired limits of accuracy, it was decided to use $\Delta = \frac{1}{8}$. A value of about 0·001 was found to be satisfactory for δx. It may be thought that the accuracy would be improved by making δx as small as possible but this did not appear to be the case because when δx was reduced much below 0·001, oscillations rapidly appeared in the values of the variables. The reason for this is not clear. It may possibly have been due to some number range trouble.

When the machine was in good working order it could integrate between two integral values of t with $\Delta = \frac{1}{8}$ in five minutes. This involved 80 applications of each of the formulae (4.4), (4.5) and (4.6).

5. *Results and conclusion.*—Most of the work consisted of preliminary integrations to determine the best values to take for parameters such as Δ, ϵ and δx. The final results are set out in the accompanying table. This shows the value of 8η (i.e. the values of $8x$ at which $v = 0$) for various values of t. The column headed $t_c = 0$ is for an instantaneous change in density when the star enters the cloud. The figures in this column converge to a value near 1·13. This may be compared with the case considered by Bondi and Hoyle who obtained 1·25. These values are the estimates of $\beta c^2/\mu$. The figures for $t_c = 1$ could not be carried far enough to get an accurate value for $\beta c^2/\mu$ because beyond $t = 7$ the accumulation of truncation errors caused the solutions to become inaccurate. They show, however, that the value of β is changed substantially from the case $t_c = 0$.

Table of 8η

t	$t_c = 0$	$t_c = 1$	$t_c = 2$
1·125	0·65	0·53	0·52
2·125	0·84	0·78	0·67
3·125	0·98	0·93	0·85
4·125	1·09	1·03	
5·125	1·116	1·11	
6·125	1·12	1·16	
7·125		1·21	

It is interesting to notice that although the curve of zero velocity (i.e. $\zeta = \eta(t)$) tends to a higher value in the case of $t_c = 1$ than in the case of $t_c = 0$, it is initially below the $t_c = 0$ curve. The first few values of the $t_c = 2$ curve show that it starts below the $t_c = 1$ curve although it is expected to go above it eventualiy.

The general conclusion from the numerical investigation is that the more violent the change of density, the smaller is the value of β. This confirms the findings of Bondi and Hoyle.

I wish to express my thanks to Professor W. H. McCrea of the Royal Holloway College for supervising the work and to Dr A. M. Turing of Manchester University for permission to use the machine.

Royal Holloway College,
Englefield Green,
Surrey:
1952 *January* 31.

CONTINUOUS ABSORPTION BY THE HYDROGEN MOLECULAR ION

R. A. Buckingham, S. Reid and R. Spence

(Communicated by H. S. W. Massey, F.R.S.)

(Received 1952 February 7)

Summary

A quantal calculation of the continuous absorption by H_2^+ ions in the transition from the bound ($1s\sigma\ ^2\Sigma_g^+$) state to the free ($2p\sigma\ ^2\Sigma_u^+$) state has been carried out for temperatures of 2 500 deg. K and less. Comparison with the results of a semi-classical approximation by D. R. Bates shows substantial agreement.

It has been suggested by Wildt* that the ($1s\sigma\ ^2\Sigma_g^+$)→($2p\sigma\ ^2\Sigma_u^+$) transition of the hydrogen molecular ion may contribute significantly to the absorption of stellar atmospheres and interstellar space. D. R. Bates† in a recent note has shown that the total absorption involved in this transition can be calculated by a semi-classical method, and though there is little reason to doubt the validity of this approach, particularly at high temperatures and for long wave-lengths, a rigorous quantal calculation provides additional information and in many respects is complementary to the classical. The H_2^+ problem is particularly interesting in being one of the very few molecular problems which can be tackled *ab initio* without recourse to empirical data. The absorption associated with bound-free transitions has been calculated in the course of a detailed investigation into the vibration-rotation levels of H_2^+ in the ($1s\sigma$) state, and compared with that derived by Bates' method over a wide range of frequency at 1 000 deg. K and 2 500 deg. K.

In one respect H_2^+ presents a complicated problem; in most previous calculations of continuous absorption by diatomic molecules ‡ the contribution of rotational levels has been adequately allowed for by treating them as independent of temperature. For H_2^+ this is unfortunately not possible, as the relative lightness of the nuclei leads to much wider spacing of vibrational and rotational levels.

1. *Formula for absorption.*—We use the quantal formula for the absorption cross-section for a transition from an initial state represented by a wave function Ψ^v to allowed final states represented by Ψ^f:

$$k_\nu(i) = \frac{32\pi^4 m^2 r}{3h^3 c} \sum_f \nu\nu |D|^2, \tag{1}$$

where

$$D = e \int (\Psi^v) \bullet \mathbf{r}\ \Psi^f\, d\tau$$

* R. Wildt, *The Observatory*, **64**, 195, 1942; *Report of Lyons International Conference*, 1947 (*Revue d'optique théorique et instrumentale*, 1949); *Astr. J.*, **54**, 139, 1949.

† D. R. Bates, *M.N.*, **112**, 40, 1952.

‡ See, e.g., O_2, E. C. G. Stueckelberg, *Phys. Rev.*, **44**, 234, 1933.
Cl_2, G. E. Gibson, O. K. Rice and N. S. Bayliss, *Phys. Rev.*, **44**, 193, 1933.
Br_2, N. S. Bayliss, *Proc. Roy. Soc.* A, **158**, 551, 1937.

and ν is the frequency of the light absorbed. In the context m_r is the reduced mass of the proton nuclei, and v their relative velocity in the $(2p\sigma)$ state after absorption of the light quantum by the system. It follows that

$$h\nu = E_i + \tfrac{1}{2}m_r v^2, \tag{2}$$

where E_i is the *binding energy* of the initial bound state relative to that for infinite proton separation.

Both the initial and final wave functions can be represented by a product of functions, ψ and ϕ, depending on nuclear and electronic coordinates respectively, i.e. $\Psi^i = \psi_i \phi_i$, $\Psi^f = \psi_f \phi_f$.

We are here concerned only with the details of the functions representing the nuclear motion. First, in the bound state,

$$\psi_i = N_{jm} R_{nj}(r) P_j^{|m|}(\cos\theta) e^{im\varphi},$$

where n, j, m refer to vibrational, rotational and magnetic quantum numbers respectively, and $rR_{nj}(r)$ satisfies the equation

$$\left\{\frac{d^2}{dr^2} - \mu(E_{nj} + V_0(r)) - \frac{j(j+1)}{r^2}\right\}(rR_{nj}) = 0, \tag{3}$$

where the binding energy E_{nj} and the potential energy $V_0(r)$ (of the $1s\sigma$ state) are in units of $e^2/2a_0$, the nuclear separation in units of a_0, and $\mu\,(=918)$ the reduced mass in units of electron mass. Moreover R_{nj} is normalized so that

$$\int_0^\infty R^2{}_{nj}\, r^2\, dr = 1 \tag{4}$$

and N_{jm} effects the normalization with respect to θ and ϕ.

In the final continuous energy state, characterized by total energy E_e and potential energy $V_1(r)$ (again in atomic units), and quantum numbers j', m',

$$\psi_f = \sqrt{(4\pi)}\, N_{j'm'} R_{\kappa j'}(r) P_{j'}^{|m'|} \cos\theta\, e^{im'\phi},$$

in which $rR_{\kappa j'}(r)$ satisfies

$$\left\{\frac{d^2}{dr^2} + \kappa^2 - \mu V_1(r) - \frac{j'(j'+1)}{r^2}\right\}(rR_{\kappa j'}) = 0, \tag{5}$$

where $\kappa^2 = \mu E_e$. In this case normalization is such that

$$R_{\kappa j'} \sim \frac{1}{\kappa r}\sin(\kappa r - \tfrac{1}{2}j'\pi + \text{const.}). \tag{6}$$

In the derivation of $|D|^2$ the degeneracy associated with the quantum number m can be removed by summing over the permitted values of m. It is well known that

$$\begin{aligned}\sum_{m=-j}^{j} |D_{njm}|^2 &= j|D^-{}_{nj}|^2 + (j+1)|D^+{}_{nj}|^2 \\ &\simeq (2j+1)|D_{nj}|^2,\end{aligned} \tag{7}$$

where

$$D^+{}_{nj} = \sqrt{(4\pi)}\int_0^\infty R_{nj} R_{\kappa,j+1} D_e r^2\, dr,$$

$$D^-{}_{nj} = \sqrt{(4\pi)}\int_0^\infty R_{nj} R_{\kappa,j-1} D_e r^2\, dr,$$

$$D_{nj} = \sqrt{(4\pi)}\int_0^\infty R_{nj} R_{\kappa j} D_e r^2\, dr,$$

and

$$D_e = e\int \phi^*{}_i r_e \phi_f\, d\tau_e;$$

D_e is the electronic dipole moment for the $(1s\sigma)\rightarrow(2p\sigma)$ transition. $|D_{nj}|^2$ is now given in atomic units $(e^2 a_0^5)$.

The approximation using D_{nj} in place of D^+_{nj} and D^-_{nj} may easily be justified by the fact that D_{nj} varies only slightly with j. The formula is indeed often simplified still further by replacing D_{nj} throughout by D_{n0}, but for H_2^+ this step is not acceptable, as the nuclear potential energy is much shallower than in most molecules and the effect of increasing rotation on the mean nuclear separation cannot be ignored. This is more effective in the bound than in the free state, and the net result is a shift of the absorption curve to lower frequencies as j increases.

The total absorption cross-section per H_2^+ molecule is now given by

$$k_\nu = \frac{1}{W} \sum_{n,j} w_{nj} k_\nu(n, j), \tag{8}$$

where w_{nj} is the statistical weight of the (n, j) state and W is the total weight of such states. Assuming Boltzmann statistics,

$$w_{nj} = (2j+1)e^{E_{nj}/kT}, \quad W = \sum_{n,j} (2j+1)e^{E_{nj}/kT}. \tag{9}$$

For astrophysical applications it is advantageous to express the absorption in terms of the densities of free hydrogen atoms and ions. If K_ν is the absorption coefficient corresponding to a final concentration of one H atom and one proton per cm^3 then

$$K_\nu = \frac{n(H_2^+)}{n(H)n(H^+)} k_\nu, \tag{10}$$

where $n(H_2^+)$ &c. are the concentrations of the several species. The ratio of concentrations is found from the usual statistical formula to be

$$\frac{n(H_2^+)}{n(H)n(H^+)} = \frac{1}{\sigma}\left(\frac{h^2}{2\pi m_r kT}\right)^{3/2} W, \tag{11}$$

where W is as defined above, and σ is the symmetry factor, which for H_2^+ has the value 2. The final formula for K_ν can be written as follows, the form emphasizing the temperature dependence:

$$\frac{K_\nu}{a_0^5} = \frac{(2\pi)^{3/2}}{6}\left(\frac{2\pi e^2}{hc}\right)\left(\frac{h\nu}{kT}\right)\sum_{n,j} w_{nj}\left(\frac{E_e}{kT}\right)^{1/2} |D_{nj}|^2. \tag{12}$$

It is assumed here that $E_e(=h\nu - E_{nj})$, $h\nu$ and kT are in the same energy units, and $|D_{nj}|^2$ is in units of $e^2 a_0^5$.

2. *Calculations and results.*—The main part of the computation to be described consists of the derivation of the bound and free radial wave functions, R_{nj} and $R_{\kappa j}$, and the subsequent evaluation of D_{nj}. The potential functions $V_0(r)$ and $V_1(r)$, as is well known, can be obtained by solving exactly the two-centre problem for an electron, though for the present purpose the available tables of these functions, e.g. the table of $V_0(r)$ by Sandeman*, were checked and extended with the help of the tables of spheroidal wave functions by Stratton, Morse, Chu and Hutner. No attempt was made to include any correction for motion of the centre of mass, although this has been estimated over a restricted range of r by V. A. Johnson.†

Fortunately no investigation of the electron dipole moment was necessary. The variation of this with nuclear separation was estimated roughly some years

* I. Sandeman, *Proc. Roy. Soc. Edin.*, **55**, 72, 1934.
† V. A. Johnson, *Phys. Rev.*, **60**, 373, 1941.

ago by Mulliken*, and in the initial calculations of absorption his results were used. As they proceeded, however, an accurate table of D_e by Bates† became available, and this has now been incorporated in the values of K_ν. The values are somewhat smaller than Mulliken's. With D_e so tabulated there is no call to use the Franck–Condon approximation in calculating D_{nj}.

Wave functions have so far been calculated by numerical integration of equations (3) and (5) for the following values of vibrational and rotational quantum numbers:

$$R_{nj} \quad n=0,1,2,3,4,5,7 \qquad j=0,4,8,$$
$$R_{\kappa j} \quad \text{Various } \kappa \qquad j=0,8.$$

This list is being extended.

In our calculations of D_{nj}, the variation with j has not been investigated in detail. Generally the elements D_{n0} have been evaluated, and a correction applied for non-zero j. Increasing j causes the peak of D_{nj} (as function of frequency) to shift relative to that of D_{n0} by an amount which is roughly proportional to the energy difference $(E_{n0}-E_{nj})$ between the rotational levels concerned. This shift can be estimated with fair accuracy by examining the effective potential energies, $V_0-j(j+1)/r^2$ and $V_1-j(j+1)/r^2$. In addition there is a small but not important change in the magnitude of D_{nj} as j increases. Some check on the adjustments made for these effects was possible by means of the exact wave functions calculated for $j=8$.

For the calculations of k_ν and K_ν the spectrum of energy values for H_2^+ is required. Sandeman‡ has given a series formula for these, based on an empirical fitting of his $V_0(r)$ function between 1·65 and 2·35a_0 by a sextic. For estimating the weights w_{nj} this formula is accurate enough, although for values of $j>20$ it is almost certainly unreliable, as the values of E_{nj} for given n cease to form a monotonic series. For $n\leqslant 7$, $j\leqslant 8$, energy values were obtained independently whilst deriving the bound wave functions $R_{nj}(r)$, and the differences between these and Sandeman's values are not significant for the absorption calculations.

Values of K_ν based on formula (12) are shown in Table I, for temperatures of 1 000 deg. K and 2 500 deg. K, and a range of frequencies from 22 000 to 115 000 cm^{-1}. These are compared with results obtained using the semi-classical method. Since the results given by Bates§ do not cover frequencies higher than 30 000 cm^{-1}, nor temperatures below 2 500 deg. K, they have been extended for this purpose.

Comparison of columns (2) and (3) at 2 500 deg. K, both of which use the same dipole moment, shows reasonably good agreement, indicating that the classical approximation is not seriously in error at this temperature, at which kT is of the same order of magnitude as the separation of successive vibrational levels (and of course appreciably greater than the separation of rotational levels). The discrepancy is largest, as might be expected, at the highest frequencies; at low frequencies the quantal and classical agree reasonably well, in spite of the fact that the quantal calculations become more difficult as ν decreases. This is because (*a*) the main contribution comes from high vibrational and rotational levels (e.g. contributions from $j=20$–25 are far from negligible), and here the

* R. S. Mulliken, *J. Chem. Phys.*, **7**, 20, 1939.
† D. R. Bates, *J. Chem. Phys.*, **19**, 1122, 1951.
‡ *Loc. cit.*
§ D. R. Bates, *M.N.*, **112**, 40, 1952.

Sandeman level scheme is not too reliable; further, the approximations made for the variation with j of the matrix element D_{nj} have not been fully tested; (*b*) the structure of the absorption curve for higher vibrational quantum numbers becomes increasingly complicated. It is not improbable that K_ν has been underestimated at the lower frequencies, and hence no attention need be given to the fact that the quantal value given at the lowest frequency (22 000 cm^{-1}) falls slightly below the classical. Calculations (2) and (3) again converge at lower frequencies.

TABLE I

Absorption coefficient K_ν, corresponding to final concentration of 1 H *atom and* 1 H^+ *ion per* cm^3

ν/c 10^3 cm^{-1}	Temperature 1 000 deg. K (1)	(2)	(3)	Temperature 2 500 deg. K (1)	(2)	(3)
	units of 10^{-30} cm^5			units of 10^{-38} cm^5		
22	...	...	...	7·5	6·3	6·4
26	...	...	...	14·8	12·4	11·4
40	2·2	1·7	0·4	95·7	77·7	63·9
55	110	79	27	348	273	238
70	652	487	411	705	533	534
85	1310	969	1570	830	619	714
100	995	738	1480	561	421	560
115	374	277	308	174	137	250

(1) quantal formula, using Mulliken's values of D_e,
(2) quantal formula, using Bates' values of D_e,
(3) semi-classical formula, using Bates' values of D_e.

The results at 1 000 deg. K show that the classical approximation is less good, but not wildly in error; it gives a sharper and higher absorption peak than the quantal calculations.

Table II contains values of k_ν, the absorption cross-section per molecule, at 0 deg., 1 000 deg. and 2 500 deg. K, using the Bates dipole moment throughout. These results indicate sufficiently well that absorption at wave-lengths in excess of 2 500 A and temperatures below 2 500 deg. K is slight.

TABLE II

Absorption cross-section k_ν per H_2^+ molecule in units of $10^{-20} cm^2$

Temp. (deg. K)	Frequency ν/c (10^3 cm^{-1}) 22	26	40	55	70	85	100	115
0	...	...	...	24	253	706	597	271
1 000	...	...	1	59	364	724	551	207
2 500	5·2	10·2	64	224	438	508	345	112

The significance of the absorption by H_2^+ in stellar atmospheres is being examined by Professor B. Strömgren.

University College,
London:
1952 *February* 5.

RADIATIVE SOLUTIONS OF THE STELLAR EQUATIONS

R. J. Tayler

(Communicated by H. Bondi)

(Received 1952 April 9*)

Summary

In Part A of the paper stellar models with energy generation according to the law $\epsilon \propto \rho T^{\eta}$ are considered for various opacity laws, and the values of η, for which a convective core is obtained, are determined. It is found that the limiting value of η varies between 1 and 8·5 for the opacity laws considered. These conclusions are compared with those of Cowling, who considered a different law of energy generation.

In Part B the model of a completely radiative star with $\eta = 3{\cdot}5$ and Kramers' opacity is investigated. The model is compared with the convective model with the same opacity law but different energy generation, and their properties are found to be not widely different. Comparison is also made with radiative models of Eddington and Biermann with other laws of energy generation.

PART A

1. *Introduction.*—Two of the most important problems in the theory of stellar structure are the origin of the radiant energy that is observed to flow across the surface, and the method of transfer of this energy through the inner regions of a star. Eddington showed that, under normal circumstances, convection would be expected to play a secondary role to radiation because of the high temperature-dependence of Stefan's law. The investigations of Cowling and others have since shown that, on the other hand, many stars will have an inner "core" in convective equilibrium, and most stellar models that have been considered are those containing convective cores. It is of interest and importance to consider the possible existence of models not possessing an inner convective region, and, if such do exist, in what physical respect they differ from those with a convective core. The latter problem will be considered in Part B of this paper.

We restrict ourselves to homogeneous gaseous stars, of ratio of specific heats $\frac{5}{3}$, that are in a steady state. Radiation pressure will be neglected everywhere.

The symbols used will be defined as usual by

r = distance from centre of star,
$P(r)$ = pressure at radius r,
$\rho(r)$ = density at radius r,
$T(r)$ = temperature at radius r,
$M(r)$ = mass contained in radius r,
G = constant of gravitation,
$\mathfrak{R}$ = gas constant (gram molecule),
μ = molecular weight,
a = Stefan's constant,
c = velocity of light,

* Received in original form 1951 November 19.

and since radiation pressure is everywhere neglected

$$P = \mathfrak{R}\rho T/\mu.$$

The solution will be performed in Bondi h-variables S, Q and N (1): these are defined in terms of the physical variables by the relations

$$S = 4\pi Pr^4/GM^2,$$
$$Q = Pr/GM\rho,$$
$$N = 1 - d\ln\rho/d\ln P.$$

The laws of opacity considered have the general form

$$\kappa = \kappa_0\rho^{\lambda-1}/T^{\nu-3},$$

and the energy generation per unit mass is

$$\epsilon = \epsilon_0\rho^{\xi-1}T^{\eta}.$$

Cowling has considered the case of $\xi = 1$ and we, in fact, restrict ourselves to the case $\xi = 2$. The equations are first obtained for the case of general ξ.

2. *Derivation of fundamental equations.*—As we are considering a steady-state problem, the hydrostatic equation takes the simplified form

$$dP/dr = -GM\rho r^{-2}, \tag{2.1}$$

while the equation of mass conservation is

$$dM/dr = 4\pi r^2\rho. \tag{2.2}$$

Using the opacity law and the energy generation of this problem, the energy transport equation becomes

$$0 = \frac{1}{r^2}\frac{d}{dr}\left[\frac{r^2cT^{\nu-3}}{3\kappa_0\rho^{\lambda}}\frac{d}{dr}(aT^4)\right] + \epsilon_0\rho^{\xi}T^{\eta}. \tag{2.3}$$

As is well known (1), equations (2.1), (2.2) can be simply expressed in h-variables by the single equation

$$\frac{S}{Q}\frac{dQ}{dS} = \frac{S+N-Q}{1+2S-4Q}, \tag{2.4}$$

which equation holds in all stars in a steady state regardless of their law of opacity or mode of energy generation.

The energy transport equation must also be transformed to h-variables, and this process requires the following relations found in (1):

$$\left.\begin{aligned}\frac{r}{T}\frac{dT}{dr} = \frac{Nr}{P}\frac{dP}{dr} = -\frac{N}{Q},\\ \frac{r}{\rho}\frac{d\rho}{dr} = -\frac{(1-N)}{Q},\\ \frac{S}{r}\frac{dr}{dS} = -\frac{Q}{1+2S-4Q}.\end{aligned}\right\} \tag{2.5}$$

Equation (2.3) may be written

$$\frac{E}{r^2}\frac{d}{dr}\left[\frac{r^2T^{\nu}}{\rho^{\lambda}}\frac{dT}{dr}\right] + \rho^{\xi}T^{\eta} = 0,$$

where E is the constant $4ac/3\kappa_0\epsilon_0$. Using (2.5) this becomes

$$\frac{E}{r^2}\frac{d}{dr}\left[\frac{-rT^{\nu+1}}{\rho^{\lambda}}\frac{N}{Q}\right] + \rho^{\xi}T^{\eta} = 0,$$

which on differentiation, and using (2.5), reduces to

$$\rho^{\xi}T^{\eta}=\frac{ET^{\nu+1}N}{\rho^{\lambda}r^{2}Q}\left[1-(\nu+1)\frac{N}{Q}+\lambda\frac{1-N}{Q}+r\frac{d}{dr}\ln\frac{N}{Q}\right].$$

If we now take logarithms and use the third relation of (2.5) we obtain

$$\xi\ln\rho+\eta\ln T-(\nu+1)\ln T+2\ln r+\lambda\ln\rho$$
$$=\ln\left\{\frac{N}{Q}\left[1-(\nu+1)\frac{N}{Q}+\lambda\frac{(1-N)}{Q}-\frac{S(1+2S-4Q)}{Q}\frac{d}{dS}\ln\frac{N}{Q}\right]\right\}+\text{const.}$$

Now we differentiate with respect to S and substitute from (2.5) to obtain

$$\frac{d}{dS}\ln\left[N\Big(S+\lambda-N(\nu+\lambda)\Big)-S(1+2S-4Q)\frac{dN}{dS}\right]$$
$$=\frac{1}{S}+\frac{(\lambda+\xi-1)-N(\lambda+\xi+\nu-\eta-1)}{S(1+2S-4Q)},$$

which finally reduces to

$$\begin{aligned}&S^{2}(1+2S-4Q)^{2}d^{2}N/dS^{2}-S(dN/dS)\{(2\lambda+\xi-1)+(4\lambda+2\xi-3)S\\&-(8\lambda+4\xi-4)Q-2S^{2}+8SQ-4Q^{2}-N[(3\lambda+\xi+3\nu-\eta-1)\\&+(6\lambda+2\xi+6\nu-2\eta-2)S-4(3\lambda+\xi+3\nu-\eta)Q]\}\\&+N\{[1+2S-4Q][\lambda-N(\nu+\lambda)]+[S+\lambda-(\nu+\lambda)N][(\lambda+\xi-1)\\&-N(\lambda+\xi+\nu-\eta-1)]\}=0.\end{aligned}\tag{2.6}$$

The equations fundamental to our problem are the standard "steady-state equation" (2.4) and the energy transport equation (2.6). We wish to investigate stellar models in which the radiative equations apply throughout the interior. The radiative equations will cease to hold if at any point the radiative temperature gradient exceeds the convective (adiabatic) temperature gradient. An equivalent condition can be seen to be

$$N>(\gamma-1)/\gamma=0{\cdot}4.$$

We require models with $N<0{\cdot}4$ throughout.

At the centre of the star S, $Q\to\infty$, but we know that

$$Q\sim Q_{E}(S;\,N_{c}),\tag{2.7}$$

the Emden solution for $N=N_{c}$ (central value of N). At the surface S, Q are both very small, and little inaccuracy is introduced by taking them both to be zero. Then, if N_{s} is the surface value of N,

$$Q\sim AS^{N_{s}}\quad\text{as}\quad S\to 0,\tag{2.8}$$

where A is an arbitrary parameter. Only one value of the parameter in (2.8) gives a solution which joins up with a central solution (2.7) to give a complete stellar model.

3. *General behaviour of solutions.*—Henceforth we consider only the case $\xi=2$. The reason why this value of ξ is of great importance is that the energy generation is believed to be caused by nuclear collisions. The number of collisions per unit mass is proportional to ρ, and thus the number per unit volume will depend on ρ^{2}.

We now require solutions of the radiative equations satisfying (2.7), (2.8) and $N_{c}<0{\cdot}4$. The variable N can also be shown to satisfy the further condition $N\geqslant N_{s}$; for it can be shown that if $N<N_{s}$ for any value of S, then $N<N_{s}$ for all smaller values of S, and the solution is then unable to satisfy the surface

boundary condition (*cf.* Hoyle and Lyttleton (**3**)). The condition can be shown to be more general than they there require, and certainly holds for $\eta > -\frac{3}{2}$. The value of N_s for the different opacity laws is given by

$$N_s = \lambda/(\nu+\lambda).$$

The problem is approached by methods of step-by-step numerical integration. No great accuracy is sought in this method, but rather a valid set of general conclusions. Outward integration is found to be more convenient than the corresponding inward process, and solutions in series of the equations, for large S, may be obtained in the form

$$Q = S/3 + (1 - N_c)/5 + O(1/S),$$
$$N = N_c - (3N_c/10S)\{(5\lambda+3) - N_c(5\lambda+5\nu-3\eta+3)\} + O(1/S^2).$$

For a given opacity law and law of energy generation the solutions form a one-parameter set with parameter N_c. The solutions obtained for N by numerical integration have the general form of Fig. 1. Because the equations are unstable with N when integrated outwards (as has been found by previous investigators), the solutions, other than the one which just satisfies the boundary conditions, will diverge to $\pm\infty$.

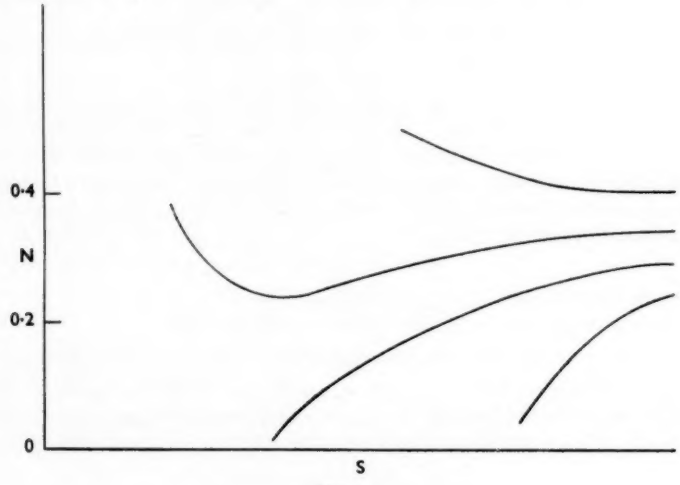

FIG. 1.

The solutions for different N_c, in all cases in which computations have been performed, appear to form a non-intersecting one-parameter family. The analytical proof of such a property would appear to present great difficulties, but we will assume it to be true in what follows.

Similarly we can consider solutions for given opacity law and $N_c = 0{\cdot}4$; these form a one-parameter family with η. Again the solutions appear to form a non-intersecting one-parameter family (Fig. 2).

We perform outward integrations for $N_c = 0{\cdot}4$ for various opacity laws, obtaining in each case a one-parameter family as above. Owing to the rough step-by-step method that we are using and the instabilities of the equation, we cannot expect to obtain the solution that just satisfies the boundary conditions. It will, however, be possible to state that the required solution, for which a

convective core is just obtained, will have an exponent of energy generation η, where

$$\eta_1 < \eta < \eta_2.$$

We require a solution of the radiative equation such that $N_c = 0{\cdot}4$ and $N < 0{\cdot}4$ for all finite S, and satisfying the surface boundary conditions.

If for $N_c = 0{\cdot}4$, $\eta = \eta_2$ we obtain an N solution which rapidly falls to $N = N_s$ and below, before the divergences of the numerical methods have become great; then we can assert that for $\eta = \eta_2$ there will be a convective core. Any solution for this value of η satisfying the boundary conditions must lie above the solution for $N_c = 0{\cdot}4$, and as N will then reach $0{\cdot}4$ for finite S, a convective core will be obtained.

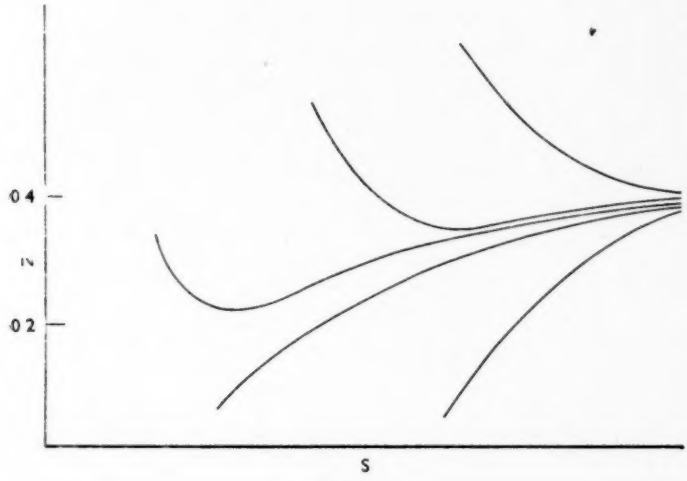

FIG. 2.

Similarly, if for $N_c = 0{\cdot}4$, $\eta = \eta_1$ the N solution becomes greater than $0{\cdot}4$ while S is still large, we can assert that the actual solution for $\eta = \eta_1$ will have $N_c < 0{\cdot}4$ and no convective core.

This enables us to state that the critical value of η must lie in a certain range $\eta_1 < \eta < \eta_2$. This range may not be made too small owing to the inaccuracies of the numerical procedure, which are of increasing importance as the values of S become smaller. The exact value of η is not normally of extreme importance and a range of variation of 1 is sufficient for most purposes.

4. *Integration procedure.*—In order to carry out a step-by-step process we change our variables by putting

$$\sigma = 1/S, \qquad \tau = 1/Q,$$

and (2.4), (2.6) take the form

$$\frac{\sigma}{\tau}\frac{d\tau}{d\sigma} = \frac{\tau + N\tau\sigma - \sigma}{\sigma\tau + 2\tau - 4\sigma},$$

$$\begin{aligned}
&\sigma(\sigma\tau + 2\tau - 4\sigma)^2\, d^2N/d\sigma^2 \\
&\quad + (dN/d\sigma)\{(2\lambda+3)\sigma^2\tau^2 + (4\lambda+9)\sigma\tau^2 - (8\lambda+20)\sigma^2\tau + 6\tau^2 - 24\sigma\tau + 28\sigma^2 \\
&\quad - N[(3\lambda+3\nu-\eta+1)\sigma^2\tau^2 + (6\lambda+6\nu-2\eta+2)\sigma\tau^2 - 4(3\lambda+3\nu-\eta+2)\sigma^2\tau]\} \\
&\quad + N\tau\{[\sigma\tau + 2\tau - 4\sigma][\lambda + N(\nu+\lambda)] \\
&\quad + \tau[1 + (\lambda - N\nu - N\lambda)\sigma][(\lambda+1) - N(\lambda+\nu-\eta+1)]\} = 0.
\end{aligned}$$

We can obtain solutions in series for N, τ for small values of σ:

$$\tau = 3\sigma + a_2\sigma^2 + a_3\sigma^3 + a_4\sigma^4 + \ldots,$$

$$N = N_c + b_1\sigma + b_2\sigma^2 + b_3\sigma^3 + \ldots .$$

It is found convenient to calculate $a_2 \ldots a_4 \ldots, b_1 \ldots b_4 \ldots$ as they are required, and not to express them in analytical form. By writing $dN/d\sigma = K$ we can obtain our equations in a first-order system suitable for the numerical integration. The series for τ, N, K give accurate values up to some value of σ normally between 0·05 and 0·1: the series for τ is sufficiently accurate to about 0·2.

We take a solution in series for τ, N, K up to some starting value of σ and then perform a step-by-step integration for N, K while still using the series for τ. When the series for τ is no longer accurate enough, we use a step-by-step method for all three variables. The method does not claim great accuracy as only the first differential coefficient is used, but it is sufficiently accurate for the general results required. If the exponent in the law of energy generation were required more precisely, a more accurate integration procedure would be necessary—together with a much greater expenditure of time. Here the emphasis has been on obtaining general results rapidly.

The series give surprisingly good agreement with the integration for quite large values of σ. Indeed, for $\sigma = 0{\cdot}5$ or 0·7 the difference between the series and the numerical integrations is often only a few per cent.

5. *Results.*—The law of energy generation was taken to be

$$\epsilon = \epsilon_0 \rho T^{\eta}.$$

Four different opacity laws were considered:

(*a*) Electron opacity; $\kappa = \kappa_0$ $(\lambda = 1$ $\nu = 3)$.

(*b*) Kramers' opacity; $\kappa = \kappa_0 \rho / T^{3{\cdot}5}$ $(\lambda = 2$ $\nu = 6{\cdot}5)$.

(*c*) Modified Kramers' opacity (i); $\kappa = \kappa_0 \rho / T^{4{\cdot}5}$ $(\lambda = 2$ $\nu = 7{\cdot}5)$.

(*d*) Modified Kramers' opacity (ii); $\kappa = \kappa_0 \rho^{0{\cdot}75} / T^{3{\cdot}5}$ $(\lambda = 1{\cdot}75$ $\nu = 6{\cdot}5)$.

It was found that there is

(*a*) A convective core for $\eta > \eta_E$ where $1 < \eta_E < 2$;

(*b*) A convective core for $\eta > \eta_K$ where $5{\cdot}5 < \eta_K < 6{\cdot}5$;

(*c*) A convective core for $\eta > \eta_1$ where $7{\cdot}5 < \eta_1 < 8{\cdot}5$;

(*d*) A convective core for $\eta > \eta_2$ where $5{\cdot}75 < \eta_2 < 6{\cdot}75$.

More detailed results for one particular case (*c*) appear in Table I.

TABLE I

$\kappa = \kappa_0 \rho / T^{4{\cdot}5}$; $\epsilon = \epsilon_0 \rho T^{\eta}$; $N_s = 0{\cdot}2105$

$\eta = 7{\cdot}5$			$\eta = 8{\cdot}5$		
σ	τ	N	σ	τ	N
0·05	0·147	0·3899	0·05	0·147	0·3827
0·1	0·289	0·3810	0·1	0·289	0·3665
0·2	0·559	0·3662	0·2	0·558	0·3368
0·3	0·809	0·3557	0·3	0·806	0·3096
0·4	1·044	0·3489	0·4	1·035	0·2836
0·5	1·265	0·3461	0·5	1·247	0·2586
0·6	1·473	0·3473	0·6	1·441	0 2343
0·7	1·671	0·3533	0·7	1·619	0·2107

6. *Conclusions and comparisons.*—Thus in all cases we expect a convective core if the energy generation is to take place according to the carbon–nitrogen Bethe cycle, or a similar process ($\eta \doteqdot 17{\cdot}5$). With the smaller value of η obtained for the proton-proton reaction a wholly radiative star will result for a Kramers' opacity law. The model of such a star forms the subject of the second part of this paper.

We may compare these results with those of Cowling (**2**), who considers energy generation per unit mass given by

$$\epsilon = \epsilon_0 T^{\eta},$$

and the two opacity laws

(*a*) Electron; $\kappa = \kappa_0$, convective $\eta > \eta_E$, $3 \leqslant \eta_E \leqslant 4$.

(*b*) Kramers'; $\kappa = \kappa_0 \rho / T^{3{\cdot}5}$, convective $\eta > \eta_K$, $7 \leqslant \eta_K \leqslant 8$.

Part B

1. *Introduction.*—It has been shown above that for energy production with low dependence on temperature an entirely radiative star results from a Kramers' opacity law.

We consider the case of pure Kramers' opacity together with energy generation per unit mass given by

$$\epsilon = \epsilon_0 \rho T^{3{\cdot}5}.$$

This law of energy generation is an approximate mathematical expression for the proton-proton reaction, which is more important than the Bethe cycle for a great number of stars. Bondi *h*-variables S, Q, N are used throughout. Radiation pressure is again neglected and the other notation is as above.

The stellar equations for

$$\kappa = \kappa_0 \rho / T^{3{\cdot}5}$$

$$\epsilon = \epsilon_0 \rho T^{3{\cdot}5}$$

are

$$\frac{S}{Q}\frac{dQ}{dS} = \frac{S+N-Q}{1+2S-4Q}, \tag{1.1}$$

$$\begin{aligned} &S^2(1+2S-4Q)^2 d^2N/dS^2 \\ &\quad - S(dN/dS)\{5+9S-20Q-2S^2+8SQ-4Q^2-N[23+46S-96Q]\} \\ &\quad + N\{(1+2S-4Q)(2-8{\cdot}5N)+(S+2-8{\cdot}5N)(3-6N)\} = 0. \end{aligned} \tag{1.2}$$

It is shown above that, for the case of Kramers' opacity and $\xi = 2$, there is no convective core for $\eta < \eta_K$ where $5{\cdot}5 < \eta_K < 6{\cdot}5$. Thus certainly for $\eta = 3{\cdot}5$ we will obtain a completely radiative star, and we require a solution of (1.1), (1.2) holding for all positive S.

2. *Solutions for large S.*—A first step consists in considering the solutions for large S. It is known (**1**) that at ∞ Q is asymptotic to $Q_E(S;\ N_c)$ where N_c is the limiting value of N and Q_E is the Emden function of S, N. Thus

$$Q = S/3 + (1-N_c)/5 + O(1/S),$$
$$N = N_c + O(1/S).$$

The problem is best tackled by a change of variables by putting

$$\sigma = 1/S, \qquad \tau = 1/Q,$$

and our fundamental equations then become

$$\frac{\sigma}{\tau}\frac{d\tau}{d\sigma} = \frac{\tau + N\tau\sigma - \sigma}{\sigma\tau + 2\tau - 4\sigma},$$

$$\sigma(\sigma\tau + 2\tau - 4\sigma)^2 d^2N/d\sigma^2$$
$$+ (dN/d\sigma)\{7\sigma^2\tau^2 + 17\sigma\tau^2 - 36\sigma^2\tau + 6\tau^2 - 24\sigma\tau + 28\sigma^2 - N(23\sigma^2\tau^2 + 46\sigma\tau^2 - 96\sigma^2\tau)\}$$
$$+ N\tau\{(\sigma\tau + 2\tau - 4\sigma)(2 - 8{\cdot}5N) + \tau(1 + (2 - 8{\cdot}5N)\sigma)(3 - 6N)\} = 0.$$

There is one parameter in our solution at the centre (N_c), and we obtain a single infinity of solutions corresponding to a single infinity of N_c values. We have as yet not specified our problem completely as we have to satisfy the surface boundary conditions

$$S = Q = 0, \qquad Q \sim AS^{4/17}, \qquad N_s = \tfrac{4}{17}.$$

Only one value of N_c will give us a solution that also satisfies the surface conditions.

The process of step-by-step integration as above is again used. These solutions will be of use up to a certain value of σ, but it will be found impossible to reach the origin as the N solutions will diverge to $\pm\infty$. A step-by-step process is carried out for several values of N_c, and we obtain two solutions for neighbouring N_c such that one diverges to $+\infty$ and the other to $-\infty$. If the divergence is sufficiently rapid for the inaccuracies to be relatively unimportant, then the above process will have obtained bounds for the required value of N_c.

Each of the solutions in series is found independently as the expression of coefficients in terms of N_c seems impracticable. It is found convenient to calculate the first four coefficients in each series.

3. *Solutions for small S.*—As we are considering a law of nuclear energy generation which depends quite critically on the temperature, the greater part of the energy production will occur in the hot central regions of the star. A first approximation is to neglect completely energy production in the outermost regions. Solutions are already known, and simply obtained (1), for the uniform Kramers' opacity star with no energy generation, and accordingly we try to fit such an envelope solution on to our central solution. This procedure has been previously followed for the convective case (Bethe cycle), where it is assumed that the generation of energy takes place in the core alone (1). This seems justified since $\rho\epsilon \doteqdot \epsilon_0\rho^2T^{18}$ and at the point of fit of the convective and radiative regions $\rho\epsilon \sim \rho\epsilon_c/150$, where ϵ_c is the value of the central energy production. Thus the rate of energy generation per unit volume is 0·66 per cent of the central rate. The use of such a method in this case is not so clear because of the smaller exponent (3·5) of T. We will attempt such a fit and consider the justification later.

Near the surface, in the case of no energy generation, we have from (1)

$$Q = \theta - \tfrac{1}{4}\theta^2 - \tfrac{7}{16}\theta^3 - \tfrac{65}{64}\theta^4 - \tfrac{667}{256}\theta^5 + \tfrac{31}{51}S\theta,$$
$$N = \tfrac{4}{17} + \tfrac{4}{51}S + \tfrac{16}{165}S\theta + \tfrac{1124}{9735}S\theta^2,$$

where $\theta = AS^{4/17}$ and A is a free parameter. The series is accurate for N up to $S = 0{\cdot}1$, but that for Q is inaccurate beyond $S = 0{\cdot}01$. Using the series for N, a few stages of step-by-step integration of $\ln Q$ against $\ln S$ cover the range between $S = 0{\cdot}01$ and $0{\cdot}1$. Thereafter the graphical method of Bondi and Bondi (1) is used.

Results were tabulated for $A = 0{\cdot}2$, $0{\cdot}22$, $0{\cdot}24$ for values of S up to 1.

4. *Fit of envelope on to central solution.*—A first fit is attempted with $S=0{\cdot}8$. The central solution for $N_c=0{\cdot}35$ is obtained, and it is found that this central solution fits quite accurately on to the envelope solution with $A=0{\cdot}24$. That is to say, that the difference in Q, N for the two solutions, at $S=0{\cdot}8$, is small compared with the value for either solution. The slopes of the two curves for N naturally do not fit. In fact they differ significantly; that is, the difference in the slopes is not negligible compared with the slopes themselves.

In order to see how sensitive the solution is for variations in N, slightly smaller values of N_c are taken, and it is found that for $N_c=0{\cdot}349$ it is impossible to obtain a fit for $S<0{\cdot}8$. Similarly consideration of solutions for slightly larger values of N_c shows that no nearer fit can be obtained for N_c much greater than 0·35. This shows that the central solution is very sensitive indeed to change of N, and that $N_c \doteqdot 0{\cdot}35$ is the accurate solution.

It is now of interest to consider what change is introduced into the physical variables by such variation in N. Taking the central solutions for $N_c=0{\cdot}35$, $N_c=0{\cdot}349$ in turn, values of P/P_c, ρ/ρ_c are obtained for the two solutions. The integrals are evaluated in terms of σ, τ either by means of Simpson's rule or graphically. We obtain

$$N_c=0{\cdot}35, \qquad (P/P_c)_{1\cdot0}=0{\cdot}324, \qquad (\rho/\rho_c)_{1\cdot0}=0{\cdot}466,$$
$$N_c=0{\cdot}349, \qquad (P/P_c)_{1\cdot0}=0{\cdot}324, \qquad (\rho/\rho_c)_{1\cdot0}=0{\cdot}463.$$

This compares with the uniform Kramers' opacity convective core solution for which $(P/P_c)_{1\cdot0}=0{\cdot}337$, $(\rho/\rho_c)_{1\cdot0}=0{\cdot}509$. It can be seen that, at any rate for $S>1{\cdot}0$, the errors introduced into P and ρ by an error in the value N_c are very small compared with the values of P, ρ themselves.

It is also convenient to consider the value of $(M/M_s)_{0\cdot8}$ for the envelope solution with $A=0{\cdot}24$ and for a neighbouring value. For

$$A=0{\cdot}24 \text{ we obtain } (M/M_s)_{0\cdot8}=0{\cdot}352,$$
$$A=0{\cdot}2351 \qquad\qquad (M/M_s)_{0\cdot8}=0{\cdot}360.$$

The error introduced in the physical variable M is thus also seen to be small for a small range in A. This will be true for all smaller values of S.

A second fit is now attempted for $S=\frac{2}{3}$. We find that such a fit is possible with $N=0{\cdot}3496$, $A=0{\cdot}2374$. The solutions for Q fit very accurately, and the discontinuity in the gradient of N is not now so serious.

We now consider the values of ρ/ρ_c, P/P_c, T/T_c for our second fit and compare the rate of energy generation per unit volume at $S=\frac{2}{3}$ with that at the centre. We obtain

$$\rho/\rho_c \doteqdot 0{\cdot}353, \qquad P/P_c \doteqdot 0{\cdot}215, \qquad T/T_c \doteqdot 0{\cdot}609,$$
$$\frac{\rho^2 T^{3\cdot5}}{\rho_c^2 T_c^{3\cdot5}} \doteqdot 0{\cdot}02.$$

The rate of generation of energy per unit volume has fallen to about 2 per cent of its central value.

By consideration of the curves of second fit and solutions for neighbouring values of N_c it seems that we can assert

$$0{\cdot}3493<N_c<0{\cdot}3497,$$

and thus, by considering such a variation in N_c we can obtain an estimate of likely errors in the physical variables. Such errors, due to incorrect N_c, but not due to errors in integration, seem unlikely to exceed 1 per cent at $S=\frac{2}{3}$.

The details that are required from our integrations are the values of the physical variables, and the exact properties of the h-variables are not required. The physical variables show a uniform behaviour in the region of second fit, and we have also reached a zone where the rate of energy production is small compared with the central value. If we are to attempt another fit at a significantly smaller value of S, then much more numerical work will be required, and an increase in the range of numerical integration will certainly increase the errors therefrom. In fact the errors due to the integration process will be expected to be large compared with the errors due to a more distant fit.

It thus seems reasonable not to attempt a closer fit, but to "round off" our solution of second fit. A smooth curve is obtained by rounding off the point of juncture, and we take this as our solution to describe the general properties of "an entirely radiative star".

What exactly have we done by performing this fit? If the integration is accurate then we have obtained a solution, prior to rounding off, in which the energy generation $\propto \rho T^{3\cdot5}$ in the inner regions, and is zero in $S<\frac{2}{3}$. We know that at the point of fit we are already in a region of low energy production, and we can expect our solution to be fairly accurate if the total production in the outer regions is small compared with that for the model as a whole.

There is, however, another way of looking at our solution. In any star the law of energy generation is highly dependent on temperature, and we would not expect any simple power law to hold throughout the star. In fact we might expect that below a certain temperature there would be a virtual cut-off in production. By rounding off above we have in effect obtained this cut-off, and, instead of regarding our solution as an inaccurate one for the law $\epsilon \propto \rho T^{3\cdot5}$ we may regard it as the solution for a star in which the energy generation $\propto \rho T^{3\cdot5}$ in inner regions and is zero in the outer regions, together with a transition zone.

5. *Calculation of results.*—There are six physical variables the values of which we require to obtain from our solution:

$$r,\ P,\ \rho,\ T,\ M \quad \text{and} \quad L(r) \text{ (luminosity at radius } r).$$

These give six fundamental parameters, r_s, P_c, ρ_c, T_c, M_s, L_s for our solution, but these are in fact not independent. We have obtained the solution of our problem in h-variables, and it must now be translated into p-variables. How many different stellar models may be obtained from such a solution? We find that if we are given the constants κ_0, ϵ_0 of our opacity and energy generation, then there is just one free parameter, and a single infinity of stellar models is obtained.

There are the following relations between our parameters:

(*a*) $P_c = \mathfrak{R}\rho_c T_c/\mu$.

(*b*) $\rho_c = \lim_{r\to 0} 3M/4\pi r^3$,

$$\text{whence } \ln \rho_c/\rho_{\text{mean}} = \ln 4\pi r_s^3 \rho_c/3M_s = \int_0^\infty \frac{(3Q-S)\,dS}{S(1+2S-4Q)}.$$

(*c*) $\ln Q = \ln P_c r_s/GM_s\rho_c + \ln r_s/r + \ln P_c/P - \ln M_s/M - \ln \rho_c/\rho$, so that

$$\ln \frac{P_c r_s}{GM_s\rho_c} = \ln Q + \int_0^S \frac{(Q-S)\,dS}{S(1+2S-4Q)} + \int_S^\infty \frac{N\,dS}{S(1+2S-4Q)}.$$

(*d*) Applying the equation of radiative transfer near the surface, we obtain the mass-luminosity-radius relation

$$A^{8\cdot5}N_s = \frac{3\kappa_0}{16\pi ac}\left(\frac{\mathfrak{R}}{\mu G}\right)^{7\cdot5}\left(\frac{1}{4\pi}\right)^2 L_s r_s^{1/2} M_s^{-5\cdot5}.$$

(*e*) Consider the equation of radiative transfer near the centre. This will only be valid in a case, such as this, when the radiative equations hold in the central regions. Then

$$\tfrac{4}{3}\,aT^3\frac{dT}{dr} = -\frac{\kappa_0 L\rho^2}{4\pi r^2 T^{3\cdot5}},$$

$$dP/dr = -GM\rho/r^2,$$

giving

$$N = \frac{P}{T}\frac{dT}{dP} = \frac{3\kappa_0 LP\rho}{16\pi acT^{7\cdot5}GM}.$$

Now let $S\to\infty$, $r\to 0$

$$N_c = \frac{3\kappa_0}{16\pi ac}\lim_{r_1\to 0}\left\{\frac{P\rho\int_0^{r_1}4\pi r^2\epsilon_0\rho^2T^{3\cdot5}\,dr}{T^{7\cdot5}G\int_0^{r_1}4\pi r^2\rho\,dr}\right\} = \frac{3\kappa_0\epsilon_0 P_c\rho_c^2}{16\pi acGT_c^4}.$$

These five relations can be shown to be independent, and thus leave us with one independent parameter, which is usually taken to be M_s.

There are in fact two other relations between our scale factors, but these may be easily shown to be consequences of the first five. The one relation is obtained by integrating the law of energy generation throughout the star to obtain a relation between L_s, T_c, ρ_c and r_s; the second is obtained by considering the expansion of $\ln S$.

If we now take M_s as a fundamental parameter, we have

$$r_s \propto 1 \text{ (constant)}$$
$$T_c \propto M_s$$
$$\rho_c \propto M_s$$
$$P_c \propto M_s^2$$
$$L_s \propto M_s^{5\cdot5}.$$

If we define the effective temperature T_e of the star by $L_s = \pi acT_e^4 r_s^2$, then

$$T_e \propto M_s^{1\cdot375}.$$

It is of interest to note that all stars given by this model possess the same radius regardless of their mass. This radius may be calculated in terms of the parameters of the solution.

Thus, having obtained the solution in h-variables, and being given the values of the three parameters, we may obtain the physical properties of a single infinity of stars each possessing the same radius.

6. *Results.*—

S	Q	N	r/r_s	M/M_s	P/P_c	ρ/ρ_c	T/T_c
0	0	0·2353	1	1	0	0	0
0·1	0·145	0·2447	0·455	0·857	0·015	0·049	0·309
0·2	0·186	0·2534	0·381	0·732	0·046	0·112	0·411
0·4	0·255	0·2708	0·310	0·533	0·121	0·230	0·526
0·6	0·323	0·2859	0·268	0·436	0·197	0·326	0·604
0·8	0·392	0·2945	0·241	0·354	0·264	0·403	0·655
1·0	0·462	0·3001	0·221	0·295	0·324	0·465	0·697
2·0	0·796	0·3181	0·165	0·148	0·527	0·652	0·808
5·0	1·797	0·3351	0·109	0·049	0·755	0·831	0·909
∞	∞	0·3496	0	0	1	1	1

We can compare this model with the Kramers' opacity convective core model (1). Three quantities which will give an idea of the relative properties of the two models are $\rho_{\text{mean}}/\rho_c$, measure of mass concentration; $\mathfrak{R}T_c r_s/\mu G M_s$, ratio of thermal energy per unit mass at centre of star to gravitational potential energy at the surface; and

$$\frac{B r_s^{0.5}}{\mu^{7.5} M_s^{5.5}} \left(\frac{\mathfrak{R}}{G}\right)^{7.5},$$

arising from the mass-luminosity-radius relation. It can be seen that the general properties of the two models are not greatly different, although in the radiative case the mass is rather more concentrated towards the centre. In particular, this model gives no great extension of radius, and is not a suitable model for red giants (6).

It is also of interest to compare the two radiative models with the same opacity law: Eddington's model with $\epsilon \propto T$ and Biermann's with $\epsilon = \epsilon_0$. In these cases radiation pressure is not neglected and the third parameter above loses its significance.

	$\frac{\mathfrak{R}T_c r_s}{\mu G M_s}$	$\frac{\rho_{\text{mean}}}{\rho_c}$	$\frac{B r_s^{0.5}}{\mu^{7.5} M_s^{5.5}} \left(\frac{\mathfrak{R}}{G}\right)^{7.5} \times 10^4$
Present paper	0·88	0·024	1·82
Bondi and Bondi (1)	0·90	0·027	1·68
Biermann (4)	0·67	0·0097	...
Eddington (5)	$0{\cdot}85\beta$	0·0184	...

We can also, on the assumption that the central law of energy generation holds up to the surface, calculate how much of the luminosity is generated interior to the final fit. This cannot be calculated to great accuracy as it involves performing a quadrature on quantities that have themselves been obtained by a quadrature on results of a numerical integration (i.e. r_s, T_c, ρ_c). However, over 90 per cent of the energy is certainly generated inside the fitting point.

In conclusion I would like to thank the Department of Scientific and Industrial Research for the award of a maintenance allowance, during the tenure of which this work was carried out.

Clare College,
Cambridge:
1951 *November* 18.

References

(1) C. M. and H. Bondi, *M.N.*, **109**, 62, 1949.
(2) T. G. Cowling, *M.N.*, **94**, 768, 1934.
(3) F. Hoyle and R. A. Lyttleton, *M.N.*, **102**, 177, 1942.
(4) L. Biermann, *Zs. f. Ap.*, **3**, 116, 1931.
(5) A. S. Eddington, *Internal Constitution of the Stars*, Cambridge, 1926.
(6) C. M. Bondi, *M.N.*, **110**, 276, 1950.

THE VELOCITY DISTRIBUTION OF SPORADIC METEORS
III. Calculation of the Theoretical Distributions

J. A. Clegg

(Communicated by A. C. B. Lovell)

(Received 1952 February 9)

Summary

The radio echo measurements of the velocities of sporadic meteors have been described in Parts I and II of this series of papers. To assess the significance of the results of these investigations it is necessary to establish a relationship between the true geocentric velocity distribution and that observed experimentally. This relationship depends essentially on the effective field of view of the radio echo apparatus, which is determined by the directional characteristics of the aerial. The present paper describes a general method of estimating the field of view of any aerial system, and hence of predicting the ratio of true to observed hourly numbers, for particles of different velocity and flight direction. It deals specifically with the measurements described in Parts I and II. Theoretical curves are derived, showing the velocity distributions that would be expected in these experiments, on the assumption that all sporadic meteors move in parabolic orbits and approach the Earth from random directions.

---

1. *Introduction.*—The development of the radio echo technique for the detection of meteor ionization in the atmosphere has provided new methods of velocity determination; and extensive radio measurements of the geocentric velocities of sporadic meteors have recently been made by McKinley* and Miss Almond, Davies and Lovell.† The primary object of these investigations was to find what proportion of sporadic meteors are moving in hyperbolic orbits round the Sun; and in order to interpret the results it is necessary to establish a relationship between the measured velocity distribution and the true heliocentric distribution for meteors detected by radio methods. This presents certain fundamental difficulties, which arise from the incomplete understanding of the processes underlying the reflection of radio waves from meteor trails.‡ Nevertheless, in view of the significance of the foregoing experiments, it appears appropriate to review the factors which determine the field of view of a meteor echo apparatus in the light of contemporary theory, and to attempt to form some estimate of the observed velocity distribution that would be expected for different heliocentric velocities and orbital motions.

In this paper the problem is resolved into three parts which may be summarized as follows:—

(i) It is assumed that all sporadic meteors move in parabolic orbits, and approach the Earth from random heliocentric directions. The radiant concentration and velocity are expressed as functions of the elongation from the

* McKinley, D. W. R., *Astrophys. J.*, **113**, 225, 1951.

† Almond, M., Davies, J. G. and Lovell, A. C. B., *M.N.*, **111**, 585, 1951; **112**, 21, 1952. These are papers I and II of this series.

‡ Herlofson, N., *Ark. Fys.*, **3**, 247, 1951.

apex of the Earth's way. This particular distribution is chosen because it provides a convenient standard of reference with which experimental results can most readily be compared.

(ii) Owing to the condition of broadside reflection of radio waves from meteor trails* the apparatus will only detect meteors whose radiants lie in a limited area of the sky. This area is found from the directional characteristics of the aerial, and is divided into a number of elementary segments, which subtend small solid angles at the observing station, so that the meteors emanating from any one have substantially the same velocity and flight direction, and each segment can be treated as the point radiant of a homogeneous meteor stream. The velocities and relative numbers of meteors from the different radiants can be found, for any position of the apex, from (i).

(iii) The probability that a meteor will be detected depends on the altitude and azimuth of its radiant, as well as on the polar diagram of the aerial. A method of finding the field of view of the apparatus, for any radiant position, is described, and is used to determine the relative probabilities of detection for particles emanating from the different segments. The observed velocity distribution can then be predicted directly.

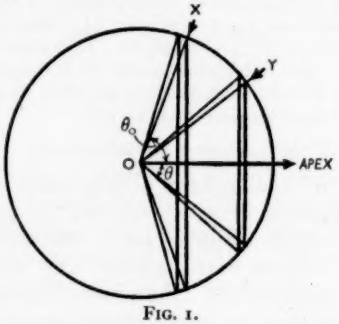

FIG. 1.

Although the treatment outlined in (iii) is perfectly general, and can be extended to the determination of the true hourly numbers and mass distribution of meteors, the present paper deals specifically with the velocity measurements made by Miss Almond, Davies and Lovell.† All calculations are based on the parameters of their apparatus, and theoretical velocity distributions are derived for comparison with their apex and antapex experiments.

2. *The radiants and geocentric velocities of sporadic meteors.*—A particular distribution will be considered, in which all sporadic meteors are assumed to travel with the same heliocentric velocity, and to fall on the Earth from random heliocentric directions. Because of the Earth's orbital motion, their radiants will be concentrated towards the apex of the Earth's way, and those emanating from radiants close to the apex will have higher velocities. Thus, for a particle approaching the Earth O (Fig. 1) from a heliocentric direction X, at elongation θ_0 from the apex, the corresponding geocentric direction of approach will be Y. If the orbital velocities of the Earth and the meteors are respectively v and $r_0 v$ it can be shown that the elongation θ of Y from the apex is given by

$$\sin\theta = (r_0 \sin\theta_0)(1 + r_0^2 + 2r_0\cos\theta_0)^{-1/2} \qquad (1)$$

* Hey, J. S. and Stewart, G. S., *Proc. Phys. Soc.*, **59**, 858, 1947.
† Prrts I and II, *loc. cit.*

while the geocentric velocity is rv, where

$$r=(r_0^2-1+\cos^2\theta)^{1/2}+\cos\theta. \qquad (2)$$

If the density of particles near the Earth is $4\pi N$ per km^3, the number approaching per second from heliocentric directions between θ_0 and $\theta_0+d\theta_0$ is $2\pi Nrv\sin\theta_0\,d\theta_0$. The corresponding geocentric flight directions lie between θ and $\theta+d\theta$ and are concentrated within a solid angle $2\pi\sin\theta\,d\theta$. The number whose radiants lie within a small solid angle $d\omega$ at elongation θ to the apex is therefore

$$N_\theta\,d\omega=Nrv\,d\omega\,(\sin\theta_0/\sin\theta)(d\theta_0/d\theta).$$

After evaluating $d\theta_0/d\theta$ from (1) and eliminating θ_0 and θ this becomes

$$N_\theta/N=2r^4v/r_0(r_0^2+r^2-1). \qquad (3)$$

The foregoing formulae take no account of the acceleration and change of flight direction of the meteors due to the Earth's gravitational attraction. The latter effect is small, and for the present purpose the consequent modification to (3) can be neglected; but a correction must be made to (2), the true geocentric velocity u being given by

$$u^2=r^2v^2+2\rho g, \qquad (4)$$

where ρ is the radius of the Earth, and g the acceleration due to gravity at the Earth's surface.

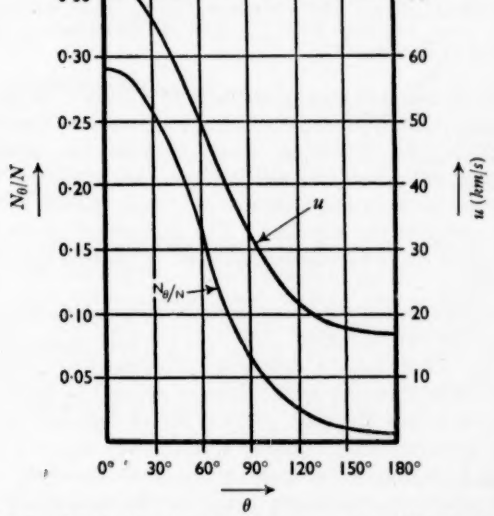

FIG. 2.—*$N\theta/N$ and u plotted as functions of θ, for meteors approaching the Earth from random heliocentric directions, with parabolic velocities.*

In interpreting the results of experimental measurements, it is most useful to compare the observed distribution with that obtained theoretically for meteors moving in parabolic orbits ($r_0=\sqrt{2}$). Fig. 2 shows values of u and of N_θ/N for such a distribution, plotted as functions of θ for a mean value of v equal to 29·8 km/s.

3. *The directional characteristics of the aerial.*—In the experiments of Miss Almond, Davies and Lovell*, a beamed aerial was directed at low

* *Loc. cit.*

elevation on an easterly bearing. This is indicated in Fig. 3, which shows the celestial sphere drawn for the observing station at O. The axis of the beam is represented by OX and the cone aOb represents the limits of the main lobe of the diffraction pattern, the side lobes of which were small and may be ignored. Radio waves of the wave-lengths employed (4·17 and 8·13 metres) suffer specular reflection from meteor trails*, so that the observations were restricted to meteors whose radiants lay in the strip of the sky enclosed by the small circle arcs xzy, x′z′y′, and lying symmetrically about the great semi-circle Sz_0N, which has X as its pole. Measurements were carried out at times when the apex (or the antapex) A was crossing this strip.

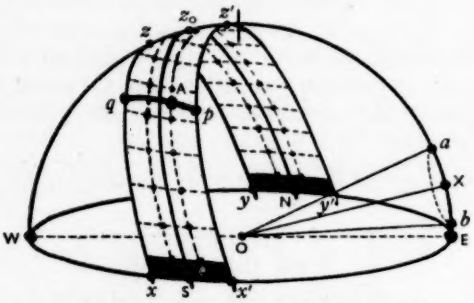

FIG. 3.—*Segments of celestial sphere representing radiants within the aerial coverage. The shaded areas close to xx′, yy′, which are 5° in vertical width, contribute a negligible number of meteors, and have been ignored.*

To find the relative numbers of meteors of different velocities which enter the aerial coverage, the strip can be divided into a number of elementary segments, in the way indicated by the dotted lines. If these are sufficiently small, the meteors emanating from any one will have the same velocity and direction of flight, and they can be treated as members of a single shower with a point radiant situated in the centre of the segment. The elongations of the centre points of the segments from A can be measured, and the values of u and N_θ/N found from the curves in Fig. 2.

Each of the apex and antapex experiments referred to above extended over several months, and in computing N_θ/N and u mean values were taken for the declination of A. Observations were made over periods of approximately two hours, during which A moved some distance across the strip via the path pq, and a mean position was assumed. It was found sufficient to divide the strip xzy, x′z′y′, into 45 segments of equal area, in the way shown in the figure. The elongation θ of the centre point of each segment from the apex, and the altitude β and azimuth χ relative to the direction OE could conveniently be measured by constructing a model of Fig. 3 on a sphere.

4. *The effective collecting area of the radio echo apparatus.*—The position of the reflecting point of a meteor trail in the aerial coverage depends on the altitude and azimuth of the radiant, and for meteors emanating from different segments in Fig. 3 there will be different probabilities of detection by the apparatus. To determine the relationship between the true hourly numbers of meteors from the

* Hey, J. S. and Stewart, G. S., *loc. cit.* Lovell, A. C. B., Banwell, C. J. and Clegg, J. A., *M.N.*, **107**, 164, 1947.

various segments, and the corresponding radio echo rates, the field of view or effective collecting area of the apparatus must be found for the individual radiant positions. A method of estimating the effective collecting area of a radio echo apparatus for meteors of a single shower has been described by Clegg* and will be considered here in greater detail.

(i) *General considerations.*—For meteors of a single stream, or from a single segment of Fig. 3, the radio echoes are all returned from the neighbourhood of a plane surface which passes through the observing station and is perpendicular to the direction of the radiant. This is indicated in Fig. 4, which shows the station at O and the curved surface OABC of the Earth. The radiant is in the

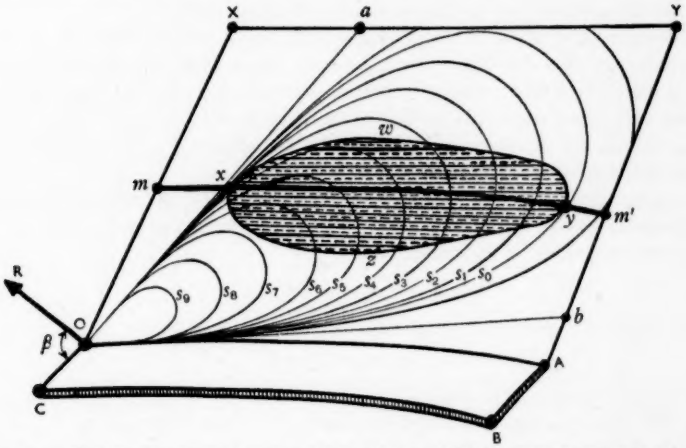

FIG. 4.—*Sensitivity contours drawn on the echo plane. The lines* Oa, Ob *indicate the limits of the aerial coverage and the shaded area represents the collecting area of the apparatus for meteors of a given mass group.*

direction OR, at altitude β, so that the echo plane OXYA is inclined at an angle $(90^\circ - \beta)$ to the horizontal. The diffraction pattern of the aerial can be represented by a series of contours drawn on this plane, which are indicated by the curved lines. The contours correspond to different values $s_0, s_1, \ldots s_q, \ldots$ of the overall sensitivity of the apparatus, so that, for a trail whose reflecting point lies on the contour s_p and which has an equivalent scattering diameter α at this point†, the amplitude A of the echo is given by

$$A = ks_p\alpha, \tag{5}$$

where k is a constant depending on the parameters of the apparatus. For the present purpose it is convenient to choose the sensitivity values in such a way that $s_{p+1} = \gamma s_p$, where γ is a numerical factor somewhat greater than unity, its exact value being determined by the required contour spacing. A method of constructing these contours for any position of the radiant is described in Appendix I.

As the velocity and flight direction are the same for meteors from the same segment, it can be assumed that particles of the same initial mass produce identical

* Clegg, J. A., *Phil. Mag.*, **39**, 577, 1948.

† The equivalent scattering diameter is defined as the ratio of the energy scattered by unit length of column to the modulus of the Poynting vector of the incident radiation.

trails. Consider meteors of a certain mass group which produce maximum electron density, corresponding to an equivalent scattering diameter α_0, at a height mm′ in the atmosphere, and assume that they are just detectable at this height out to the points x, y on the contour s_0. Particles of the same mass which cross the echo plane at points closer to the axis of the beam, and therefore cut contours of higher value, will be detectable for some distance above and below mm′, and we can define a curve xwyz, inside which meteors of this class will be observed. Similar collecting areas bounded laterally by other contours can be defined for mass groups whose scattering diameters, at the points of maximum electron density, differ from α_0 by factors of $\gamma^{\pm p}$ where p is an integer. The conditions which determine the shapes of these areas, and the method adopted for their delineation, are discussed in the following section.

Although an infinity of areas larger than xwyz can be defined, it is found experimentally that for any radiant position there is a well-defined range limit beyond which no echoes appear.* The largest area that need be drawn is therefore the one extending outwards to this distance from the station. The value of α_0 corresponding to this area (which will be designated α_M) can be found from the parameters of the apparatus.

Suppose now that the number of meteors falling on the Earth from the lth segment, whose trails have scattering diameters between α_0 and $\alpha_0+d\alpha_0$ at the points of maximum ionization, is

$$dN_{\alpha_0,l}=\eta_l F(\alpha_0)\,d\alpha_0, \tag{6}$$

where $F(\alpha_0)$ is a predetermined function and

$$\eta_l \propto (N_\theta/N)\Delta S, \tag{7}$$

ΔS being the area of the segment.

It will be assumed that this law holds up to a value of α_0 equal to α_M. A family of curves such as xwyz, corresponding to maximum scattering diameters α_M, α_M/γ, . . . α_M/γ^p . . . , can be constructed for any radiant position, and their areas a_0, a_1, . . . a_p, . . . can be measured. There will in general be a finite number n of such curves, the smallest having an area a_{n-1} (i.e. the area a_n corresponding to α_M/γ^n being zero).

Consider first the trails whose maximum scattering areas lie between α_M and α_M/γ. The largest of these will be seen whenever they pass through the area a_0, while the smallest will only be detected when they pass inside a_1. If a_0 and a_1 differ by a sufficiently small factor, the effective collecting area for meteors of this group is therefore approximately equal to $\frac{1}{2}(a_0+a_1)$ and the total hourly number detected will be

$$\tfrac{1}{2}(a_0+a_1)\eta_l\int_{\alpha_M/\gamma}^{\alpha_M} F(\alpha_0)\,d\alpha_0.$$

Similar expressions can be obtained for other groups, and the total echo rate N_l for meteors from this particular segment is found to be

$$N_l=\tfrac{1}{2}\eta_l\sum_{p=0}^{n}(a_{p-1}+a_p)\int_{\alpha_M/\gamma^p}^{\alpha_M/\gamma^{p-1}} F(\alpha_0)\,d\alpha_0 \text{ per hour.} \tag{8}$$

Thus if $F(\alpha_0)$ is known, and if the collecting areas can be accurately constructed, a relationship can be established between the factor η_l and the observed hourly numbers.

* Clegg, J. A., *loc. cit.*

(ii) *Construction of the collecting areas on the echo plane.*—The shapes and sizes of the collecting areas depend on:

(*a*) the relationship between the equivalent scattering diameter of the trail and the electron density at the reflecting point, and

(*b*) the way in which the electron density varies along the trail.

These factors will be considered separately.

(*a*) It will be assumed that the electrons in the trail behave as individual scatterers of radiation.* The scattering area of the column is then directly proportional to the number of electrons present; and α can be taken to represent the electron line density at the reflecting point, the constant of proportionality being included in the factor k of equation (5).†

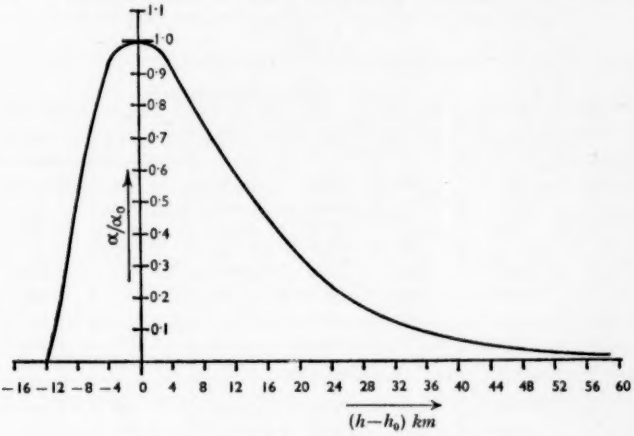

FIG. 5.—*Theoretical ionization curve for a meteor.*

(*b*) The experimental and theoretical data concerning the evaporation and ionization of meteors have been reviewed by Herlofson‡, who concludes that the relationship between the electron line density α in the trail, and the height h in the atmosphere, is of the form

$$\alpha = \tfrac{9}{4}\alpha_0 \left\{ 1 - \tfrac{1}{3} \exp\left(\frac{h_0 - h}{H}\right) \right\}^2 \exp\left(\frac{h_0 - h}{H}\right), \qquad (9)$$

where H is the scale height and h_0 is the height of maximum ionization. The value of α_0 is given by the proportionality

$$\alpha_0 \propto m f(u) \sin \beta, \qquad (10)$$

where m and u are the initial mass and velocity of the meteor and β is the altitude of the radiant. The dependence of h_0 on m, u and β will not be taken into account, as the errors thereby introduced in computing the field of view of the apparatus are small in comparison with those discussed in Section 6 below. The value of α/α_0 is plotted as a function of $(h - h_0)$ in Fig. 5, for a scale height of 10 km.

* Blackett, P. M. S. and Lovell, A. C. B., *Proc. Roy. Soc.* A, **177**, 183, 1941.

† Lovell, A. C. B., *Nature*, **160**, 372, 1947. Lovell, A. C. B. and Clegg, J. A., *Proc. Phys. Soc.*, **60**, 491, 1948.

‡ Herlofson, N., *Phys. Soc., Rep. Prog. Phys.*, **11**, 444, 1946–1947.

This curve can be used directly to find the overall collecting area of the apparatus for any given radiant position. Consider, for example, the delineation of the area xwyz of Fig. 4. A plan of the echo plane, showing the configuration of the sensitivity contours, is first constructed in the way described in Appendix I, and the position of the line mm′, corresponding to the height of maximum ionization, is estimated. The area extends laterally to the points x, y, where this line cuts the contour s_0, and its boundary cuts the inner contours at points where the electron density has fallen by successive multiples of the chosen factor γ. The vertical distances of these points above and below mm′ can be read off from Fig. 5. To find the corresponding distances along the echo plane, which is inclined at an angle β to the vertical, we must multiply by sec β. Corresponding areas for meteors of other mass groups can be drawn in a similar manner.

TABLE I

χ	β	Collecting areas in km²						
		$s_6=2{\cdot}07$	$s_5=1{\cdot}44$	$s_4=1{\cdot}00$	$s_3=0{\cdot}69$	$s_2=0{\cdot}48$	$s_1=0{\cdot}34$	$s_0=0{\cdot}23$
°	°							
83·5	10		386	1 350	2 580	3 800	5 150	6 450
92	10	645	1 820	2 900	4 030	5 150	6 540	8 050
100	10	65	965	1 830	2 990	4 350	5 860	7 080
85	20		370	1 450	2 580	3 540	5 060	7 250
93·5	20	645	1 770	3 310	4 760	6 120	7 020	9 170
102·5	20	166	677	1 925	3 060	4 180	5 320	6 830
86·5	30		96·5	1 350	2 580	4 030	5 320	6 920
96	30	680	2 160	3 640	4 990	5 630	7 730	9 170
105·5	30	322	1 060	2 060	3 280	4 180	5 320	6 550
88	40			370	1 930	3 600	5 310	7 570
98·5	40	805	2 250	3 600	5 220	6 920	8 370	9 660
109·5	40	129	1 130	2 090	3 150	4 180	5 410	6 700
90	50				1 290	3 220	5 480	7 570
102	50	900	2 250	3 700	5 960	7 510	9 350	11 920
116	50		935	1 770	2 740	3 860	5 320	6 510
91·5	60					645	2 570	5 800
108	60	645	2 540	4 570	6 770	9 180	10 950	13 350
126	60	481	1 450	2 800	3 770	5 080	6 450	7 950
94	70							
119	70	805	3 000	5 800	8 220	10 700	13 700	16 730
154	70		741	2 090	3 280	4 770	5 800	7 410
100·5	80							
180	80	805	3 220	8 050	11 300	14 500	19 300	23 400

Collecting areas, corresponding to the various segments shown in Fig. 3, have been constructed in this way for the apparatus used by Miss Almond, Davies and Lovell.*

These areas, for the aerial used in the second apex (1949) and the antapex (1950) experiments†, are given in Table I. The two left-hand columns indicate the altitude β and the azimuth χ of the centre points of the segments relative to the axis of the aerial beam. Other columns show the measured areas for values of the limiting sensitivity contour differing by factors of $s=1{\cdot}44$. It was found

* *Loc. cit.*

† Almond, Davies and Lovell, Part I.

experimentally that the most distant meteors detected by the apparatus had their reflecting points on the contour $s=0{\cdot}23$, and the largest area in each case has been taken as the one extending outwards to this contour. Of the total of 45 segments, all except the one nearest to the zenith were situated symmetrically in pairs, on either side of the axis of the beam, so that only 23 radiant positions were required.

5. *The velocity distribution.*—In order to use the set of collecting areas of Table I to find the numbers of meteors from each segment detected by the apparatus, the functions $F(\alpha_0)$ and $f(u)\sin\beta$ of (6) and (10) must be known.

$F(\alpha_0)$ depends on the mass distribution of the meteors. It is believed* that the absolute numbers of sporadic meteors vary inversely as the mass m and, since $m \propto \alpha_0$, we may take $F(\alpha_0)$ to be α_0^{-1}. Substituting this value in (8) we have, for the number N_l of meteors emanating from the lth segment,

$$N_l = \tfrac{1}{2}\eta_l \ln \gamma \sum_{p=1}^{n} (a_{p-1} + a_p). \qquad (11)$$

The experiments of Miss Almond, Davies and Lovell indicated that $f(u)=u^{\sigma}$, where $\sigma \simeq 1$.† It may be assumed, therefore, that the meteors detected out to the farthest contour $s_0=0{\cdot}23$ were those of such a velocity and radiant altitude that $u\sin\beta$ had its maximum value $(u\sin\beta)_M$. In the apex experiments this condition was fulfilled for particles emanating from the segment at an altitude of 70°, while for the antapex experiment the corresponding altitude was 35°. In the case of a segment for which $u\sin\beta$ is lower than the maximum value by a factor γ^{-p}, where p is a positive integer, the outermost collecting area must be taken as the one extending outwards to the contour $s_p=0{\cdot}23\,\gamma^p$. For segments for which $u\sin\beta$ does not differ from $(u\sin\beta)_M$ by an integral power of γ the areas can be estimated by interpolation. After correcting the figures of Table I in this way for each radiant position in turn, the appropriate values of $\sum_{p=1}^{n}(a_{p-1}+a_p)$ can be found for the various segments. Since η is known from (7) the relative values of N_l can be determined from (11) and, using (2), can be plotted as a function of velocity.

Theoretical velocity distributions obtained by this method are shown in Fig. 6.

6. *Accuracy.*—The greatest uncertainty in these calculations arises from the present incomplete understanding of the scattering processes which occur when radio waves are incident on a meteor trail. It has been pointed out by Herlofson‡ that if the volume density of electrons in the ionized column is of the order of the critical density for the wave frequency employed, plasma resonance may occur. In this circumstance the echo amplitude will be increased, and the effective echoing area will no longer be linearly related to the electron line density. Such resonance phenomena have been observed by Clegg and Closs.§

It is difficult to assess the effect of plasma resonance on the field of view of the apparatus, as its magnitude depends on the sharpness of the boundary of the ionized column, but recent estimates, based on theoretical and experimental work‖, indicate that it is unlikely to change the collecting areas by a factor

* Fletcher Watson, *Between the Planets*, 1941 (Philadelphia : Blakiston and Co.) gives a review of the evidence for this conclusion.

† The experimental evidence for this is outlined in Appendix II.

‡ Herlofson, N., *Ark. Fys.*, **3**, 247, 1951.

§ Clegg, J. A. and Closs, R. L., *Proc. Phys. Soc.* B, **64**, 718, 1951.

‖ Closs, R. L. and Kaiser, T. R., *Phil. Mag.*, **43**, 1, 1952.

greater than 1·2. It therefore appears adequate, until further data are available, to use the simple scattering formula for their delineation. It is interesting to note, however, that as plasma resonance is only produced by the component of

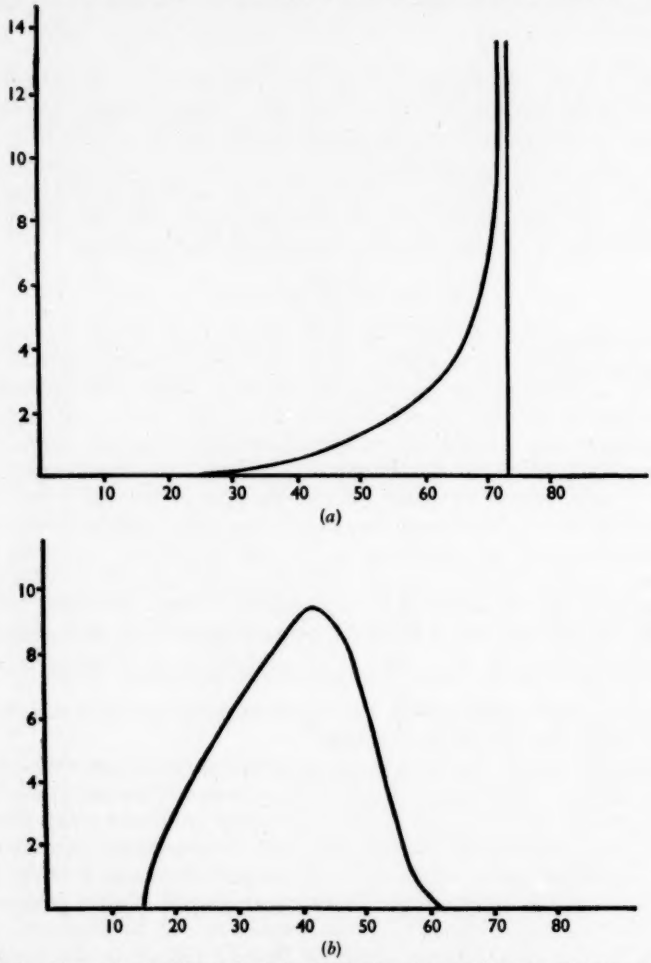

FIG. 6.—*Curves showing observed velocity distributions that would be expected during the experiments of Almond, Davies and Lovell, assuming that all sporadic meteors travel with parabolic velocities and approach the Earth from random directions.*

Ordinates : Relative numbers.
Abscissae : Velocity (km/s).

(*a*) *Distribution for second apex experiment* (1949).
(*b*) *Distribution for antapex experiment* (1950).

the incident wave polarized perpendicularly to the trail, and as the aerials used for velocity measurements were horizontally polarized, this phenomenon would tend to increase the probability of detecting meteors from radiants close to the zenith. In the case of the apex experiments, such meteors would have relatively

high velocities, so that the peak of the curve in Fig. 6(*a*) would be shifted to the right. In Fig. 6(*b*), on the other hand, the peak would be moved in the direction of lower velocity.

The observed velocity distribution also depends critically on $f(u)$ of (10). The choice of u^{σ}, where $\sigma = 1$, is purely empirical and is not in agreement with Öpik's theory of meteor ionization, which predicts an exponent of 2·5.* But if the value of σ is increased, greater weight is given to high velocities, and the maxima of the curves of Fig. 6 are shifted to the right. This shift is very pronounced, even when σ is increased to 1·5; and if a value of 2·5 is chosen, the curve of Fig. 6(*a*) shows approximately 95 per cent of measured velocities in excess of 50 km/s.

On the other hand, it is difficult on theoretical grounds to justify the choice of a value less than unity, which would shift the predicted distributions in the opposite direction. The discrepancy between the experimental value for σ and that obtained by Öpik† may partly be accounted for by destructive interference across the diameter of the column, which reduces the apparent number of electrons in the trail. The change in the scattering area due to this effect will be greater for faster meteors, which produce columns of greater width.

7. *Acknowledgments.*—The author is indebted to Professor A. C. B. Lovell, Director of the Jodrell Bank Experimental Station, and to Dr J. G. Davies for many valuable discussions and for helpful criticism. He also wishes to thank Miss M. Almond, who was responsible for a considerable part of the computational work required for the derivation of the theoretical velocity distribution curves.

University of Manchester,
Jodrell Bank Experimental Station,
Cheshire:
1952 *February* 8.

APPENDIX I

In constructing the collecting areas of the aerial, contours corresponding to different values of the sensitivity must be delineated on the echo plane. This

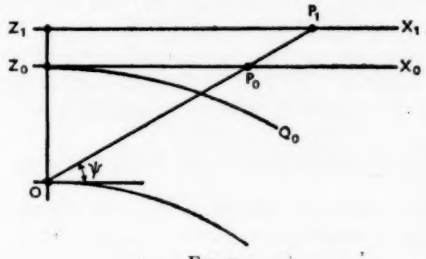

FIG. 7.

can conveniently be done for any radiant position, by a geometrical construction. The contours are first drawn on a horizontal plane Z_0X_0 (Fig. 7) at an arbitrary height OZ_0 above the station at O. They are formed by the intersection of this plane with a set of equisensitivity surfaces, defined by the general equation

$$G(\phi, \psi)/R^{3/2} = s, \qquad (12)$$

* Öpik, E. J., *Tartu Obs. Pub.*, **30**, No. 5, 1, 1940; *The Observatory*, **68**, 228, 1948.
† Öpik, E. J., *loc. cit.*

where G is the absolute power gain of the aerial, and R, ϕ and ψ are the range, azimuth and altitude measured from the station.* The height OZ_0 may be taken as the unit of distance, so that the distances of any point P_0 in the plane from O and Z_0 are given respectively by

$$R = \operatorname{cosec} \psi; \quad R_0 = \cot \psi. \tag{13}$$

On combining this value of R with (12), we have for the equation of the contours

$$G(\phi, \psi) \sin^{3/2} \psi = s. \tag{14}$$

The contour $s = 1$ therefore corresponds to the sensitivity at a point at unit height situated vertically above an isotropic radiator.

The gain function $G(\phi, \psi)$ is usually determined experimentally in the way indicated in Fig. 8, which shows the station at O and the axis of the beam OX.

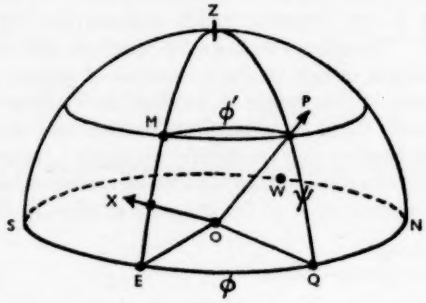

FIG. 8.

The horizontal and vertical polar diagrams $H(\phi)$ and $V(\psi)$ are found by measuring the relative intensity of radiation as a function of angular distance from E, round the horizon circle EQNWS and the meridian EZ respectively. The absolute power gain G_0 in the direction OX can then be determined. For the aerials used during the velocity measurements, it can be shown that the effective gain in a direction OP with coordinates (ϕ, ψ) can be expressed as $G_0 V(\psi) H(\phi')$, where the angle ϕ' is measured along the great circle arc PM and is given by

$$\sin \phi' = \sin \phi \cos \psi = R_0 (1 + R_0^2)^{-1/2} \sin \phi. \tag{15}$$

After introducing this value for $G(\phi, \psi)$ in (14), we define $G_0 V(\psi) \sin^{3/2} \psi$ as a function $W(R_0)$ of R_0, obtaining,

$$W(R_0) H(\phi') = s. \tag{16}$$

The functions $W(R_0)$ and $H(\phi')$ can be plotted graphically for any particular aerial. To draw the sensitivity contour for any chosen value of s, the values of $H(\phi')$ corresponding to different values of $W(R_0)$ are obtained from (16), and the appropriate values of ϕ' and R_0 are read off from the graphs. The true azimuth ϕ is then found in each case from (15) and the contour is constructed by plotting R_0 against ϕ.

* Clegg, J. A., *loc. cit.*

A typical set of sensitivity contours $s_0, s_1, \ldots s_6$ drawn in this way, for a beamed aerial directed at low elevation, are shown in Fig. 9 (*a*). The point Z_0 is situated vertically above the station, and the heavy line OW represents the horizontal direction of the beam axis. For a radiant in the azimuthal direction Z_0R from the station, and at altitude β, the echo plane cuts the horizontal surface, on which contours are drawn, in a straight line X_0Y_0, which is perpendicular to Z_0R, and intersects the contours at points $P_0, P_0' \ldots, Q_0, Q_0', \ldots$. Since the height of the contour plane is taken as the unit of distance, it follows that $Z_0S = \tan \beta$.

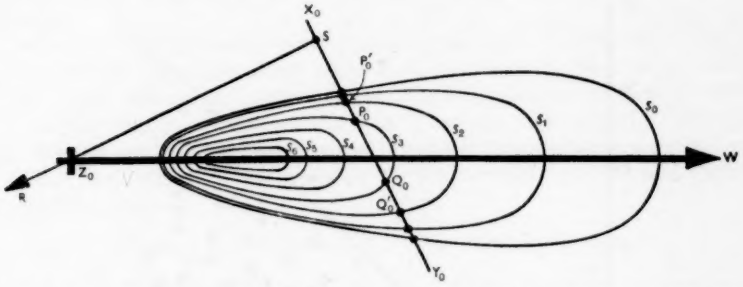

FIG. 9 (*a*).—*Typical map of sensitivity contours, on horizontal plane at arbitrary height above the observing station, for beamed aerial directed at low elevation in azimuthal direction* Z_0W. X_0Y_0 *represents intersection of echo plane with this surface for radiant in azimuthal direction* Z_0R *and at altitude* $\tan^{-1} Z_0S$.

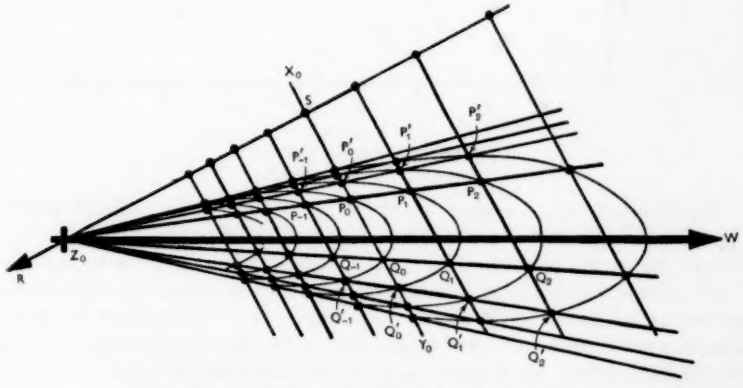

FIG. 9 (*b*).—*Sensitivity contours drawn in plan on echo plane. The lines* Z_0S, Z_0W, *and* X_0Y_0 *correspond to those in Fig.* 9 (*a*).

A map such as this can be used to delineate the sensitivity contours on each echo plane for any radiant position. Let the sensitivity values be chosen so that $s_{p+1} = \gamma s_p$, and consider a second horizontal plane Z_1X_1 (Fig. 7) at a height OZ_1 equal to $\gamma^{2/3} \times OZ_0$. If the sensitivity at the point P_0 in the lower plane is s_p, and if OP_0 be produced to P_1 in the higher plane, then according to (12), since P_0 and P_1 are at the same azimuth and altitude from the station, the sensitivity at P_1 will be

$$s_p' = (OP_0/OP_1)^{3/2} s_p = \gamma^{-1} s_p = s_{p-1}.$$

Thus the values of s corresponding to all such pairs of points as P_0 and P_1 differ by the same numerical factor γ. It follows that if the contours of Fig. 9(*a*) are reproduced for the new plane, they will have the same form, but that each will be increased in scale by a factor $\gamma^{2/3}$, and will have a value corresponding to that of the next outermost contour on the surface below. This argument can be extended and in general, for a horizontal surface at a height $\gamma^{\pm 2/3p}$, where p is an integer, the scale of the contours is changed by a factor $\gamma^{\pm 2/3p}$, and the contour s_q becomes $s_{q \mp p}$.

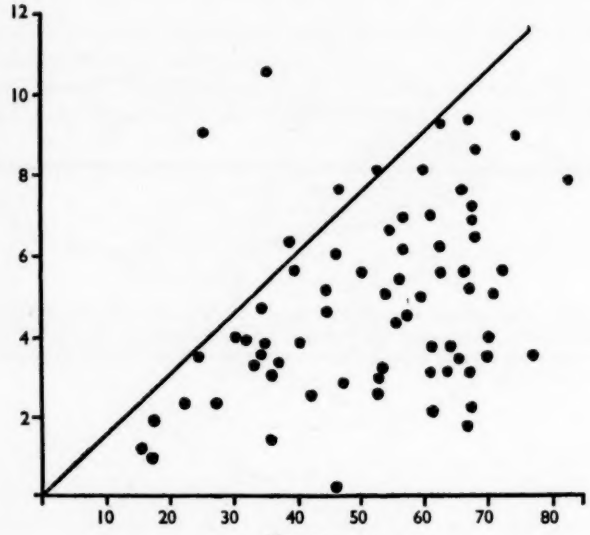

FIG. 10.
Ordinates : Relative values of α_0.
Abscissae : Velocity (km/s).

To delineate the contours on the echo plane for the radiant position of Fig. 9(*a*), the procedure indicated in Fig. 9(*b*) is therefore adopted. A series of lines are drawn parallel to X_0Y_0, at distances from Z_0 equal to $Z_0S \times \gamma^{\pm 2/3p}$. These represent in plan the intersections of the echo plane with other horizontal surfaces at heights of $\gamma^{\pm 2/3p}$ above the station. It is evident that the sensitivity value at a point such as P_0' will exceed that at the corresponding point P_1' on the next higher surface by a factor γ, and will therefore be equal to that at P_1. The curves of equisensitivity on the skew plane are therefore constructed by joining each of the intersection points to the next outermost point on the surface below.

Fig. 9(*b*) evidently represents a horizontal projection of the echo plane, and to obtain a plan of the contours, distances in the direction Z_0S must be increased by a factor cosec β.

APPENDIX II

The function $f(u)$ of the proportionality (10) was determined in the following way. It was found, during the apex experiments, that meteors of high velocity were detected out to greater range, and this was interpreted as evidence that

more intense ionization is produced by faster particles. The mean height of maximum ionization of the meteors was taken to be 95 km *, and a map of the contours on the 95 km surface, Z_0Q_0 (Fig. 7), was drawn by a construction similar to that described in Appendix I. It was assumed that all echoes are returned from points close to the central axis of the contours, so that by measuring the range, a sensitivity value s could be ascribed to each. The measured echo amplitude was then divided by s to find the scattering diameter α_0 of the column. The results obtained during the second apex experiment are shown in Fig. 10. Relative values of α_0 are shown as ordinates, and the measured velocities as abscissae.

Individual echoes are indicated by separate points on the diagram. Although the assumption that echoes occur close to the centre of the beam is not valid in all cases, it can be assumed to hold for those showing the largest scattering diameter. It is evident from the diagram that for such echoes, with only two exceptions, there is a well-marked linear relationship between the maximum observed value of α_0 and the velocity u, as indicated by the straight line. It was therefore assumed that $f(u) \propto u^{\sigma}$, where $\sigma = 1$.

* Clegg, J. A. and Davidson, I. A., *Phil. Mag.*, **41**, 77, 1950.

MOTIONS IN THE SUN AT THE PHOTOSPHERIC LEVEL
I. METHODS

H. H. Plaskett

(Received 1952 May 1)

Summary

Methods for determining sight-line velocities at specified points on the solar photosphere are described. The portion of the solar image, the spectrum of which is to be photographed, is observed with an angular magnification of 390 times. The image may be guided, independently of the telescopic controls, and the photograph taken at the instant of best seeing. The spectra are measured against a centre spectrum by Evershed's positive-on-negative method on a self-recording micrometer; possible line displacements due to the asymmetry of the horizontal apparatus function of the spectroscope are thus eliminated. An equation of condition between the three rectangular velocity components of motion in the photosphere and the measured sight-line velocity is derived.

Introduction.—The deepest layers which are observationally accessible in the Sun lie in the photosphere. It is these layers which transform by absorption and re-emission the radiant energy of the Sun in the optical range, that is, some 67 per cent of the total solar output. By contrast, the chromosphere and the corona, in spite of the many fascinating and difficult problems which they present, transform solar radiation primarily in the radio range, or only a few ten-millionths of the total energy output. It is therefore to the photosphere that we must look for information about the energetically significant physics of the Sun.

The photosphere is normally considered to be in a steady state with energy transport effected wholly by radiation. On this hypothesis there is a constant net flux of radiation through the photosphere, isothermal and isobaric surfaces are level surfaces, and temperature and pressure increase monotonically with optical depth. Such a stratification is mechanically stable if,

$$\frac{d\ln T}{d\ln p} < \frac{\gamma-1}{\gamma} \qquad (=0{\cdot}4 \text{ for a monatomic gas}),$$

where γ is the ratio of specific heats. The temperature in a photosphere in radiative equilibrium is known as a function of optical depth, and the pressure as a function of optical depth may be found once the mass coefficient of continuous absorption is known. Either on the hypothesis of low hydrogen abundance and continuous absorption by the photo-ionization of the metals, or on the hypothesis of high hydrogen abundance and absorption by the photo-ionization of the negative hydrogen ions, it is found that below an optical depth of unity a photosphere in radiative equilibrium would be unstable and would tend to turn itself over. This tendency would be accentuated at still greater depths where, because of the ionization of hydrogen, the value of $(\gamma-1)/\gamma$ is less than its monatomic value of 0·4. A photosphere, stratified as in radiative equilibrium, would thus convert some of its potential energy to kinetic, and the dissipation of this kinetic

energy to heat by viscous forces would itself make some contribution to the energy transport. In the actual photosphere, as opposed to a hypothetical photosphere in radiative equilibrium, some account must be taken of the internal energy carried by moving photospheric matter and of the degradation of its kinetic energy to heat, as well as of the energy transport by radiation. The first step towards this end is a more detailed knowledge of the motions of photospheric matter.

The velocity component in the sight-line of photospheric matter moving at a particular point can be found from the Doppler displacement of lines in the spectrum of that point. If, however, accurate sight-line velocities, referable to specified points in the photosphere, are to be obtained, certain precautions must be adopted. It is the purpose of the present paper to give some account of the methods of observation, measurement and reduction which are common to a number of investigations now in progress at Oxford. The results of these investigations will, it is hoped, be communicated to the Society under the general title of "Motions in the Sun at the photospheric level".

1. *Methods of observation.*—No very fine-scale analysis of motions in the solar photosphere is to be expected from measurements of Doppler displacements. A single height in a spectrum of a portion of the photosphere has thrown on it light from more distant regions, to some extent because of the vertical apparatus function of the spectroscope and the aberrations of the telescope, both of which are determinable so that their effect may be eliminated, but overwhelmingly because of atmospheric tremor and bad definition. Nominally a height of 0·1 mm in an Oxford spectrum corresponds to some 750 km on the photosphere, but under bad conditions of seeing and atmospheric tremor light from many times this distance is superposed on the 0·1 mm. To minimize these effects it is essential to have some means of making exposures of photospheric spectra only at those times when the solar definition is as perfect as possible.

For this purpose an instrument known as a Guiding Plate, illustrated in Plate 4, 1, has been in use since 1947. Its essential feature is the glass cube of 5·1 cm edge shown at A. This consists of two 90°-prisms cemented on their hypotenuse faces with a cement, the refractive index of which is very nearly that of the glass. This cube transmits some 97 per cent of the flux of the axial beam from the solar telescope, and this flux, after passage through a Compur shutter, B, forms on the slit of the spectroscope a focused image of the portion of the solar image which lies on the axis of the telescope. Some 1·6 per cent of the flux incident on the hypotenuse face of the first prism is, however, reflected at right angles and is focused by the solar telescope on cross-wires where it is viewed by a positive eyepiece C of 5 cm focal length. The resultant angular magnification is 390 times.

Because of the large focal ratio, $f/62$, of the solar telescope (**7**), the aberrations introduced by the cube are negligible. The depth of focus of the telescope, defined as that range within which optical path differences from the focal point are less than $\lambda/4$, is 0·92 cm; compare Conrady (**1**). The difference in focus produced by the cube for light of 4000 A and 6600 A is only 0·04 cm, and the primary longitudinal spherical aberration at 5900 A is only 0·000 4 cm. Both aberrations therefore produce path differences which are well below the Rayleigh limit.

The Guiding Plate is placed on an optical bench in front of the spectroscope slit (**8**). The observer watches the portion of the photosphere, the spectrum of which is to be photographed, through the eyepiece, and opens the shutter by means of a release near his right hand at the instant when the definition is sharpest and the image appears most steady. The exposure times in the 5900 A region, where spectra for sight-line velocities are taken, vary for Ilford Rapid Process Panchromatic plates between 0·5 and 5 seconds, depending upon the transparency of the sky and the portion of the photosphere being photographed. The seeing is described on a subjective scale from 0 to 5 as follows:

0....absence of definition,
1....penumbrae of spots just visible (tremor disk 20″),
2....penumbrae clearly visible (tremor disk 10″),
3....penumbral structure visible (tremor disk 7″),
4....granulation just visible (tremor disk 5″),
5....granulation easily visible and steady (tremor disk 3″).

The estimates of diameters of tremor disks are only a rough guess. Good seeing conditions in Oxford occur in the early autumn and to some extent in the spring. The best seeing so far recorded is 4 on the above scale.

The following additional features of the Guiding Plate may be noted. The cube A is adjustable for azimuth, and the cross-wires and the eyepiece for height, so as to bring the point of the solar image which is on the centre of the slit on to the centre of the cross-wires. Either fixed cross-wires, as illustrated in the photograph, or a filar micrometer is available; both are adjustable to bring the centre of the cross-wires on to the axis of rotation of the engraved circle from which the position angle is read. On the telescope side of the cube A is an optically plane parallel piece of glass (bloomed) of 1 cm thickness. This plate may be rocked about a vertical axis by the handle on the base of the instrument to the right of the eyepiece, and about a horizontal axis by the handle to the left. The resulting image movement is $\pm 1{\cdot}5$ mm to the north or south and to the west or east respectively. In this way it is possible accurately to centre the image before an exposure, and actually to guide should the exposure be sufficiently prolonged. It is interesting to note that Evershed (**3**) used a rocking plane plate for guiding in solar spectroscopy as early as 1916.

2. *Measurement of spectra.*—As already noted, the spectra for sight-line velocities are invariably taken in the 5900 A region. The water-vapour lines present in this region act as wave-length standards, and are subject, should there be any non-uniform illumination of the collimator, to identically the same spurious displacements as the solar lines. The high humidity of the Oxford climate is a guarantee that the water-vapour lines will be sufficiently strong to be easily measurable at any time of the day. Water-vapour lines, rather than oxygen lines farther to the red, are chosen as wave-length standards to take advantage of the higher prismatic dispersion at 5900 A. In this region 16 strong water-vapour lines (Rowland numbers 1 to 7), unblended with solar lines, lie between 5885 A and 5959 A; in this same range and well distributed through it are, exclusive of the *D* lines, 10 unblended solar lines with Rowland numbers from 1 to 6. These lines, due to silicon, titanium, iron and nickel, and, if necessary, fainter solar lines are suitable for measurement of Doppler

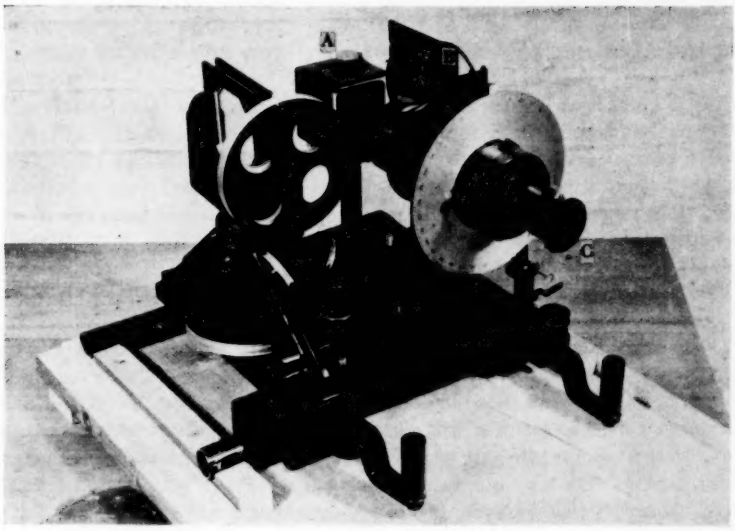

1

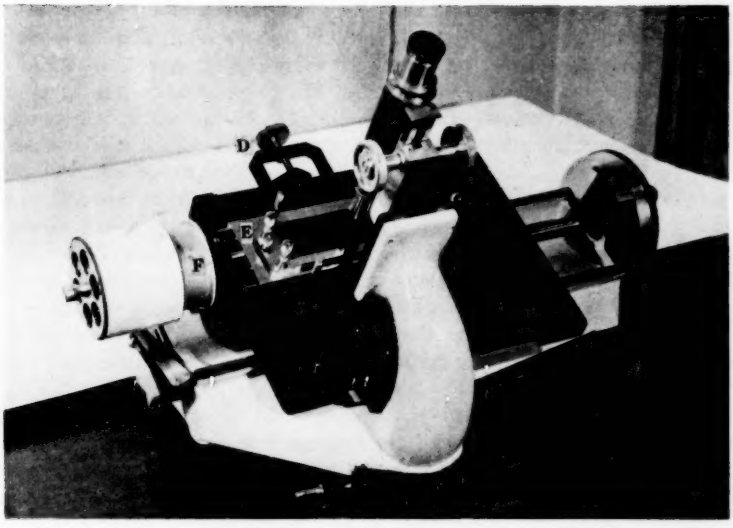

2

H. H. Plaskett, Motions in the Sun at the photospheric level. I. Methods

displacements. They will give sight-line velocities for photospheric matter at some mean, non-zero, optical depth; following Strömgren (**11**), this means optical depth may be put at 0·25 for the centre of the solar image. The Doppler displacement for a sight-line velocity of 1 km/s averages 13·3 microns for this range of spectrum.

The Oxford solar spectroscope has a very asymmetrical horizontal apparatus function (**8**). To avoid the danger that the measured position of a line is some function of its equivalent width or Rowland number, it is necessary to measure the position of each line from the same line in some known or standard position. A line in the spectrum of the centre of the solar image is in such a known or standard position, and one centre spectrum, taken at any convenient time, will serve as a standard against which to measure all photospheric spectra with approximately the same water-vapour line intensities. On account of the curvature of the spectrum lines, measurement must be made at the same height in both the standard centre spectrum and in the photospheric spectrum.

The spectra may be measured on an ordinary photo-measuring micrometer. First in the centre spectrum the linear positions of the water-vapour and the solar lines are found by setting with a line graticule, and a series of such measures are made for all possible heights. These measures give the standard positions of the lines for each height. The Hartmann dispersion constants for each height are then found from the water-vapour lines, preferably using Stratton's least squares method (**10**). The photospheric spectrum, in which the sight-line velocity at some definite height is required, is then measured in the same way. The differences of micrometer settings (centre spectrum at this height minus photospheric spectrum) for the water-vapour lines are then plotted as a function of wave-length. The corrections read from this curve, and applied to the differences of settings for the solar lines, will give the displacements of the solar lines in the photospheric spectrum from their positions in the centre spectrum in units of the dispersion of the latter. Multiplication of these corrected displacements by the appropriate velocity factor, derived from the Hartmann constants at this height, will give the sight-line velocity difference between the photospheric spectrum and the centre.

2.1. *Evershed micrometer.*—Alternative and simpler methods of carrying out this measurement are provided by the Hartmann spectrocomparator (**4**), and by the Evershed positive-on-negative micrometer (**2**). The latter method, to which an ordinary photo-measuring micrometer can readily be adapted, must be used for the present purpose with an ordinary contact positive of the centre spectrum, not a reversed positive. Otherwise the asymmetrical lines in the positive of the centre spectrum and in the negative of the photospheric spectrum would be asymmetrical in opposite directions, and consistent matching would be difficult or impossible. Further, since it is necessary to match the contact positive and the negative at a number of different heights, the same in each spectrum, the simple but elegant adaptation by Evershed of the photo-measuring micrometer cannot be followed.

The Evershed micrometer in use at Oxford is illustrated in Plate 4, 2. On the travelling stage of a Hilger micrometer is a vertical slide moving in ways at right angles to the direction of motion of this stage. This vertical slide may be moved up or down on the stage by a screw D. The negative spectrum (of the photosphere) is held, emulsion side up, on the vertical slide by spring clips.

Any desired line in this spectrum can be brought to a fixed point (to avoid parallactic displacement) in the field of view of the microscope by turning the micrometer head at the right, thus moving the travelling stage, and any desired height on this line can be obtained by adjusting the screw D. A variable aperture in the focal plane of the eyepiece confines the height of the spectrum between limits of 0·05 and 1·0 mm. Permanently fixed to the vertical slide is a bridge with ways parallel to the direction of motion of the travelling stage. On these ways a slide E moves under kinematical constraints. This slide, driven against springs by a Moore & Wright 0·5 mm-pitch micrometer F, carries the positive of the central spectrum with its emulsion side down and almost in contact with the emulsion side of the negative spectrum of the photosphere. The displacement of the positive is read on the head of the micrometer F. The setting is always made from one side against the action of the springs to avoid lost motion, and is judged to be satisfactory when the appropriate line in the spectrum of the positive is exactly superposed on the same line in the negative spectrum of the photosphere. Before measurement commences the positive is adjusted by three spring-loaded screws and by a rotatable stage on the slide E to bring it as close as possible and parallel to the negative spectrum.

The features so far described are common to the Evershed micrometer pictured in Plate 4, 2, and a prototype micrometer used by T. D. Kinman in his measurement of the Evershed effect in sunspots (**5**). Two points distinguish the micrometer in the photograph. In the first place a number of removable carriers, to which positives may be cemented, is provided. Two positives of the same centre spectrum may thus be cemented on separate carriers, one red right and the other red left; this means that the negative spectrum of the photosphere can be measured both direct and reversed. Secondly the instrument is self-recording. The head of the micrometer F carries a removable metal sleeve, held in position to the head by a screw. This sleeve is covered by a thin cylinder of rubber on which may be wrapped and fixed a piece of recording paper. A needle, operated by a shutter-release, can be driven into the paper to make a small hole. Each setting of the positive can therefore be recorded by pressing the shutter-release. When at the same height we move to the next line in the spectrum of the negative, by moving the travelling stage by the micrometer head on the right, the sleeve carrying the recording paper moves past the needle point to the right. The needle holes recording the settings of the positive appear the same distance to the left on the recording paper. Before the measurement of a spectrum at a given height, a series of needle holes is made in the paper at intervals of 0·01 mm on the drum of the Moore & Wright micrometer. A motion of the positive of this amount corresponds to a distance of about 5 mm on the recording paper. A similar series of holes is made at the conclusion of the measurement; the two series provide a scale by which to read the record. The advantages of self recording are not so much in saving eye strain, though this is a consideration, as in avoiding prepossessions in the measurement of differential displacements (**6**).

The preliminaries and the method of reduction are the same for the Evershed micrometer as those already described for measurement with a line graticule. The positive is first measured once and for all at a number of heights with a line graticule and the Hartmann dispersion constants found for each height. When a negative spectrum at a given height has been measured against the positive at the same height, the recorded readings for the water-vapour lines are used to

construct a correction curve; the corrections from this curve, applied to the recorded readings of the solar lines, give the displacements of the solar lines in the negative from their positions in the positive in units of the dispersion of the latter. These displacements are converted to a sight-line velocity of the photosphere relative to the centre by multiplication by velocity factors found from the Hartmann constants for the given height of the positive.

2.2. *Accuracy of measurement.*—To test the accuracy of measurement with the ordinary photo-measuring micrometer on the one hand and the Evershed micrometer on the other, seven of Miss A. B. Hart's solar-rotation spectra have been measured by her and by me. Table I contains the results of measurement with the ordinary micrometer and a line graticule. The table is divided into two parts, one for each measurer. The first column in each part contains the mean displacement in km/s for 10 solar lines between the solar-rotation spectrum and the centre spectrum, the second column gives the r.m.s. residual from this mean for a single line, and the third column the R–D discordance. It will be noted that the consistency of measurement, as shown by the r.m.s. residual for a single line, is effectively the same for each measurer with a mean of ±0·28 for A.B.H. and of ±0·25 for H.H.P.

TABLE I

Photo-Measuring Micrometer

Sp.	A.B.H.			H.H.P.			Mean V*
	V*	r.m.s.e.	R–D	V*	r.m.s.e.	R–D	
1	2·33	±0·27	−0·28	2·30	±0·17	−0·28	2·32
2	1·80	·35	− ·31	1·84	·20	− ·04	1·82
3	2·27	·33	− ·08	1·94	·22	− ·11	2·10
4	2·01	·16	− ·10	1·94	·28	+ ·03	1·98
5	1·46	·33	− ·17	1·56	·19	− ·45	1·51
6	1·82	·28	− ·04	1·78	·35	− ·23	1·80
7	1·69	·24	− ·24	1·97	·37	+ ·08	1·83
	Means	±0·28	−0·17		±0·25	−0·14	

The results of measurement of the same spectra with the Evershed micrometer are shown in Table II. The first point to be noted about these measures is the low consistency obtained by myself with a mean r.m.s. residual for a single line of ±0·38. These are the first measures I have made with the Evershed micrometer, and bear out a remark of Evershed that measurement by the positive-on-negative method has to be learned. Miss Hart, who has had a great deal of experience with the Evershed method, obtains a much higher degree of consistency, though her r.m.s. residual for a single line is not substantially different from that obtained by both of us with the ordinary micrometer. The high accuracy achieved by Evershed himself with his method presumably arises from the doubled displacement obtained with the reversed positive.

The second and somewhat puzzling point about measurement with the Evershed micrometer is the large R–D discordance obtained by both measurers. This discordance was first discovered by Miss Hart and shows the importance of taking the mean of a direct and a reverse measure. Coming up from one side to set the line of the positive centre spectrum on the same line of the negative spectrum, the measurer gets a satisfactory match earlier on solar lines than on water-vapour lines. These particular spectra of the centre and for solar rotation

were exposed on days of relatively low humidity, so that the solar lines are on the average stronger than the water-vapour lines. The R–D discordance thus appears to be an intensity phenomenon; it would presumably be less marked the more nearly comparable in intensity were the two classes of lines.

3. *Determination of solar velocities.*—If V be the component in the sight-line of the velocity of photospheric matter at a point Q on the surface of the Sun, then

$$V=(c/\lambda_1)(\lambda-\lambda_1)+C_1.$$

In this equation λ is the wave-length (as it would be found interferometrically at Q), and λ_1 is the true wave-length at Q (as it would be found interferometrically in the absence of relative motion of Q and the observer). C_1 is the correction for the component in the sight-line of the observer's motion. The true wave-length, λ_1, at Q differs from λ_0, the true wave-length at the sub-terrestrial point E (the apparent centre of the solar image), by the so-called limb effect. In the extreme case where Q is on the limb of the Sun, $\lambda_1-\lambda_0$ probably does not exceed 0·02 A. Without making an error as great as that arising from the uncertainty in our knowledge of the velocity of light, c, we may substitute c/λ_0 for c/λ_1. Hence

$$V=(c/\lambda_0)(\lambda-\lambda_1)+C_1=(c/\lambda_0)(\lambda-\lambda_0)+C_1-\Delta_1, \qquad (1)$$

where $\Delta_1=(c/\lambda_0)(\lambda_1-\lambda_0)$ may be defined to be the limb effect expressed in km/s.

TABLE II

Evershed Micrometer

Sp.	A.B.H.			H.H.P.			
	V•	r.m.s.e.	R–D	V•	r.m.s.e.	R–D	Mean V•
1	2·42	±0·14	+0·65	2·22	±0·19	+1·21	2·32
2	1·83	·20	+ ·74	1·72	·37	+0·52	1·78
3	2·18	·31	+ ·67	1·95	·32	+ ·90	2·06
4	2·02	·21	+ ·89	2·30	·38	+ ·69	2·16
5	1·72	·25	+ ·37	1·61	·42	+ ·58	1·66
6	1·94	·21	+ ·94	1·84	·35	+ ·71	1·89
7	2·04	·28	+ ·54	1·97	·62	+ ·66	2·00
Means		±0·23	+0·69		±0·38	+0·75	

The method of measurement and reduction described in the previous section gives a sight-line velocity

$$V^\bullet=(c/\lambda_0)(\lambda-\lambda').$$

Here λ' is the wave-length as it would have been found interferometrically for the line at the centre of the solar image at the time when the photograph of the centre spectrum was taken. Hence we may write (1) in the form

$$V=(c/\lambda_0)(\lambda-\lambda'+\lambda'-\lambda_0)+C_1-\Delta_1=(c/\lambda_0)(\lambda-\lambda')-C_0+C_1-\Delta_1,$$

or

$$V=V^\bullet+C_1-C_0-\Delta_1. \qquad (2)$$

C_0 is the correction for the component of the observer's velocity in the sight-line to the sub-terrestrial point E at the time when the centre spectrum was taken; consequently

$$C_0=-(c/\lambda_0)(\lambda'-\lambda_0),$$

provided the photospheric matter at the sub-terrestrial point has on the average no vertical component of velocity.

With origin at Q (see Fig. 1) erect a right-handed system of rectangular axes. The xy-plane is tangent to the solar surface at Q with the x-axis pointing in the direction of solar rotation, the y-axis tangent to a meridian to the Sun's north pole of rotation, and the z-axis pointing radially outwards. Then if u, v, and w are the components of the photospheric velocity at Q along these axes, and $\cos\gamma_1$, $\cos\gamma_2$, and $\cos\gamma_3$ are the direction cosines of the sight-line directed from the observer to Q, then

$$(u+U)\cos\gamma_1+v\cos\gamma_2+w\cos\gamma_3=V=V^{\bullet}+C_1-C_0-\Delta_1, \qquad (3)$$

where U is the velocity due to solar rotation at Q. If the photospheric matter has any common motion, (3) is an equation of condition which may be solved by least squares to find the u, v and w components of this motion. In this equation the direction cosines may be found once the heliographic coordinates of Q are known, and the corrections for the observer's motion when the equatorial coordinates of Q are known. For most purposes the solar rotation U and the limb effect Δ_1 may be taken from previous observations.

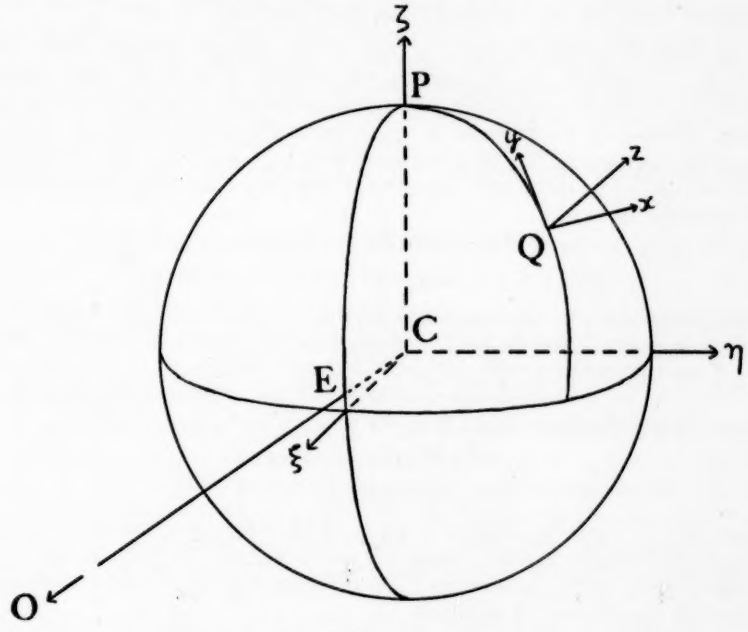

FIG. 1.

3.1. *Heliographic and equatorial coordinates of Q.*—By means of a polar coordinate disk, mounted on the optical bench in front of the spectroscope slit, the radius vector ρ from the centre of the solar image and the position angle ϕ (measured from the west) may be found for any readily identifiable point on the solar image. If this identifiable point be used for guiding with the Guiding Plate (Section 1), the polar coordinates for any other point (that is the image of Q) on the illuminated slit may be found. ρ is measurable to 0·1 mm (roughly 1″

of arc) and ϕ to 0°·1. Then θ_1, the angle subtended at the observer, O, by Q and the sub-terrestrial point E, is given by

$$\tan\theta_1 = \rho/f,$$

where f is the focal length of the telescope. Correspondingly if ρ_0 be the radius of the solar image measured with the polar coordinate disk, the angular semi-diameter S of the Sun is given by

$$\tan S = \rho_0/f.$$

Hence to the nearest second of arc, corresponding to the limit of measurement with the polar coordinate disk,

$$\theta_1 \simeq (\rho/\rho_0)S. \tag{4}$$

Note, however, that if this accuracy is to be maintained, a correction for differential refraction must be applied to ρ and to ϕ when the altitude of the Sun is less than 30°.

The angle θ subtended at the centre of the Sun, C, by Q and E is found from the plane triangle CQO to be given by

$$\sin(\theta+\theta_1) = \sin\theta_1/\sin S \simeq \theta_1/S, \tag{5}$$

to the accuracy of measurement. Then in the spherical triangle PEQ, where P is the Sun's north pole of rotation, we have the arc $EQ=\theta$. The spherical angle $\psi = \angle PEQ$ is equal to the plane angle measured at the centre of the solar image between the direction of the Sun's north pole and the point Q. Thus in the NW quadrant of the solar image $\psi = \pi/2 + P - \phi$ where P is the position angle of the Sun's north pole measured from the north. We then have from the spherical triangle

$$\left.\begin{aligned} \sin B &= \cos\theta\sin B_0 + \sin\theta\cos B_0\cos\psi, \\ \cot(L-L_0) &= (\cos B_0\cot\theta - \sin B_0\cos\psi)\operatorname{cosec}\psi. \end{aligned}\right\} \tag{6}$$

These equations give the required heliographic latitude, B, and longitude, L, of Q in terms of B_0 and L_0 for E, and the measured quantities θ and ψ. B_0, L_0 and P are tabulated for each day in the *Nautical Almanac*.

If α_0, δ_0 are the equatorial coordinates of the sub-terrestrial point E, the equatorial coordinates of Q are given by $\alpha = \alpha_0 + \Delta\alpha$, $\delta = \delta_0 + \Delta\delta$, where

$$\left.\begin{aligned} \Delta\alpha &\simeq -\theta_1\cos\phi\sec\delta_0, \\ \Delta\delta &\simeq \quad \theta_1\sin\phi. \end{aligned}\right\} \tag{7}$$

Note that ϕ, as already defined, is the position angle measured from the west. The position angle measured from the north will therefore be $\phi - \pi/2$. The accuracy given by (7), better than 5″, is sufficient for the purpose for which the equatorial coordinates are required.

3.2. *Correction for the observer's motion.*—At the instant of photographing the spectrum of the photosphere at Q, the observer's motion may be analysed into a rotation about the Earth's axis, and a motion of the Earth's centre about the centre of the Sun. The correction in km/s for the Earth's rotation is, as is well known,

$$-\frac{2\pi a r'\cos\phi'}{86164\cdot1}\cos\delta\sin H = -0\cdot2885\cos\delta\sin H \quad \text{(for Oxford)}.$$

Here r' is the observer's distance from the Earth's centre, including his height above sea level, measured in units of the Earth's equatorial radius a; ϕ' is his

geocentric latitude, and the numerical constant 86164·1 is the number of mean solar seconds in a sidereal day. It should be noted that δ and $H = \text{L.S.T.} - \alpha$ are defined with respect to the instantaneous axis of rotation and the true equinox; consequently the apparent equatorial coordinates of Q are required. They may be found by adding $\Delta\alpha$ and $\Delta\delta$ from (7) to the apparent equatorial coordinates of the centre of the Sun at the time of observation.

The centre of the Earth, and with it the observer, are moving about the centre of gravity of the Earth–Moon system, and the latter is moving in a perturbed elliptical orbit about the centre of the Sun. These various motions are fully included in the geocentric equatorial rectangular coordinates (X, Y, Z) of the Sun, tabulated for each day in the *Nautical Almanac*. Then following Schlesinger (**9**) the correction to the sight-line velocity for the motion of the Earth's centre is

$$-(\dot{X}\cos\delta'\cos\alpha' + \dot{Y}\cos\delta'\sin\alpha' + \dot{Z}\sin\delta')$$

and this may be expressed in km/s by multiplying it by the mean distance of the Sun in km and dividing by the number of mean solar seconds in a mean solar day. The geocentric equatorial rectangular coordinates X, Y, Z are defined with respect to a mean equator and equinox (say, 1950·0). The equatorial coordinates α', δ' must then be defined with respect to the same equator and equinox. For the Sun's centre they are found most easily, as pointed out to me by Dr. Merton, from $\tan\alpha_0' = Y/X$, and $\sin\delta_0' = Z$. The corresponding coordinates for Q are then found by adding $\Delta\alpha$ and $\Delta\delta$ from (7).

Summarizing, the correction in km/s for the component of the observer's motion along the sight-line to Q is

$$C_1 = -\frac{2\pi a r'\cos\phi'}{86164\cdot1}\cos\delta\sin H - 1732\cdot34(\dot{X}\cos\delta'\cos\alpha' + \dot{Y}\cos\delta'\sin\alpha' + \dot{Z}\sin\delta'). \tag{8}$$

The corresponding correction, C_0, along the sight-line to the sub-terrestrial point E is found by substituting the appropriate equatorial coordinates for the centre of the Sun and the values of $\dot{X}$, $\dot{Y}$, $\dot{Z}$, both for the instant when the centre spectrum was taken.

3.3. *Direction cosines of the sight-line.*—The direction cosines of the sight-line OQ with respect to the rectangular coordinate system, x, y, z, with origin at Q (*cf.* Fig. 1) may be found by considering another right-handed system of axes, ξ, η, ζ, with origin at the Sun's centre, C. The $\xi\eta$-plane is the equatorial plane of the Sun and the ξ-axis lies on the intersection of this plane by the plane through O and the Sun's axis of rotation. The η-axis has the heliographic coordinates $B = 0$, $L - L_0 = \pi/2$, and the ζ-axis the heliographic coordinate $B = \pi/2$. The direction cosines of the x, y and z axes with respect to the ξ, η, ζ axes are clearly

$l_1 = -\sin(L - L_0)$	$m_1 = \cos(L - L_0)$	$n_1 = 0$
$l_2 = -\cos(L - L_0)\sin B$	$m_2 = -\sin(L - L_0)\sin B$	$n_2 = \cos B$
$l_3 = \cos(L - L_0)\cos B$	$m_3 = \sin(L - L_0)\cos B$	$n_3 = \sin B$

Further the direction cosines of the sight-line OQ in the ξ, η, ζ system are

$$(1/d')[R\cos B\cos(L - L_0) - d\cos B_0], \quad (1/d')R\cos B\sin(L - L_0),$$
$$(1/d')[R\sin B - d\sin B_0],$$

where R is the radius of the Sun, $d = \text{OC}$ is the distance of the observer from the centre of the Sun, and $d' = \text{OQ}$, his distance from Q.

Then the cosine of the angle γ_1 between the sight-line OQ and the x-axis is

$$\begin{aligned}\cos\gamma_1 &= (1/d')[-\{R\cos B\cos(L-L_0)-d\cos B_0\}\sin(L-L_0)\\ &\quad + R\cos B\sin(L-L_0)\cos(L-L_0)]\\ &= (d/d')\sin(L-L_0)\cos B_0.\end{aligned}$$

However from the plane triangle CQO, $d\sin\theta_1 = d'\sin(\theta+\theta_1)$, so that finally

$$\cos\gamma_1 = \sin(L-L_0)\cos B_0\sin(\theta+\theta_1)\operatorname{cosec}\theta.$$

Similarly the cosine of the angle γ_2 between the sight-line OQ and the y-axis is found to be

$$\cos\gamma_2 = [\sin B\cos B_0\cos(L-L_0)-\cos B\sin B_0]\sin(\theta+\theta_1)\operatorname{cosec}\theta.$$

The same procedure, after a little algebra, gives the cosine of the angle γ_3 between the sight-line OQ and the z-axis to be

$$\cos\gamma_3 = -\cos(\theta+\theta_1).$$

This result may also be found directly from the plane triangle OCQ. As may be readily verified, the sum of the squares of these three direction cosines is unity.

Summarizing the results of this section, the equation of condition connecting the measured sight-line velocity V^* with the velocity components u, v, w of the photospheric matter at Q is

$$u\cos\gamma_1 + v\cos\gamma_2 + w\cos\gamma_3 = V^* + C_1 - C_0 - \Delta_1 - U\cos\gamma_1 \tag{3}$$

where
$$\left.\begin{aligned}&\cos\gamma_1 = \sin(L-L_0)\cos B_0\sin(\theta+\theta_1)\operatorname{cosec}\theta,\\ &\cos\gamma_2 = [\sin B\cos B_0\cos(L-L_0)-\cos B\sin B_0]\sin(\theta+\theta_1)\operatorname{cosec}\theta,\\ &\cos\gamma_3 = -\cos(\theta+\theta_1).\end{aligned}\right\} \tag{9}$$

$$C_1 = -\frac{2\pi a r'\cos\phi'}{86164{\cdot}1}\cos\delta\sin H - 1732{\cdot}34[\dot{X}\cos\delta'\cos\alpha' + \dot{Y}\cos\delta'\sin\alpha' + \dot{Z}\sin\delta']. \tag{8}$$

C_0, the correction for the component of the observer's motion along the sight-line to the sub-terrestrial point E, is found from (8) by substituting the appropriate equatorial coordinates for the centre of the Sun, and $\dot{X}$, $\dot{Y}$, $\dot{Z}$, all for the instant when the centre spectrum was taken.

In conclusion I wish to express my thanks to Miss A. B. Hart for her careful investigations of the accuracy of measurement by the Evershed micrometer, and for the use of some of her measures. I also wish to thank Mr R. M. Abraham of Casella & Co. for the detailed mechanical design of the Guiding Plate and for its construction by his firm. Thanks are also due to Mr H. G. East, a local instrument maker, for the construction of the Evershed micrometer.

University Observatory,
Oxford:
1952 *April* 30.

References

(1) A. E. Conrady, *Applied Optics and Optical Design*, p. 136, Oxford, 1929.
(2) J. Evershed, *Bull. Kodaikanal Obs.*, **3**, 17, 1913.
(3) J. Evershed, *Bull. Kodaikanal Obs.*, **3**, 167, 1916.
(4) J. Hartmann, *Ap. J.*, **24**, 285, 1906.
(5) T. D. Kinman, *M.N.*, **112**, 425, 1952; *Comm. Univ. Obs., Oxford*, No. 35.
(6) H. H. Plaskett, *Jour. R.A.S.C.*, **10**, 220, 1916.
(7) H. H. Plaskett, *M.N.*, **99**, 219, 1939; *Comm. Univ. Obs., Oxford*, No. 14.
(8) H. H. Plaskett, *M.N.*, **112**, 177, 1952; *Comm. Univ. Obs., Oxford*, No. 33.
(9) F. Schlesinger, *Ap. J.*, **9**, 159, 1899.
(10) F. J. M. Stratton, *M.N.*, **71**, 663, 1911.
(11) B. Strömgren, *Festschrift für E. Strömgren*, Copenhagen, p. 251, 1940.

MOTIONS IN THE SUN AT THE PHOTOSPHERIC LEVEL

II. The Evershed Effect in Sunspot Mt. Wilson No. 9987

T. D. Kinman

(Communicated by the Director, University Observatory, Oxford)

(Received 1952 May 1)

Summary

Sight-line velocities are measured for 237 points in the penumbra and surrounding photosphere of a large regular spot (Mt. Wilson No. 9987), from short exposure spectra obtained under good conditions of seeing. These spectra are measured by Evershed's positive-on-negative method with an r.m.s. error of 0·1 km sec^{-1} per point.

The sight-line velocity is a linear function of the cylindrical components of the velocity at any point in the penumbra and these cylindrical components may be found from the sight-line velocities of a group of points which have a motion in common. Least squares solutions for the 237 points show that the penumbral motion has cylindrical symmetry. This motion is found to consist of an outward horizontal radial velocity which increases from approximately 1 km sec^{-1} at the edge of the umbra to 2 km sec^{-1} in the middle zone of the penumbra and finally falls to zero in the photosphere well outside the spot. Tangential and vertical velocity components are less than the errors of measurement.

In a brief investigation of the energy exchange in the penumbra, it is shown that the energy required both to warm up the penumbral material and to provide its kinetic energy is comparable with the radiation absorbed by the material.

Introduction.—Radial motion in sunspots was discovered by Evershed (**3**) in 1909 from the Doppler displacements of the spectrum lines. His spectra were taken of spots in various positions on the disk and with the slit of his spectroscope at different angles to the solar radius. He measured these spectra at points on the outer edge of the penumbra and found displacements of the lines which could be explained by a radial horizontal outflow of about 2 km sec^{-1}. He also judged from the appearance of the lines that the velocity increased outwards from the umbra to a maximum at the outer edge of the penumbra where it ceased abruptly. According to his later work, there were also tangential components of 0·25 km sec^{-1} (**6**) and 0·35 km sec^{-1} (**5**) and a velocity of descent in the umbra of 0·4 km sec^{-1} (**5, 6**). In his last paper (**7**), however, Evershed found no evidence for a regular tangential component although irregular velocities were sometimes present.

St. John (**21, 22**), in 1913, compared the displacements of the lines at the outer edge of the penumbra on two opposite sides of the spot. He placed his slit along a solar radius with an occulting device in front which enabled him to photograph the spectra of the limb-edge and the centre-edge of the penumbra side by side but not simultaneously on the same plate. A measurement of the differential displacement of 506 different lines ($\lambda\lambda$ 3624–6644) showed that it was proportional to wave-length and so confirmed Evershed's hypothesis of a Doppler effect due to motion in the spot. Besides this, the displacement was

greater for weak lines than for strong, ranging from 1·02 km sec^{-1}, for lines of Rowland number −1, to zero or negative values for Rowland numbers greater than 15. St. John, however, contended from the appearance of the lines that the motion continued beyond the penumbra into the photosphere, while Evershed (**7**) maintained that, although this happened occasionally in some spots, his previous observation was generally true.

In 1932, Abetti (**1**) determined the displacement at two points in the penumbrae of spots by comparison of their spectra with a spectrum of the centre of the disk. Besides radial velocities varying from 0·2 to 5·8 km sec^{-1} outwards, he found irregular tangential velocities of from 0 to 5·0 km sec^{-1} and concluded that the motions must vary markedly from spot to spot. Further details of previous observations are given in Table I. Column one gives the observer, the second the reference, the third the scale of the solar image in seconds of arc per mm, the fourth the mean diameter of the umbrae (corrected for foreshortening) in seconds of arc, the fifth the number of spots observed, the sixth the linear dispersion in A per mm (for grating spectroscopes in all cases), the seventh the region of the spectrum, the eighth the exposure time and lastly the mean radial velocity at the photospheric level in km sec^{-1}.

TABLE I

Previous observations of the Evershed effect at the photospheric level

Observer	Ref.	Image scale ″/mm	Mean umbral diameter ″	No. of spots	Disp. A/mm	Mean wave-length A	Exp. s	Mean rad. velocity km sec^{-1}
Evershed	(3)	16, 30	14	12	1·1	4 650	⩾30	+1·6
	(4)	16, 30	13	4	1·1	4 650	⩾30	+1·9
	(5)	16, 30	17	5	1·1	4 650	⩾30	+2·0
	(6)	16, 30	...	...	1·1	4 650	⩾30	+2·0
	(7)	22	20	2	...	4 650	5–30	+1·9
St. John	(21)	11	12	11	0·56	4 490	60–180	+1·0
					0·86	6 120		
Abetti	(1)	11	13	26	1·2	4 800	...	+1·4

Now these observations do not determine the velocity field of a spot since they refer to only two or at most four points in the spot, and even at these points the agreement between different observers is only rough. The purpose of this paper therefore is to present as complete a determination of the velocity field of a spot as possible. The first section deals with the determination of the sight-line velocities and the second with their reduction to actual velocities in the spot. A physical discussion of these results forms a short concluding section.

1. *The determination of the sight-line velocities*

1.1. *Observational material.*—A series of 40 spectra of the large regular spot Mt. Wilson No. 9987 (heliographic latitude and longitude: −12° 07′; 268° 05′) were taken by H. H. Plaskett on 1949 September 8, 10, 11 and 13 using the Oxford Solar Telescope (**13**) and spectroscope (**14**). The sight-line component of a horizontal or vertical velocity in a spot varies as sin ρ or cos ρ respectively, where ρ is the angle subtended by the spot and the observer at the centre of the Sun. The geometrical foreshortening of the spot varies as cos ρ, so the best position for determining all velocity components is when $\rho = 45°$.

The fifteen spectra taken on September 11 ($\rho = 38°$) when the seeing was particularly good were therefore chosen for measurement.

The Oxford telescope gives a strictly achromatic image on a scale of 10″ per mm, so that the spot umbra of 20″ angular diameter had an image diameter of 2 mm, which is nearly twice that of any previous observer. A spot may be set and maintained on the spectroscope slit with the Guiding Plate (**15**) and this also allows the exposure to be made at the instant of best seeing. Table II gives the time, the exposure, the seeing and the position of the slit on the umbra for each spectrum together with further details of the apparatus. Comparison with Table I shows that the exposures are considerably shorter than for the grating spectra of previous observers with comparable solar images; the effect of unsteadiness is therefore minimized and each height in a spectrum tends to correspond closely to a single point in the spot.

TABLE II

Measured Plates

Dispersion: 1·5 A/mm (λ5935); Image scale: 10″·3/mm; Umbral diameter: 20″;
Slit height: 12 mm; Slit width: 0·030 mm; Emulsion: Ilford Rap. Process Pan.

Spectrum	Slit position
1	On central notch in umbra
2	On N. edge of umbra
3	On S. edge of umbra
4	20″ N. of centre of umbra
5	20″ S. of centre of umbra

Centre of slit approx. on N.–S. line through spot centre in each case.

Spectrum	Plate E7			Plate E8			Plate E9		
	U.T. h	Exp. s	Seeing	U.T. h	Exp. s	Seeing	U.T. h	Exp. s	Seeing
1	8·78	4	2	9·84	6	4	11·32	5½	3
2	8·85	5	3	9·88	6	3	11·35	5½	3+
3	8·89	5	3	9·91	6	2	11·39	5½	2+
4	8·93	5	3	9·95	6	3	11·42	5½	2+
5	8·96	5	3	9·98	6	1+	11·44	5½	3

The seeing refers to a scale of 5.

By using atmospheric lines as standards, spurious displacements due to non-uniform illumination of the collimator may be avoided. Consequently the spectra are taken in the region of λ5900 where there are many atmospheric water vapour lines. The linear dispersion in this region (1·5 A/mm) is smaller than that used by previous observers, but this is partly offset by a larger Doppler shift in angstroms per unit velocity. The Doppler shift in microns for a velocity of 1 km sec^{-1} is 13·1 for the present observations, as compared with 14·1 for Evershed, 21·4 and 24·8 for St. John and 13·2 for Abetti.

A single spectrum of the centre of the disk for use with the Evershed micrometer was taken using an out-of-focus solar image to avoid the effects of granules. Kodak Press Contrast developer was used throughout.

1.2. *The measurement of the plates.*—The positions of measurement on the plates are identified by marks made at half millimetre intervals in a direction perpendicular to the dispersion using a needle pivoted on a Hilger photomeasuring micrometer. Both ends of the spectra are marked so that a series of lines is defined on the plate parallel to the dispersion and along or between which the

spectra are measured. The position of measurement is then found from the measured positions of these marks and spot features such as the edges of the umbra and penumbra.

Since the micrometer can only accommodate some five inches of plate, the region λλ5886–5968, where atmospheric lines are most frequent was selected. Table III gives a list of the wave-lengths and Rowland numbers of 22 of these lines whose Rowland number is not less than one and which are not blended with solar lines. Table IV gives a list of 15 solar lines chosen for their freedom from blends with atmospheric lines. These lines have Rowland numbers from 0 to 6 (mean number 3) and are thus representative of lines originating at the photospheric level. Two other solar lines: λ5922·123 and λ5965·836 of Ti I were used in some of the first measurements but were rejected later on account of their faintness in these plates. In Table IV, the first column gives the wave-lengths taken from Rowland's Revision (**20**), and corrected according to I.A.U. recommendations (**8**). The second gives the element and the third and fourth columns the Rowland number of the line in disk and spot respectively (**20**). The last two columns give the transitions responsible for the line and the corresponding *J* values for the states, both being taken from the *Revised Multiplet Table* (**10**).

TABLE III

Atmospheric water vapour lines

Wave-length A	Rowland No.	Wave-length A	Rowland No.	Wave-length A	Rowland No.
5 885·977	5	5 912·996	3	5 944·313	1
5 887·222	5	5 919·055	5	5 946·006	3
5 887·660	3	5 919·643	7	5 947·066	2
5 891·661	4	5 924·272	4	5 954·952	1
5 892·397	3	5 928·292	2	5 957·880	1
5 901·468	6	5 932·093	5	5 958·622	1
5 908·997	3	5 932·784	2	5 966·666	1
				5 968·276	2

Taken from Rowland's Revision and corrected according to the I.A.U. recommendations (**8**).

TABLE IV

Solar lines

Wave-length	Element	Rowland No. Disk	Rowland No. Spot	Transition	*J*
5 892·881	Ni I	4	4	y^3D^0–f^3F	3–4
				a^3P–z^1P^0	0–1
5 899·304	Ti I	1	6	a^3P–y^3D^0	1–2
5 902·478	Fe I	0	0	d^3F–t^3G^0	4–5
5 905·680	Fe I	4	3	y^3F^0–f^3D	2–1
5 909·981	Fe I	1	2	z^5D^0–e^7D	4–5
5 916·258	Fe I	3	6	a^3H–y^3F^0	4–4
5 927·796	Fe I	2	1	y^3F^0–g^5F	2–1
5 929·682	Fe I	2	2	y^3F^0–h^5D	4–3
5 930·190	Fe I	6	6	y^3F^0–e^5G	2–3
5 934·665	Fe I	5	5	z^3D^0–e^3F	2–3
5·948·548	Si I	6	2	$4s^1P^0$–$5p^1D$	1–2
5 949·348	Fe I	1	4	y^5F^0–h^5D	3–2
				a^5F–z^7P^0	4–3
5 952·726	Fe I	4	4	z^3F^0–e^3F	4–3
5 953·170	Ti I	1	6	a^3G–z^3H^0	5–6
5 956·705	Fe I	4	10	a^5F–z^7P^0	5–4

The plates were measured on a prototype of the Evershed type positive-on-negative photomeasuring micrometer described by H. H. Plaskett (**15**). By means of this micrometer the negative spectrum may be measured against a contact positive of a spectrum of the centre of the solar disk. The negative spot spectrum is mounted with its emulsion side uppermost on a slide that can be moved at right angles to the run of a Hilger micrometer. The field of view in this direction is restricted to 0·3 mm by a diaphragm in the microscope eyepiece so that this width of spectrum can be measured at any desired height. The positive spectrum with its emulsion side downwards is mounted on a carrier so that it may be superposed on the negative without actually touching it; the separation is of the order of 0·10 mm. A micrometer screw drives this carrier against a resisting spring along ways parallel to the dispersion so that a setting on a line in the negative spectrum may be made by the corresponding line at the same height in the positive spectrum. The design of the prototype Evershed micrometer does not allow the positive to be reversed on its carrier. Consequently the positive spectrum always approaches the negative spectrum from the same direction before a setting, since the micrometer drive is only used against the resisting spring. This lack of reversal of the positive spectrum may introduce a systematic error in the measurement and this is discussed with other errors in Section 1.4.

A setting is made by superposing the positive image of a line in the centre spectrum on the negative image of a line in the spot spectrum so that the contrast between the resulting line and its surroundings is the same on both sides. Each setting is made on a single line at a time at a particular point in the field of view and not with a number of lines together as in Evershed's original method. This precaution is necessary to avoid the parallax caused by viewing the positive and the negative spectra at different angles. To avoid prepossession when several settings on one line are made together, only one setting is made on each line for a single run of the spectrum. The complete run is then repeated twice more and the mean of the three runs taken. A reversing prism, fitted over the eyepiece on alternate runs, removes any systematic bias to left or right. An analysis of fifteen solar lines in five spectra, however, shows that the mean difference between settings with and without the prism is only 0·2 microns with an r.m.s. residual for a single line of 0·6 microns. Each spot spectrum was measured at from 15–20 points, the first measures being made at the marked points and later at those intermediate points where the velocity in the spot appeared to change rapidly.

If the dispersion of the negative spot spectrum were identical with that of the positive spectrum of the centre of the Sun, the micrometer settings for all the atmospheric lines would be a constant independent of wave-length. In general, however, there will be a difference in dispersion which may be found by plotting a curve of errors of the micrometer settings of the atmospheric lines as a function of wave-length. Hence the measured micrometer setting for a solar line minus the micrometer setting from the curve of errors will give the displacement of the spot line from the same line in the centre spectrum for a dispersion identical with that of the centre spectrum. The differential nature of the measurement removes any error due to the asymmetrical profile of the line or to line curvature.

The dispersion curve of the positive spectrum of the centre of the disk was found from crosswire measurements, also using a reversing prism for alternate

runs. These measurements, together with the solar wave-lengths (Table IV) which are corrected for the effect of the Earth's motion at the time of observation, and the atmospheric wave-lengths (Table III), then give a Hartmann dispersion curve by Stratton's method (**23**). The dispersion factor for each line is then obtained by differentiating the dispersion curve. The measurements were made at five slit heights to see if the change of line curvature with wave-length produced any variation of dispersion with slit height. The maximum variation detected however is only 0·02 per cent.

The displacement in microns is then converted to angstroms by multiplying by the dispersion factor for that line and further converted to a velocity in km sec^{-1} by multiplying by the frequency (c/λ) of the line.

The velocity at a given point in the spot is then equal to the mean velocity from all the solar lines in the spectrum of that point. The mean r.m.s. residuals of a single line are 0·34, 0·28 and 0·36 km sec^{-1} and the r.m.s. residuals for the mean of all lines at a single point are 0·10, 0·08 and 0·10 km sec^{-1} respectively for the three plates. These values are based on one point in each spectrum selected at random.

To obtain sight-line velocities on the Sun, these velocities which are relative to the centre of the disk must be corrected for the relative motion of the Sun and the observer in both the negative spot and positive centre spectra. Details of these corrections are given by H. H. Plaskett (**15**). The resulting sight-line velocities (V) in the sunspot are given for the 237 points of measurement in Table V.

1.3. *The determination of the positions of measurement in the spot.*—The slit positions given in Table II are only approximate. To find the positions of the measured points in the spectrum with respect to the centre of the umbra, use was made of a positive copy of the Greenwich photograph of the Sun at $08^h\ 49^m$ U.T. on 1949 September 11. This copy, together with three others taken on September 8, 10 and 13, were kindly given to us by H. W. Newton with the permission of the Astronomer Royal.

The heliographic latitude and longitude (B, L) of the centre of the umbra may be calculated from the coordinates of the spot on the solar disk which were measured on a polar coordinate disk (**15**) at the focus of the telescope, and also may be checked from measurements of the Greenwich plates. The position angle of the slit with respect to the East–West line was marked on an enlargement (scale: 1 mm = 1″·10) of the Greenwich plate of September 11. The maximum error due to distortion by foreshortening in assuming that this plate and the spectra were taken simultaneously is only 1·6 per cent and is in general much less than this.

If the measured positions of the umbra and penumbra in the spectra are converted to the scale of the enlargement and copied on to Kodatrace strips, then, knowing the position angle of the slits, their exact position may be found by comparing the features on the strips with those on the enlargement. One spectrum, however (No. 4, Plate 3), contains no penumbral features so that no fit is possible. It is concluded therefore that a mistake was made in adjusting the spot on the slit and this spectrum is not considered further. With the slit positions determined, the heliographic coordinates B, L can be found for all the measured points in the spectra. Fig. 1 is a diagram of the spot with coordinates $x = L \cos B$, $y = B$ on which the measured points are shown by small filled circles.

TABLE V

Sight-line velocities at 237 positions in the spot

$\bar{r}^*$	ϕ	E7	E8	E9	$\bar{r}^*$	ϕ	E7	E8	E9	$\bar{r}^*$	ϕ	E7	E8	E9
−0·1	7°	2·00			+0·7	4°		2·56		+1·0	152°		0·00	
	16		1·86			19	2·16				154			0·25
	73		1·44			21			2·23		176		0·68	
	105	1·01				24		1·87			182			0·09
	112	0·66				31			1·62		205	0·65		
	146		0·56			34		1·55			278	1·74		
	152			0·46		41	1·54				281		1·78	
	201			0·72		48		1·36			338			2·86
	344		1·56			61		1·31						
						73	0·96			+1·2	0°		2·32	
+0·1	7°			1·73		76		0·80			8			1·50
	99		1·00			88	0·54				11		1·68	
	106			0·86		94			0·65		112		0·91	
	119			0·26		130	0·81				118	0·99		1·06
	124	0·00				154			*0·36*		158	0·00		
	149		0·09			190			0·62		178			0·02
	153			0·13		202		0·94			179	0·36		
	163	0·30				216	0·74				194		1·01	
	198		1·13			228	0·78				197	0·66		
						246	1·49				292		1·66	
+0·3	3°			2·37		266		1·59			311			1·71
	113		0·61			297	2·38				313		1·62	
	161	*0·32*				339			2·95		334	2·23		
	196	0·22				340		2·68			338			2·13
	274		1·86	1·86							340		1·94	
	280	1·81			+0·9	14°			2·01		356	2·72		
	340			1·88		16		2·20						
	341		2·39			92		0·69		+1·4	7°	1·60		
						100	0·82				120		1·12	
+0·5	0°	2·33				105			0·82		121			1·06
	8		2·29			128		0·74			153		*0·28*	
	28	1·67				154			*0·02*		288	1·79		
	47			1·45		159	*0·03*				312	2·19		
	56	1·55				181		0·79			334	2·24		
	62			1·33		184	0·22				354	2·10		1·97
	78			0·66		263	1·43				358		1·88	
	121		0·57			305		2·02						
	151		*0·36*			306	2·54		2·32	+1·6	123°	1·07		
	188		0·61			334	2·27				134			0·55
	192	0·06				357			2·69		136	1·06		
	214		0·89								155			*0·19*
	230		1·12		+1·0	1°		2·84			188		1·15	
	248		1·34			13	1·99				296	1·44		
	294			2·24		104		0·79			300		1·53	
	296		2·14			110	0·88		0·92		317		1·63	
	332	2·03				114			0·16		352	1·89		
	341		2·88			131			*0·37*					

Negative velocities are given in italics.

TABLE V (*continued*)

$\bar{r}^\bullet$	ϕ	E7	E8	E9	$\bar{r}^\bullet$	ϕ	E7	E8	E9	$\bar{r}^\bullet$	ϕ	E7	E8	E9
+1·7	4°			1·34	+2·4	0°	1·41		1·27	+3·4	157°	1·14		
	6		1·43			120		1·12			167		1·30	
	126			0·67		140			1·03		168	1·16		
	132		0·92			141	1·25				169	1·23		1·04
	158	0·43				154		0·51			177	1·26		
	173		0·71			170	1·15				316	1·44	1·36	
	174			0·48		179		1·28			323	1·40		1·47
	190	0·70				182	1·18				324		1·35	
	316	1·75		1·59		310		1·47			335	1·47		
	338			1·54		335	1·48				337			1·40
	339		1·59			350	1·51		1·23		346	1·30		1·34
											350		1·32	
+2·0	3°	1·50			+2·8	0°		1·44			356	1·54		1·25
	128	1·32				139		1·19						
	138			0·95		154		1·14		+4·3	136°	1·12		
	154		0·25			155			1·15		137			1·06
	155			0·53		158	1·24				138		1·26	
	158	0·93				169		1·43			139	0·82	1·16	
	170		1·16			170			1·26		140			1·05
	172			1·07		176		1·38			143		1·14	
	173	0·87				179	1·15				146			1·18
	186	1·03				311	1·43				155			0·84
	302	1·38				335	1·35				155		0·67	1·17
	306		1·58			337			1·51		162		1·27	
	319	1·30		1·35		338		1·47			166			1·03
	320		1·56			349	1·48				320	1·52	1·38	
	334	1·83									326	1·28		1·38
	351			1·69	+3·4	132°			0·97		327		1·55	
	355		1·49			144			0·74		335	1·46		
						145	1·21				343			1·46
						155		1·01			348		1·30	

Negative velocities are given in italics.

The main outlines of the umbra and penumbra are shown in this figure by continuous lines.

To reduce the sight-line velocities to velocities in the spot, it is necessary to know the positions of the measured points in polar coordinates (r, ϕ) with origin at the centre of the umbra. In this system, r is the horizontal radius from the centre of the umbra and ϕ is the position angle measured counter-clockwise from the direction of solar rotation. If ΔB and $\Delta\lambda$ are the differential heliographic coordinates measured from the centre of the umbra, then

$$r = R_0[(\Delta\lambda \cos B)^2 + (\Delta B)^2]^{1/2} \text{ and } \tan\phi = \frac{\Delta B}{\Delta\lambda \cos B},$$

where R_0 is the radius of the Sun in kilometres. It is shown in Section 2.3, however, that it is better to use $r^\bullet$, the radial distance from the edge of the umbra, instead of r. The position of the edge of the umbra can be found from the enlargement so that $r^\bullet$ can be calculated from r.

The sight-line components of velocity (V) at 237 positions in the spot are given in Table V together with their coordinates (r^*, ϕ). The measured points are grouped together in eighteen annular zones, of which the mean value of r^* is given in the first column and the value of ϕ for each point in the second column. The third, fourth and fifth columns give the sight-line velocity derived from the three plates. In this table the run of V against ϕ for a given $\bar{r}^*$ for the three plates can be compared, and it will be seen that there is satisfactory agreement between the three plates for points with approximately the same ϕ.

1.4. *The errors in the sight-line velocities.*—The sight-line velocities contain no errors due to non-uniformity of the illumination of the collimator, since they are determined differentially using the atmospheric lines as standards. There are other systematic errors which will now be discussed.

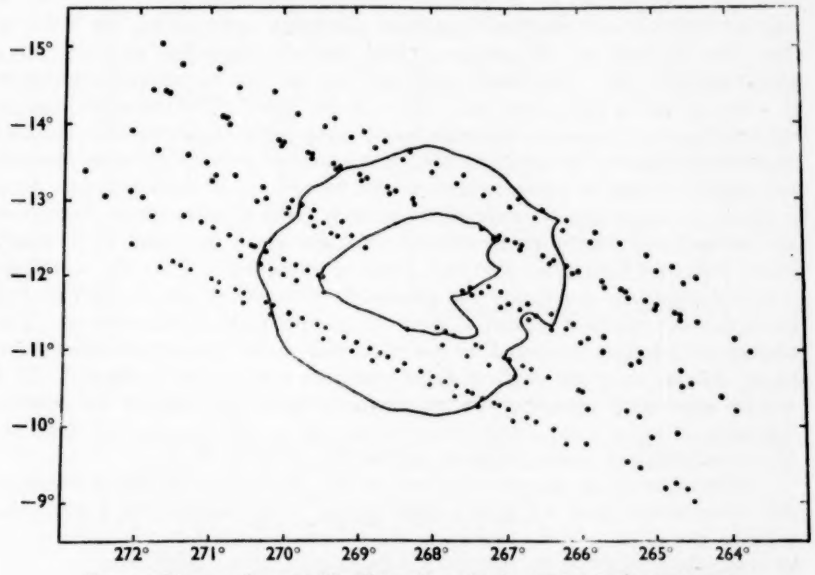

FIG. 1.—*Diagram of sunspot Mt. Wilson No. 9987 showing points of measurement. The ordinate and abscissa are heliographic latitude and longitude respectively.*

The horizontal apparatus function of the spectroscope.—It is known (**14**) that the horizontal apparatus function of the Oxford spectroscope is asymmetrical and that consequently the centre of intensity of an observed line is displaced towards the red from that of the true line by an amount which is nearly proportional to the logarithm of its equivalent width. The centre of gravity of the line however remains undisplaced with change in intensity. It is to avoid this error that lines in the spot are measured against the same lines in the centre of the disk. However, as may be seen from Table IV, some lines change their Rowland number in passing from the photosphere to the umbra, and for these lines an error due to this asymmetry will be present. An extreme upper limit to the error introduced can be found by assuming that settings are made on the centre of intensity of the line and that the lines in the penumbra have the same intensity as lines in the umbra. It is found that this limit to the error for the

mean of the fifteen lines in Table IV is 0·13 km sec^{-1}. The actual error will be a small fraction of this.

Zeeman effect.—The central field strength of the spot is 3200 gauss (**11**) and since the field drops to zero at the outer edge of the penumbra (**2**) this is an upper limit to the penumbral field. The Zeeman splitting for these lines is approximately given by the mean of the separations of the strongest σ-components. The mean splitting so calculated for all the solar lines is 0·97 Lorentz units, which gives an upper limit of $5{\cdot}1 \times 10^{-2}$ A, corresponding to 2·6 km sec^{-1} for the above field. Since a linear Zeeman pattern, such as may be expected in these lines, is symmetrical in intensity about the undisplaced line, a shift in the centre of gravity of the line can only occur if the relative intensities of the two groups of σ-components are changed by the apparatus. In the case of a spot field the σ-components are in general elliptically polarized. Each σ-component may be resolved into two plane polarized secondary components, one being in the plane defined by the magnetic field and the sight-line and the other perpendicular to it. The phase angle between the two secondary components is $+\pi/2$ for one σ-component and $-\pi/2$ for the other. The telescope changes the intensities of corresponding secondary σ-components in a given ratio and also alters their phases by the same amount. The telescope does not therefore produce any relative change in intensity between the two groups of σ-components, since it affects corresponding σ-components similarly. The absolute changes in phase and intensity for the 5-mirror Oxford telescope are in any case quite small. Plane polarized light from the Sun, when at three hours from the meridian, becomes elliptically polarized; the amplitude of the minor axis is 3 per cent of the major axis which is rotated 2° from the original plane of polarization. The changes in intensity produced by the spectroscope are greater but there is no phase change, since the single metallic reflection is at normal incidence. By a similar argument, therefore, the spectroscope does not change the relative intensities of the two groups of σ-components either, and consequently there are no errors in the sight-line velocities due to the Zeeman effect.

Obliteration of the image.—A point source photographed with a telescope and spectroscope does not give a point image. This means that a measured velocity at a point in the spectrum is the velocity averaged over an area of the corresponding point in the Sun. This averaging may be ascribed to:

(1) bad seeing;

(2) diffraction and aberration in the telescope;

(3) the vertical apparatus function of the spectroscope.

Since the spectra show streaks of 5″ height due to granules in the photosphere, the smearing of a point image into one of 5″ diameter is the maximum effect which can occur. The application of a geometrical construction due to Rayleigh (**17**) to the velocity curves to correct for such a smearing shows that a maximum error of 0·1 km sec^{-1} is introduced at a few turning points but that for over 80 per cent of the curves the error does not exceed 0·02 km sec^{-1}.

Scattered light.—Atmospheric and instrumental scattering cause some bright photospheric light to be scattered on to the darker image of the spot. Let the light scattered from an annulus of width δr and radius r on to its centre be $2\pi r U(r)\delta r$, where $U(r)$ is a scattering function. Zanstra (**26**) has shown that $U(r)$ behaves like an exponential function for $r<5''$ and as an inverse

square function for $r>40''$. A more complex function holds for intermediate distances but Redman's observations (**18**) on the distribution of light in a star image show that $U(r)$ is approximately an inverse square function for $r>5''$. This type of function (shown in Fig. 2B) is therefore used and constant scattering is assumed within $5''$.

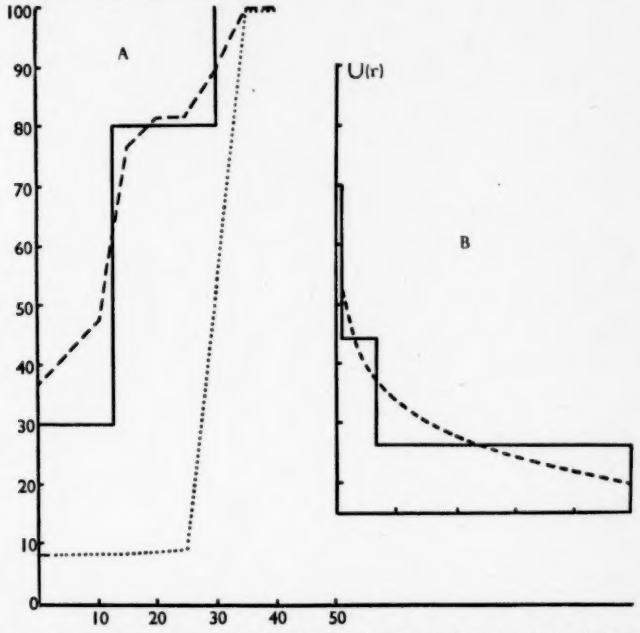

FIG. 2.—*A. The assumed true intensity profile of the spot is shown with a full curve. The distorted intensity profile is shown by a dashed curve. (Photosphere equal to 100 per cent.) The percentage scattered photospheric light is given by the dotted curve. The abscissa is in seconds of arc.*
B. The normalized function U(r) (dashed curve) and the step function (full line) which is an approximation to it. The abscissa is in minutes of arc.

The unpublished spectrophotometric observations of Miss Hart, with the Oxford telescope, show that on the average there is 2·7 per cent scattered light at a distance of $40''$ from the solar limb. If it is imagined that there are two such limbs on either side of the point, then there will be 5·4 per cent scattered light at the point and this will approximately equal the amount of light which would be scattered on to the point from distances greater than $40''$ (**12**). The light scattered from an annulus of radii r_1 and r_2 ($r_1>r_2$) on to its centre is $C \ln (r_1/r_2)$ if an inverse square scattering function is assumed. It is here assumed for simplicity that no light was scattered from beyond $5'$, but the exact value of this outer limit makes little difference to the resulting scattered light. Putting $C \ln (r_1/r_2)$ equal to 0·054, and substituting for r_1 and r_2, C can be found. The amount of light scattered between $5''$ and $40''$ can therefore be found and that remaining within $5''$ by subtracting the sum of that from the two outer zones from 100 per cent.

From the observations of Richardson (**19**) and others the true intensity profile of a spot may for the present purposes be represented by a step function

where the ratio of the intensities in umbra, penumbra and photosphere are as 0·3 : 0·8 : 1·0. The total light scattered on to any point and the region from which it came can be calculated from the true profile and this gives the apparent profile. The true profile is shown by a full curve in Fig. 2A, the apparent profile is shown by a dashed curve, while the amount of photospheric light falling on the penumbra is shown by a dotted curve. There is therefore about 9 per cent photospheric light falling on to most of the penumbral image, while the amount of the penumbral light scattered on to the photosphere is negligible. No correction for scattered light is in fact applied to the observed sight-line velocities which are about to be discussed. It must be remembered therefore that errors from this cause are undoubtedly present and that a correction would lead to an increase in the penumbral sight-line velocities of about 9 per cent and a general steepening of the velocity curve, especially at the outer edge of the penumbra.

Reversal of the positive spectrum.—Miss A. B. Hart, using the Evershed micrometer (**15**), in which the spectra can be reversed, has found a systematic difference in velocity for direct and reverse measurements of $R-D=+0{\cdot}6$ km sec^{-1}. This discordance has been confirmed by another measurer on the same negative and positive spectra, in which the atmospheric water vapour lines are weak relative to the solar lines. It would presumably entirely disappear if the atmospheric and solar lines were of comparable intensity.

As already noted, the present series of spectra in which the atmospheric water vapour lines were more nearly comparable with the solar lines was only measured in one direction. They are therefore presumably subject to a constant error of $\frac{1}{2}(R-D)$ or something of the order of 0·3 km sec^{-1}. We are, however, only interested in velocities in the penumbra relative to the photosphere and such velocities will not be affected by an error of this kind which is constant for all velocities.

Summarizing, it will be seen that line asymmetry, Zeeman effect and obliteration produce either negligibly small or zero errors. Further, the constant error of the order of 0·3 km sec^{-1} originating from measuring the spectrum in one direction only, applies equally to all points in the spot and in the photosphere outside; the velocities in the spot relative to the photosphere are therefore unaffected. The measured sight-line velocities in the spot relative to the photosphere are therefore only distorted by scattered light. The effect of this is to reduce the penumbral velocities by approximately 9 per cent and to cause a slight flattening in the velocity curve at the outer edge of the penumbra.

2. *The reduction of sight-line velocities to velocity components in the spot*

2.1. *Preliminary least-squares solutions.*—In the preceding paper (**15**) an expression has been given for the sight-line velocity (corrected for the observer's motion) in terms of the velocity components along three rectangular axes at any point on the solar surface. In considering motion in the sunspot it is more convenient to use the cylindrical velocity components, denoted here by $u=\dot{r}$, $v=r\dot{\phi}$ and $w=\dot{z}$, where r, ϕ and z are the cylindrical coordinates. The corrected sight-line velocity is then given by

$$V=v_s\cos\gamma_1+u\,(\cos\phi\cos\gamma_1+\sin\phi\cos\gamma_2)$$
$$+v\,(\cos\phi\cos\gamma_2-\sin\phi\cos\gamma_1)+w\cos\gamma_3,$$

where the direction cosines, cos γ_i, are defined in the preceding paper, and where the velocity, v_s, due to solar rotation may be taken from any standard source (**16**). Since the angle subtended at the centre of the Sun by the whole extent of the spot does not exceed 4°, we may treat the solar surface at the spot as plane with the origin of the cylindrical coordinate system at the centre of the umbra. Assuming the motion of the photospheric matter to have cylindrical symmetry about this origin, so that the velocity components u, v and w are functions of r alone, the foregoing equation of condition may be solved by least squares.

Each spectrum on a single plate gives two heights with the same value of r. Each plate with its five spectra (only four in the case of the third plate) thus gives ten measured sight-line velocities at a common value of r, from which by least squares the values of u, v and w may be found for this r. Twelve least-squares solutions at four values of r for each of the three plates showed that the tangential component, v, at each of these four values of r was less than its r.m.s. error, and that the vertical component, w, averaging $-0{\cdot}28$ km sec^{-1}, was constant over the whole penumbra and surrounding photosphere. Since the coefficient of w in the equation of condition is constant for this region (in accordance with our assumption that the surface is plane), this constant value of w is the anticipated result of a constant error ϵ in V (due to non-reversal when the spectra were measured) which would appear as $\epsilon \sec \gamma_3$ in the w-component alone. From these preliminary least-squares solutions only the radial component, u, was many times larger than its r.m.s. error, and for a given value of r was the same within its error on each of the three plates. Since the interval covered by the plates was of the order of two and a half hours this radial flow, u, may be regarded as a steady motion.

Assuming from these preliminary solutions a steady motion with $v=0$ and $w=-0{\cdot}28$ km sec^{-1}, each of the measured sight-line velocities in Table V gives a corresponding value of the velocity component u. When plotted against r these values of u show a large scatter, though with a well-marked tendency for the radial flow, u, to increase from 1·2 km sec^{-1} at the edge of the umbra to a maximum of some 2 km sec^{-1} near the centre of the penumbra, followed by a steady decrease to zero in the photospheric regions well outside the penumbra. When, however, u is plotted against $r^\bullet$ (the radial distance measured from the edge of the umbra rather than its centre) the scatter both graphically and from a computation of the r.m.s. error of u for a given $r^\bullet$, is greatly reduced.

2.2. *Definitive solution for u, v and w.*—A solution for u, v and w can now be made on the basis of these preliminary results. The points with measured sight-line velocities are divided into 16 annular zones in $r^\bullet$, the n points in a zone being assigned the mean value of $r^\bullet$ for that zone. Then, since V and ϕ are known for each point, the equation of condition for this point contains as unknowns only u, v and w, and these may be found by least squares from the n points in the zone in question.

Consider the results from this solution for the tangential component, v (shown in Fig. 3). The run of v with $r^\bullet$ is irregular and its value is generally less than its r.m.s. error (shown by a vertical line through the plotted v for a given $r^\bullet$). It is therefore probable that the calculated v is entirely due to accidental errors in the measured sight-line velocities. This hypothesis can be tested by finding the tangential velocity due to a sight-line velocity at the limit of its accidental error. The value of this limit is not less than 0·05 km sec^{-1},

since the r.m.s. residual of a single point on each plate is 0·10 km sec^{-1} (Section 1.2). If β_i is the direction cosine of the tangential velocity v_i with respect to the sight-line component V_i, then

$$V_i = \beta_i v_i$$

and the smallest observable tangential component is (0·05) β_i^{-1} km sec^{-1}. Therefore for a given zone containing n points, the mean tangential component, $\bar{v}_i$ is given by

$$\bar{v}_i = \frac{1}{n}\Sigma V_i = \frac{1}{n}0{\cdot}05\Sigma(\beta_i)^{-1} \text{ km sec}^{-1}.$$

This limiting mean component $\pm\bar{v}_i$ is shown in Fig. 3 by two broken lines. Since the observed tangential components lie almost wholly within these lines, it may be concluded that they are spurious and that there is no evidence for the existence of a tangential velocity.

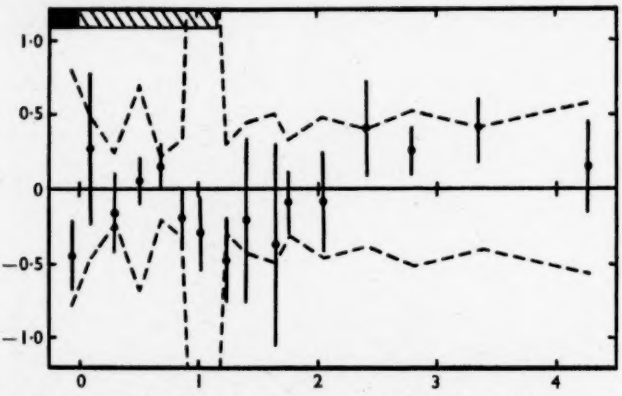

FIG. 3.—*The tangential velocity component v as a function of the radial distance r* from the edge of the umbra. The ordinate is in km sec^{-1} and the abscissa is in units of ten thousand kilometres. The penumbra extends over the range* 1·2 > r^* > 0.

The final values of u and w may now be found from a least-squares solution for these two quantities alone. The results of this solution are shown in Fig. 4, while Table VI gives the values of u and w and their r.m.s. errors, σ_u and σ_w, and the mean radius, r^*, in units of ten thousand kilometres for each annulus. The radial velocity increases from the umbra outwards to reach a maximum of about 2 km sec^{-1} in the middle of the penumbra and then decreases to zero in the photosphere outside the spot. The vertical velocity is constant within its r.m.s. error at about 0·25 km sec^{-1} over both the spot and photosphere. There is thus no vertical motion in the spot relative to the photosphere and the constant value in the photosphere is probably due to a constant systematic error of this order due to the non-reversal of the positive (Sections 1.4 and 2.1). The positions of the umbra and the penumbra shown in Figs. 3 and 4 are the mean values of r^* for twelve directions 30° apart. The outer edge of the penumbra is diffuse, so the position of this edge is only approximate.

A test of the modified cylindrical symmetry.—In making the least squares solution it has been assumed that all points in the penumbra have a common motion with cylindrical symmetry about the edge of the umbra. The validity

of this assumption can be tested by examining the residuals of the observed sight-line velocities from the sight-line velocities computed by the least-squares solution for the same position. The mean value without regard to sign of these residuals for all observed points is 0·26 km sec^{-1}. The distribution of the residuals with ϕ is found by dividing the spot into eighteen sectors of 20° each

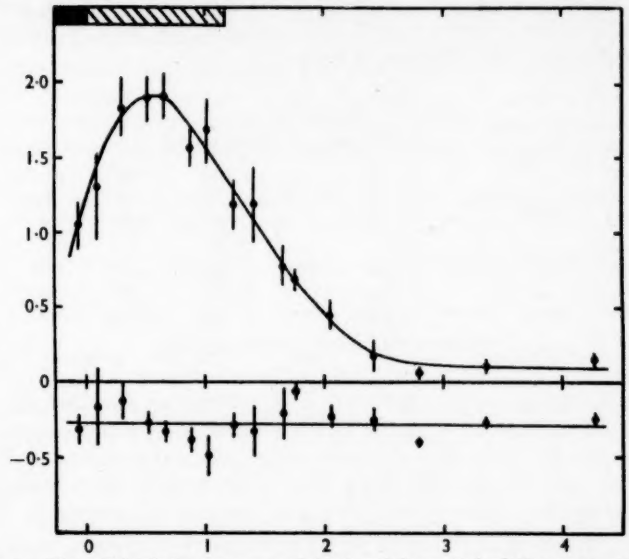

FIG. 4.—*The radial velocity component u (above) and the vertical velocity component w (below) as a function of the radial distance r^* from the edge of the umbra. The ordinate is in km sec^{-1} and the abscissa is in units of ten thousand kilometres. The penumbra extends over the range $1{\cdot}2 > r^* > 0$.*

TABLE VI

Final least squares solution for u and w in km sec^{-1}

Mean r^*	−0·1	0·1	0·3	0·5	0·7	0·9	1·0	1·2
No. of points	8	9	9	12	17	16	15	18
Mean u	+1·05	+1·30	+1·84	+1·90	+1·92	+1·67	+1·79	+1·19
σ_u	±0·16	±0·36	±0·19	±0·15	±0·15	±0·13	±0·21	±0·17
Mean w	−0·32	−0·17	−0·14	−0·28	−0·33	−0·39	−0·49	−0·29
σ_w	±0·10	±0·25	±0·12	±0·08	±0·07	±0·08	±0·14	±0·11
Mean r^*	1·4	1·6	1·7	2·0	2·4	2·8	3·4	4·3
No. of points	10	9	12	18	13	14	22	21
Mean u	+1·20	+0·78	+0·68	+0·45	+0·17	+0·05	+0·10	+0·15
σ_u	±0·24	±0·24	±0·08	±0·10	±0·11	±0·04	±0·05	±0·06
Mean w	−0·33	−0·21	−0·06	−0·24	−0·25	−0·40	−0·27	−0·25
σ_w	±0·17	±0·17	±0·06	±0·08	±0·08	±0·03	±0·04	±0·04

r^* is in units of ten thousand kilometres.

and evaluating the algebraic mean residual, $\bar{\delta}$, for each sector. These algebraic mean residuals, $\bar{\delta}$, are given in Table VII, where $\bar{\phi}$ is the mean position angle for the sector and n the number of points within it.

It will be seen from the table that in no case does $\bar{\delta}$ exceed the mean residual of all points without regard to sign of 0·26 km sec^{-1} and only for two sectors

with $\bar{\phi}$ equal to 110° and 150°, does it approach this value. It may be significant that the boundaries of the umbra and penumbra are somewhat irregular within these two sectors, and that they also contain a disturbed region in the surrounding photosphere.

Over the greater part of the penumbra, however, positive and negative residuals are equally frequent, supporting our hypothesis that the motion has cylindrical symmetry, and we shall only consider this kind of motion in the physical discussion which follows in Section 3.

TABLE VII

Distribution of mean residuals with $\bar{\phi}$

$\bar{\phi}$	10°	30°	50°	70°	90°	110°	130°	150°	170°
n	22	5	4	6	4	13	24	34	23
$\bar{\delta}$	*0·03*	*0·18*	*0·08*	*0·03*	0·00	0·26	0·10	*0·21*	0·04
$\bar{\phi}$	190°	210°	230°	250°	270°	290°	310°	330°	350°
n	14	5	2	2	5	8	18	27	22
$\bar{\delta}$	0·11	0·09	*0·06*	0·03	*0·12*	*0·09*	*0·03*	0·05	0·04

Negative residuals are given in italics.

The radial position error (Δr^*).—It is of interest to note that the random error in radial position (Δr^*) can be calculated from the r.m.s. errors of u which include, in general, errors in both sight-line velocity and position. In the outer photospheric zone, however, the r.m.s. error is almost solely due to the sight-line velocity and its mean value for the three outer zones is 0·05 km sec^{-1}. It can be shown that for a point in the penumbra with an r.m.s. error σ_u:

$$\Delta r^* = [\sigma_u{}^2 - (0{\cdot}05)^2]^{1/2} \left(\frac{du}{dr^*}\right)^{-1}.$$

The mean value of Δr^* for eight positions in the penumbra is 1 700 km on the Sun, which is of the same order as the width of the annular zones.

2.3. *Summary of results.*—Summarizing these results: the motion in the spot is shown to have modified cylindrical symmetry about the edge of the umbra rather than its centre. The velocity field in the spot at the photospheric level is wholly radial and horizontal. The calculated tangential component is shown to be entirely due to random error and the vertical velocity in the spot relative to the photosphere is zero within the error of measurement. The constant value of this component in both spot and photosphere is probably due to the constant systematic error of this order which may arise from the non-reversal of the positive spectrum (Sections 1.4 and 2.1). The radial velocity component increases outwards from the umbra to reach a maximum value of about 2 km sec^{-1} in the middle of the penumbra and then decreases smoothly to zero well out in the photosphere. There is no evidence for the sharp break in velocity at the outer edge of the penumbra suspected by Evershed. Our observed variation in u cannot be due to scattered light on the penumbra; the scattered light is only of the order of 9 per cent and any correction for this error would lead to an increase and sharpening of the curve in both spot and photosphere. As already shown, and as is evident from Table V, the flow is steady. Further, since the scatter in the velocities is within the errors of observation, there is no turbulence greater than these errors. Consequently, we may assume the flow to be laminar.

3. *A physical discussion*

The filamentary appearance of a sunspot penumbra suggests that a layer of cool umbral material is flowing radially outwards and is being gradually warmed up by the hotter sub-photospheric layers beneath it. The present observations show that such a radial horizontal flow does occur and give no evidence for vertical or tangential motion in the penumbra. Continuity demands however that there must be some vertical motion in the umbra to maintain the flow and also a corresponding subsidence in the photosphere surrounding the spot. The former phenomenon occurs outside the region of the present observations and in the latter case the cross-section of the surrounding photosphere is so large that continuity would be satisfied by a vertical velocity smaller than the limit of observation.

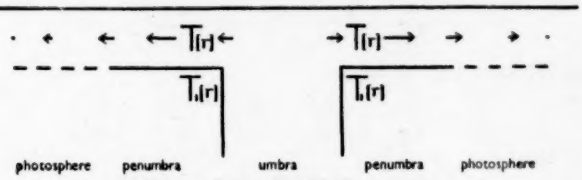

FIG. 5.—*Assumed model of a sunspot.*

In order to find a physical interpretation of the observed motion, we adopt the following simple model of the spot, which is shown in Fig. 5. The cool material from the umbra flows radially and horizontally outwards in a thin layer of optical depth τ over an infinitely deep sub-photospheric layer; the temperatures (assumed uniform with depth) of the two layers being $T(r)$ and $T_1(r)$ respectively at a distance r from the centre of the umbra. The penumbral material is neutral monatomic hydrogen and helium with spectroscopic quantities of metals, so that it is permissible to assume that its specific heat is constant at the value for an ideal monatomic gas in the range of the temperatures encountered (5000 deg. K–6000 deg. K). In accordance with observation, the flow is steady and laminar; viscous forces are ignored for the sake of mathematical simplicity.

Material at the penumbral level is not subject to the mechanical effect of the magnetic field of the spot, since it is almost wholly un-ionized. All the observed absorption lines are due to neutral atoms (mostly Fe I), at a temperature well above the Curie point of iron. A neutral atom with an atomic moment $\mathbf{m}$ in a non-uniform magnetic field $\mathbf{H}$ is however subject to a body-force $(\mathbf{m} \cdot \text{grad})\,\mathbf{H}$ (Stern–Gerlach effect), but since on the average half the atoms will be aligned with their atomic moments parallel to the field and half antiparallel, the net body-force on a macroscopic quantity of neutral matter at this temperature in any magnetic field will be zero. Changes in gravitational potential are zero, since the flow is horizontal, and the radiation pressure is ignored, since it is negligible compared with the gas pressure.

Only the mechanical and heat energies are therefore considered when this simple model is used to estimate the energy exchanges which are occurring in the penumbra and surrounding photosphere.

3.1. *Estimation of the energy exchanges in the penumbra and surrounding photosphere.*—Euler's equations of motion in their Lagrangian form give for the moving gas in our penumbral layer:

$$\frac{D}{Dt}\left(\frac{u^2}{2}\right)+\frac{1}{\rho}\frac{Dp}{Dt}=0, \qquad (1)$$

where u, ρ and p are the velocity, density and gas pressure for a unit mass of penumbral material. In the steady state observed $\partial/\partial t$ terms are zero, and (1) becomes:

$$u\left[u\frac{du}{dr}+\frac{1}{\rho}\frac{dp}{dr}\right]=0, \tag{2}$$

which is the relation between the kinetic and potential energies per unit mass. The first law of thermodynamics is:

$$\frac{Dq}{Dt}=\frac{DE}{Dt}+p\frac{D(1/\rho)}{Dt}, \tag{3}$$

where q and E are the heat absorption and internal energy per unit mass. For an ideal gas in the steady state, (3) may be written:

$$\frac{Dq}{Dt}=\frac{u}{\gamma-1}\left[\frac{1}{\rho}\frac{dp}{dr}-\gamma p\frac{d(1/\rho)}{dr}\right]. \tag{4}$$

Subtracting (2) from (4), we have:

$$\frac{Dq}{Dt}=u\left[\frac{2-\gamma}{\gamma-1}\frac{1}{\rho}\frac{dp}{dr}+\frac{\gamma}{\gamma-1}p\frac{d(1/\rho)}{dr}-u\frac{du}{dr}\right]. \tag{5}$$

Now for an ideal gas

$$\frac{dp}{dr}=C_v(\gamma-1)\left[T\frac{d\rho}{dr}+\rho\frac{dT}{dr}\right], \tag{6}$$

so that (5) becomes:

$$\frac{Dq}{Dt}=u\left[(2-\gamma)C_v\frac{dT}{dr}-2C_v(\gamma-1)\frac{T}{\rho}\frac{d\rho}{dr}-u\frac{du}{dr}\right]. \tag{7}$$

The equation of continuity for radial horizontal outflow is:

$$\frac{1}{\rho}\frac{\partial\rho}{\partial r}+\frac{1}{u}\frac{\partial u}{\partial r}+\frac{1}{r}=0. \tag{8}$$

Therefore, eliminating ρ between (7) and (8), we finally obtain:

$$\frac{Dq}{Dt}=u\left[\frac{2-\gamma}{\gamma}C_p\frac{dT}{dr}+\left(2\frac{(\gamma-1)}{\gamma}\cdot\frac{C_pT}{u}-u\right)\frac{du}{dr}+2\frac{(\gamma-1)}{\gamma}\frac{C_pT}{r}\right], \tag{9}$$

which is an expression for the heat absorbed per second per unit mass in terms of the velocity u and temperature T at a radial distance r from the centre of the umbra. The velocity u is known from the present observations, and the temperature T is calculated from the intensity profile of a spot given by Richardson (**19**), assuming that the intensity is proportional to T^4. The calculated values of Dq/Dt in erg g^{-1} sec^{-1} for sixteen values of r are given in Table VIII and illustrated in Fig. 6. It is seen that in most of the penumbra from the umbra outwards, Dq/Dt is positive, showing that heat is being absorbed to warm the cool penumbral material and also to increase its kinetic energy. Outside this region in the photosphere, Dq/Dt is negative, i.e. heat is transferred from the material to its surroundings presumably in the form of radiation, and this may account for the bright ring which, according to Waldmeier (**25**), is observed outside the penumbra.

3.2. *Estimation of the radiation absorbed in the penumbral layer.*—Milne (**9**) has shown that for a thin layer of optical depth τ at a uniform temperature T, which overlies an infinitely deep layer at a uniform temperature T_1, the net gain of radiation of the thin upper layer per unit area per second is:

$$2\pi\tau B(T_1)-4\pi\tau B(T)=2\tau\sigma[T_1^4-2T^4], \tag{10}$$

where σ is Stefan's constant. The lateral temperature gradient in the penumbral layer (0·04 deg. C per km) is small enough for this to be applicable to our model. The mass per unit area of the layer is $\tau/\bar{\kappa}$, where $\bar{\kappa}$ is the mean mass absorption coefficient in the layer, so that the net gain of radiant energy per gram is:

$$\frac{dq}{dt} = 2\bar{\kappa}\sigma[T_1^4 - 2T^4]. \qquad (11)$$

In a steady state, such as must occur in the photosphere, $dq/dt = 0$ and therefore in the photosphere $T = 0{\cdot}84T_1$. It is improbable that the penumbral material is actually in equilibrium with the radiation field. If this were the case, the transition from umbra to photosphere would be exceedingly rapid and there would be

TABLE VIII

Rate of heat absorption per gram in the penumbra

r	1·0	1·1	1·3	1·6	1·7	1·9	2·1	2·3
$\frac{Dq}{Dt}$	+3·3	+3·0	+2·2	+1·3	+0·8	−0·1	−0·3	−0·6
r	2·4	2·7	2·8	3·1	3·4	3·8	4·4	5·3
$\frac{Dq}{Dt}$	−0·8	−0·8	−0·7	−0·6	−0·3	−0·1	0·0	0·0

Dq/Dt is given in units of 10^8 erg g^{-1} sec^{-1}; r is in units of ten thousand kilometres.

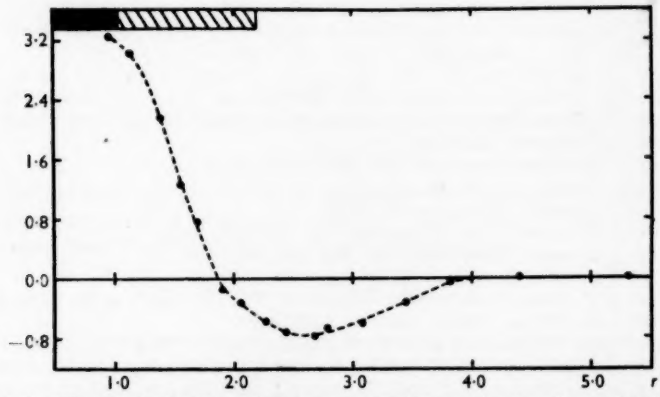

FIG. 6.—*The rate of absorption of heat per gram (Dq/Dt) as a function of the radial distance r from the centre of the umbra. The ordinate is in units of 10^8 erg g^{-1} sec^{-1} and the abscissa is in units of ten thousand kilometres. The penumbra extends over the range $2{\cdot}2 > r > 1{\cdot}0$.*

no penumbra. The time taken for the umbral material to reach equilibrium with the radiation field is thus of the order of 10^4 seconds, i.e. the time taken by it to cross the penumbra. It is however of interest to assume that equilibrium exists and to equate the rate of absorption of radiant energy by the penumbral layer given by (11) with the rate of heat absorption in the layer given by (9) at each point in the penumbra and photosphere. The temperature of the sub-photospheric layer in our model may thus be calculated and is given in Table IX for sixteen values of r. It is seen that this very rough approximation yields a reasonable value of T_1. The actual temperature of the sub-photospheric layer

would be expected to decrease inwards towards the umbra, as is found, due to the lateral transfer of radiation in the neighbourhood of the umbra.

It may therefore be concluded that the radiant energy absorbed in the penumbral layer of our simple model is of the same order as that which is required both to warm the penumbral material and increase its kinetic energy.

TABLE IX

The temperature T_1 of the sub-photospheric layer as a function of r

r	1·0	1·1	1·3	1·6	1·7	1·9	2·1	2·3
T_1	6 303°	6 397°	6 429°	6 545°	6 602°	6 682°	6 767°	6 825°
r	2·4	2·7	2·8	3·1	3·4	3·8	4·4	5·3
T_1	6 825°	6 824°	6 825°	6 825°	6 825°	6 826°	6 826°	6 826°

Assuming $\bar{\kappa}=0{\cdot}24$ as given by Strömgren (**24**) for $\tau=0{\cdot}3$,
r is in units of ten thousand kilometres.

It is a pleasure to express my sincere thanks to Professor H. H. Plaskett, not only for suggesting the investigation and providing the observational material but also for his constant help. The theory of the physical discussion, in particular, is largely due to him. I should also like to thank Miss A. B. Hart for many helpful discussions.

University Observatory,
Oxford:
1952 *April* 30.

References

(1) G. Abetti, *Publ. R. Osserv. Arcetri*, **50**, 47, 1932.
(2) S. Chapman, *M.N.*, **103**, 116, 1943.
(3) J. Evershed, *Kodaikanal Obs. Bull.*, **2**, 63, 1909.
(4) J. Evershed, *M.N.*, **69**, 454, 1909.
(5) J. Evershed, *M.N.*, **70**, 217, 1910.
(6) J. Evershed, *Mem. Kodaikanal Obs.*, **1**, Part I, 1909.
(7) J. Evershed, *Kodaikanal Obs. Bull.*, **51**, 167, 1916.
(8) *Trans. I.A.U.*, Vol. IV, p. 60, 1932.
(9) E. A. Milne, *Handbuch der Astrophysik*, Vol. III, Part I, p. 84, Springer, 1930.
(10) C. E. Moore, *Revised Multiplet Table*, 1945.
(11) "Mt. Wilson magnetic observations of sunspots", *P.A.S.P.*, **61**, 263, 1949.
(12) E. Pettit and S. B. Nicholson, *Ap. J.*, **71**, 153, 1930.
(13) H. H. Plaskett, *M.N.*, **99**, 289, 1939; *Comm. Un. Obs., Oxford*, No. 14.
(14) H. H. Plaskett, *M.N.*, **112**, 177, 1952; *Comm. Un. Obs., Oxford*, No. 33.
(15) H. H. Plaskett, *M.N.*, **112**, 414, 1952; *Comm. Un. Obs., Oxford*, No. 34.
(16) J. S. Plaskett, *Ap. J.*, **42**, 373, 1915.
(17) Lord Rayleigh, *Scientific Papers*, Vol. I, p. 135, Cambridge, 1899.
(18) R. O. Redman and E. G. Shirley, *M.N.*, **98**, 613, 1938.
(19) R. S. Richardson, *Ap. J.*, **78**, 359, 1933.
(20) Rowland's Revision, *Publ. Carnegie Inst. Washington*, 1928.
(21) C. E. St. John, *Ap. J.*, **37**, 322, 1913.
(22) C. E. St. John, *Ap. J.*, **38**, 341, 1913.
(23) F. J. M. Stratton, *M.N.*, **71**, 663, 1911.
(24) B. Strömgren, *Pub. og Meddel. Kobenh. Obs.*, No. 138, 1944.
(25) M. Waldmeier, *Astron. Mitt. Zurich*, No. 138, 439, 1939.
(26) H. Zanstra, *M.N.*, **103**, 265, 1943.

ON THE SHARPENING OF OBSERVATIONAL DATA WITH SPECIAL APPLICATION TO THE DARKENING OF THE SOLAR LIMB

P. B. Fellgett and F. B. Schmeidler†*

(Communicated by the Director of the Cambridge Observatories)

(Received 1952 March 8)

Summary

Numerical observations are sometimes blurred by convolution with some known scattering function, and it is desired to sharpen them so as to obtain the numbers that would have been observed in the absence of the blurring. It is suggested that a method of doing this by Fourier transformation has marked advantages. Although the method requires rather more arithmetical operations than are in principle necessary, the computation of the Fourier transforms on Lipson-Beevers strips so simplifies these operations that the method is economical. Moreover, when the calculation is made in this way, the effect of errors in the data is apparent both during the work and in the final result. These errors prevent complete sharpening, but a degree of sharpening can be chosen which minimizes the sum of the systematic and random differences between the reconstruction and the true distribution. This optimum sharpening depends on the statistical properties of the errors, and it is therefore suggested that in future work these properties should be measured in order that the required sharpening can be determined uniquely.

The brightness near the solar limb is recalculated by the suggested method from the results of the Göttingen measurements at the partial eclipse of 1949 April 28. It appears that photoelectric measures of brightness distributions are preferable to photographic determinations.

1. *Introduction.*—It is sometimes desired to determine a true function $T(x)$ from experimental data which give $E(x)$, the convolution of T with a known scattering or weighting function W according to the relation

$$E(x)=\int_{-\infty}^{\infty} W(y)T(x-y)dy. \tag{1}$$

This equation occurs, for example, in stellar statistics, in measurements of limb darkening, in the determination of line profiles from spectra of limited resolution and in the analysis of the spectra of rotating bodies. The solution of the equation presents no fundamental difficulty, but the calculation tends to be laborious unless some simplifying approximation is introduced.

The amount of computation that is necessary can be understood by considering that the functions E, T and W are specified numerically by ordinates at equal intervals of the arguments. Let m non-zero ordinates be necessary to define W with sufficient accuracy. Then the effect of the convolution is to blur T so that each ordinate T_n makes a contribution to m of the ordinates of E. The solution of equation (1) may be regarded as the process of collecting these m contributions together again into T_n. Since the solution depends linearly on E, T_n may be written in the form

$$T_n=\sum_{r=1}^{m} a_r E_r. \tag{2}$$

* Now at the Lick Observatory, University of California.
† Now at Universitäts-Sternwarte, München.

The evaluation of each ordinate T_n therefore requires a number of multiplications and additions of the order of m. Since the a_r are each dependent on all the ordinates of W, the order of m^2 additional operations are necessary to determine the a_r; but in many cases W is independent of n, or varies only slowly, and therefore the same values of a_r may be used to determine a large number of ordinates of T.

Numerical work can sometimes be saved by fitting W to some analytic form. The solution of equation (1) is notoriously sensitive to E, however, and we shall see from equation (4) below that it is equally sensitive to W. The use of an analytic form for W is therefore objectionable if it involves any approximation greater than the uncertainty of the data.

A procedure that has often been used is to find by trial and error a T which is consistent with W and E within the experimental error. This simplifies the computation because the solution for E is relatively insensitive to W and to the T-function assumed. The objection to the method is that although it does give a possible solution, it gives no direct indication of the extent to which this solution is demanded by the data. It seems that some such indication of the uncertainty in T is essential if misinterpretation is to be avoided, especially since this uncertainty may be large. It can probably be indicated most satisfactorily by finding the solution which follows literally from the data taken at their face value. The uncertainty is then shown by random differences between the ordinates, in the same manner as if T has been directly observed.

2. *Solution by Fourier transforms.*—A method of solution which appears to have marked advantages is that of Fourier transforms. Taking the Fourier transform of both sides of equation (1) yields

$$\int_{-\infty}^{\infty} E(x)\,e^{ix\omega}dx = \int_{-\infty}^{\infty}\int_{-\infty}^{\infty} W(y)\,T(x-y)\,e^{i.x\omega}\,dy\,dx$$

$$= \int_{-\infty}^{\infty} W(y)\,e^{i\omega y}\,dy \int_{-\infty}^{\infty} T(x-y)\,e^{i\omega(x-y)}\,dx,$$

$$\int_{-\infty}^{\infty} T(x)\,e^{ix\omega}\,dx = \frac{\int_{-\infty}^{\infty} E(x)\,e^{i\omega x}\,dx}{\int_{-\infty}^{\infty} W(y)\,e^{i\omega y}\,dy}. \qquad (3)$$

Writing the operation of Fourier transformation as F, and performing this operation on both sides of equation (3)

$$T = \mathrm{F}\cdot\left\{\frac{\mathrm{F}\cdot E}{\mathrm{F}\cdot W}\right\} \qquad (4)$$

since $\mathrm{F}^2 = 1$. In words, T is found by taking the Fourier transform of the quotient of the Fourier transforms of E and W.

In numerical Fourier transformation, the number n of ordinates in the transform is equal (by conservation of data) to the number in the original function. Since each ordinate of the transform depends on all the n input ordinates, the computation of the transform therefore requires the order of n^2 numerical operations. Using the symmetry properties of the trigonometrical functions, the number can actually be reduced to $n^2/4$. In the solution of equation (4) for n ordinates of T, it is necessary to work with n ordinates of E. The number of ordinates of W which must be used is also n, of which only m will be non-zero, in order that the transform may have n ordinates which can be divided into the n ordinates in the transform of E. (The effect of the zero ordinates in W is to introduce correlation between neighbouring ordinates of the transform :

there is a corresponding redundancy such that the transform could be adequately specified by only m ordinates, were it permissible to chose the spacing of these ordinates independently of those in the transform of E.) The three transforms of equation (4) therefore require a total of $3n^2/4$ numerical operations. According to equation (2), however, each ordinate of T is derived from the m ordinates which lie in the vicinity of the corresponding part of E. There is insufficient information in the n ordinates of E to determine fully those ordinates of T which lie near the ends of the corresponding section of E. If W is symmetrical, this will be true of the $m/2$ ordinates at each end of the range calculated. In any case, the ordinates affected will be m in number, and these must be rejected, leaving only $n-m$. The number of operations per ordinate computed is therefore $(3n^2/4)/(n-m)$, which has a minimum value of $3m$ at $n=2m$. Hence computation is minimized by dividing E into sections of twice the total width of W, and working with these separately.

It is convenient to calculate the required transforms using Lipson-Beevers strips (**1**), which were designed for Fourier transformation in X-ray crystallography. Numerical Fourier transformation involves forming sums of the kind $\Sigma a_r \cos rx$ and $\Sigma b_r \sin rx$. The strips are printed with a row of numbers representing the variation of these trigonometric functions with x at 6° intervals (3° in a later version). Each strip corresponds to a given value of a or b, and of r. Strips are selected with amplitudes a and b corresponding respectively to the ordinates of the symmetrical and anti-symmetrical parts of the function to be transformed, and with values of r corresponding to the serial numbers of these ordinates. The strips are placed in a square array, each strip forming one row. The sum of each column is then an ordinate of the required transform. Full instructions for using the strips have been given by Ross (**2**). (In understanding these instructions it is helpful to remember always that Fourier analysis and synthesis are identical operations; and also that the symmetry properties, which are used to simplify the calculation, are indicated by whether or not a row or column ends in a zero.) The strips correspond to all integral amplitudes a and b between ± 99, and enable transforms to be performed on 15, 30 or 60 ordinates (120 ordinates for the 3° strips) with 1 per cent accuracy.

It has so far appeared that the Fourier method of solving equation (1) involves some three times as many arithmetical operations as are required according to the general considerations given previously. The use of Lipson-Beevers strips, however, makes it unnecessary to perform any multiplications of the kind indicated in equation (2) (these were done once and for all in creating the strips) or even to write down the products to be added. It is only necessary to select the appropriate strips and to add in columns. This simplification greatly outweighs the apparent disadvantage, and in practice the method is relatively fast.

A further advantage of the Fourier method is that on performing the calculation it becomes obvious that equation (1) is a very idealized representation of the problem and that it is not possible to obtain a perfectly sharp representation of T. Instead of $E(x)$, there should be written $E(x)+R_1(x)$, where R_1 is a random function representing the errors of measurement. The W-function should be written $W(y)+R_2(y)$. The scattering function is essentially smooth, and by equation (1) E cannot be substantially sharper. The transforms of both W and E are therefore deficient in higher terms, and on calculating these transforms it is seen that the higher terms are in fact largely derived from the errors R_1, R_2, and therefore contribute nothing useful to the calculation of T. Consequently it is impossible

to perform literally the operation defined by equation (4), and some cut-off function must be applied to reduce the higher terms in (F.E/F.W). If this cut-off is too severe, the calculated T will be insufficiently sharpened and will differ systematically from the true T-function. If the cut-off is insufficient, the calculated T will have large random errors arising from R_1, R_2. Wiener (**3**) has discussed this problem and has shown that there exists a unique cut-off function which minimizes the mean square error due to these two causes. (The present problem is sometimes called the "infinite delay case", since the entire E-function is given before the attempt is made to estimate any ordinate of T (**4**).) The optimum cut-off depends on the auto-correlation functions of E, W, R_1, R_2 or of their sums : this function for W is defined as

$$\int_{-\infty}^{\infty} W(y)\, W(x-y)\, dy,$$

and it is equivalent to a knowledge of the power spectrum, by Kinchin's theorem. It is important, therefore, in the measurement of a quantity that is blurred by convolution, that the experiment should include a determination of the quantities necessary to fix the required cut-off. In particular, the magnitude and shape of the auto-correlograms of the errors should be measured.

3. *Application.*—We have applied the Fourier method to a re-calculation of the intensity near the solar limb using the measurements of ten Bruggencate, Gollnow and Jäger (**5**). We are greatly indebted to Professor ten Bruggencate for communicating to us unpublished details of his experimental results. In the method used by these authors, intensity measurements are made at a partial eclipse of the Sun. The radii of curvature of the limbs of the Sun and Moon are large compared with the scale of the scattering caused by atmospheric turbulence. The scattering is therefore regarded as one-dimensional (an equation analogous to (4) is applicable to the two-dimensional case but is much more laborious to evaluate).

Within the part of the photographic image corresponding to the Moon, the intensity is caused entirely by scattered light. The intensity just outside the limb of the Moon is correspondingly reduced by the scattering. If the eclipse is not too nearly total the gradient of solar intensity near to the lunar limb will be small, and it can be shown that the scattering function W is then the gradient of the intensity observed along a lunar radius in the neighbourhood of the limb. The apparent intensity across the limb of the Sun gives E. Three sets of observations were made, using photographs exposed for $\frac{1}{40}$, $\frac{1}{100}$, and $\frac{1}{200}$ second. Fig. 1 shows the "true" intensity T which we have derived from these three sets. The apparent intensity for the $\frac{1}{100}$ second exposure is also shown for comparison. The curves are drawn through the computed ordinates without any smoothing, and for clarity the three curves are separated by a vertical displacement.

The observed intensities were extrapolated in order to avoid the loss of ordinates of T which we have seen must otherwise occur at each end of the range calculated. Outside the limb, the extrapolation involves only the assumption that the intensity remains zero once it has fallen to that value. On the solar disk, several seconds of arc away from the limb, the intensity varies sufficiently smoothly for the scattering to have little effect on the observed values. Conversely, the reconstruction process produces only small corrections, and consequently it was found that the results were insensitive to the extrapolation used. The portions of T corresponding to the regions of zero intensity outside the limb are shown dotted in Fig. 1. These should differ from zero only because of rounding-off errors of the strips, and

because of errors in the observations "diffracted" into these regions by the reconstruction. They therefore provide a check on the accuracy of the method of calculation and on the presence of any arithmetical errors. This check is the more useful and sensitive because these approximately zero values are obtained by the algebraic addition of columns of which the arithmetical sums are as large as those corresponding to the ordinates on the solar disk.

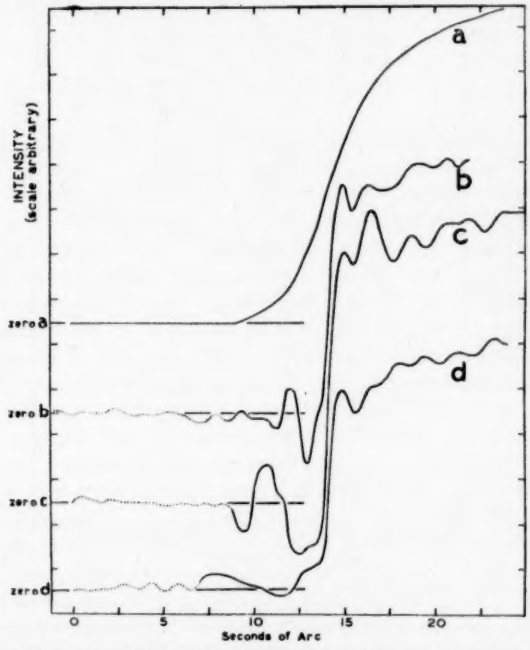

FIG. 1.—*(a) Observed intensity near the Sun's limb according to the* $\frac{1}{100}$ *second exposure of the Göttingen photographic observations. (b) Reconstructed "true" intensity derived from the* $\frac{1}{200}$ *second exposure ; (c) . . . . from the* $\frac{1}{100}$ *second exposure ; and (d) . . . from the* $\frac{1}{10}$ *second exposure. The curves are drawn through discrete ordinates every* $\frac{1}{2}$ *second of arc, and the intensity scale for each curve is arbitrary.*

The data have a relative accuracy of 0·001 and the Lipson-Beevers strips only 0·01. The computation was therefore performed on the first differences of E, which contain the same information as E but are within the accuracy of the strips. The scattering function W was already, as we have seen, obtained by differencing observed intensities. Since differencing E commutes with the operation defined by equation (4), the computation gave the differences of T, from which T was obtained by summation. As the statistical properties of the errors had not been determined, smooth cut-offs were found by trial which appeared to give the arithmetically smallest values outside the limb. The cut-offs used reduced to one half, respectively, the 15th, 20th and 25th ordinates of the transform of T, where the intervals at which the data are given are in each case sufficiently close to determine ordinates up to the 30th. The observed W was slightly skew. It is hard to see how this skewness can arise in the Earth's atmosphere, and it seems most likely that it is caused by proximity effects in the photographic plate. Such effects are non-linear and will therefore differ at the solar and lunar limbs. In the absence of

any more definite information than that the effects would probably be greater at the sharper lunar limb, it seemed best to ignore this skewness. The modulus of the Fourier transform of W was therefore used in the calculation.

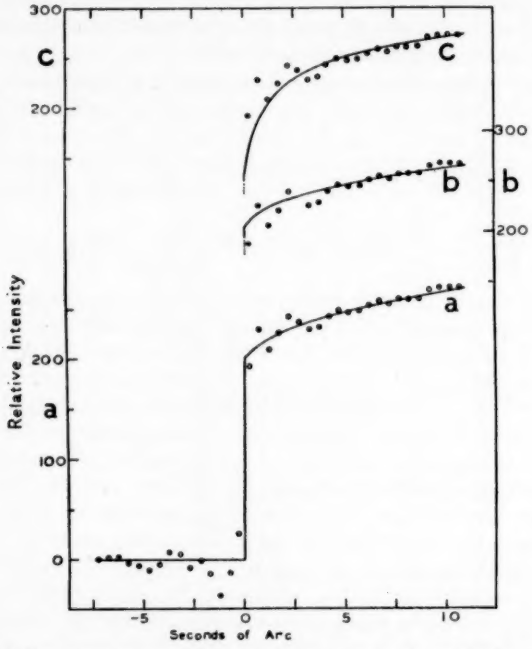

FIG. 2.—*(a) True intensity near the Sun's limb according to the weighted mean of the reconstructions for the three exposures shown in Fig. 1. The curve is drawn through the points on the assumption that the intensity is discontinuous at the limb. (b) Comparison of the points with the intensity curve calculated from the theoretical temperature distribution of de Jager and Voigt. (c) Comparison with the intensity curve derived from the original Göttingen calculations.*

It will be seen that the curves show a consistent peak where the intensity begins to flatten out after the steep rise at the limb. This persists when the cut-off is more severe than is desirable on other grounds, and cannot therefore be caused by oversharpening. It would indeed correspond to the Eberhard effect (**6**), but an at least equal effect would be expected at the limb of the Moon, in which case it would cancel out in the right hand side of equation (4). Accurate photographic photometry depends very greatly on matching the densities produced under identical conditions. When this cannot be done, as here in the comparison of E and W, the complexity of the factors determining photographic density is liable to lead to uncertainties. There would seem to be considerable advantages in making the measurements photoelectrically. The accuracy of such measures can be very high, they may be made substantially free from non-linear and from proximity effects, and the properties of the noise disturbing the measurements are better understood than is photographic granularity.

Fig. 2 shows the smoothed curve based on the mean of all the data. Weights of 2, 3 and 4 respectively were assigned to the three sets, in order to allow to some

degree for the narrower W of the shorter exposures. The curve was drawn by eye on the assumption, which is at least not contradicted by the points, that there is a discontinuity at the limb. Some values read from the curve are given in Table I.

TABLE I

Distance from limb	Relative Intensity	Distance from limb	Relative Intensity
"		"	
0·0	(0—200)	4·0	240
0·5	208	5·0	246
1·0	216	6·0	250
1·5	222	7·0	255
2·0	226	8·0	260
2·5	230	9·0	264
3·0	234	10·0	267

In the upper part of Fig. 2 the points are compared with the intensity distribution according to the original Göttingen calculations, and with that calculated at Göttingen from the temperature distribution predicted theoretically by de Jager and Voigt. The curves are drawn from the data given in Table I of ten Bruggencate, Gollnow and Jäger's paper (**5**). The intensity scale of the present calculations is arbitrary, and in both comparisons it has been adjusted to give a good overall fit. It will be seen that the two calculations agree closely, but that near the limb the present results are in better accord with the de Jager-Voigt curve. Indeed it now appears that, in the region shown in the figure, the de Jager-Voigt curve is consistent with the Göttingen observations. Nevertheless it will be noticed that the points near the limb are slightly lower, relative to the theoretical curve, than those at the opposite end of the diagram. This circumstance may indicate that the intensity varies a little more steeply than the theory predicts ; the Göttingen observers drew a similar conclusion from their calculations.

4. *Acknowledgments.*—The calculations on the intensity near the solar limb were made possible by the kindness of Professor ten Bruggencate in allowing us to use his original observational data for this purpose. The authors are also grateful to Professor Sir Lawrence Bragg and to Professor R. O. Redman for their interest, help and advice ; and to the Crystallographic Department of Cavendish Laboratory for allowing us to use their computing facilities including the Lipson-Beevers strips. One of the authors (F. B. S.) is indebted to the British Council for a Fellowship which enabled him to work at the Cambridge Observatories, and the other author (P. B. F.) was supported by an Isaac Newton Studentship during the period within which the investigation was made.

The Observatories,
Madingley Road,
Cambridge :
1952 *March* 7.

References

(1) Lipson, H. and Beevers, C. A., *Proc. Phys. Soc.*, **48,** 772, 1936; *Nature*, **137,** 825, 1936. The strips may be obtained through Dr C. A. Beevers, Dewar Crystallographic Laboratory, King's Buildings, Edinburgh, 9.

(2) Ross, M. A. S., *Nature*, **152,** 302, 1943.

(3) Wiener, N., *Extrapolation, Interpolation and Smoothing of Stationary Time Series*, Willey and Sons, New York, 1949.

(4) Bode, H. W. and Shannon, C. E., *Proc. Inst. Radio Engrs.*, **38,** 417, 1950.

(5) ten Bruggencate, P., Gollnow, H. and Jäger, W., *Zs. f. Astrophys.*, **27,** 223, 1950.

(6) Mees, C. E. K., *The Theory of the Photographic Process*, p. 875, Macmillan and Co., New York, 1942.

ON TELESCOPIC STAR IMAGES

E. H. Linfoot and E. Wolf

(Received 1951 December 5)

Summary

Diffraction theory is applied to discuss the properties of the polychromatic, three-dimensional star images formed by refracting doublet objectives. The effects of the secondary spectrum on the light distribution in the diffraction image and on the position of best focus are examined quantitatively in two special cases: (A) an $f/15$ refractor of $24\frac{7}{8}$ inches aperture, (B) a similar refractor of one-third the linear dimensions. The image formed by an $f/15$ reflector working without central obstruction (Case R) is analysed for comparison purposes.

1. *Introduction*

The first explanation of the main features of the stellar images seen in a good telescope was given by Airy (1835) (**1**). He showed that, as a direct consequence of the undulatory theory of light, a stellar image should exhibit the well-known appearance of a bright central dot (the "star disc") surrounded by faint concentric rings. Airy assumed the telescope to be of circular aperture and free from aberrations or central obstruction, the effects of air tremor to be negligible, and the light to be monochromatic. Thus his analysis, of fundamental importance as the starting point for later work, was far from providing an adequate treatment of the formation of star images in the large astronomical telescopes which have been developed since his day.

Rayleigh (**2**) in 1880 carried the theory forward by investigating the case where small amounts of primary spherical aberration are present; like Airy, he took the light to be monochromatic. He did not discuss the image in detail, but showed that, with amounts of spherical aberration not exceeding one-quarter of a wave-length, the intensity at the centre of the star disk at paraxial focus was diminished by not more than 20 per cent.

Lommel (1885) (**3**)*, in a paper of great power and scope, discussed in detail the properties of the out-of-focus, aberration-free monochromatic image of a point source by a circular objective and confirmed the predicted appearances experimentally, using a monochromatic light source. The numerical part of his work was only carried through for images fairly close to focus. A more convenient method of calculating the images far from focus was developed thirteen years later by K. Schwarzschild (**4**), who used asymptotic expressions for the intensities.

Almost at the same time as Lommel, H. Struve (1886) (**5**) published an independent and very similar analysis; he did not work out the numerical consequences in such detail, but he gave valuable approximate expressions for the intensity near the edge of the geometrical shadow, where the Lommel–Struve expansions are rather slowly convergent.

* The date of this paper is sometimes given as 1884 or 1886. A later paper (Lommel, *ibid.*, 531–664, 1886) deals with diffraction by rectangular apertures, obstacles and slits.

These investigations still left a rather wide gap between the theory of telescopic star images and their observed appearance. Not only did they leave out of account the effects of atmospheric tremor, but they did not discuss the powerful effects of the secondary spectrum on star images in large refracting telescopes. However, by 1886, Lommel's and Struve's work had provided a means of predicting the three-dimensional light distribution near the focus of an error-free monochromatic image.

No actual diagram of this distribution was published until Berek's paper (**6**) appeared in 1926. A new and more accurate diagram, based on a different expansion of the Huygens–Kirchhoff diffraction integral from those obtained by Lommel and Struve, was recently worked out by Zernike and Nijboer (**7**); it is reproduced as Fig. 2 below.

The delay in working out the light-distribution diagram was the more surprising since Dennis Taylor, in his stimulating and entertaining paper (**8**) on the secondary colour aberrations of visual telescopes, had in 1894 made abundantly clear the importance of a knowledge of this distribution to the makers and users of astronomical refractors.

It was not until 1919 that the subject was carried further by A. E. Conrady (**9**), who worked out in some detail the light distribution in slightly defocused images, and in images possessing small amounts of spherical aberration, the receiving plane in the latter case being placed at paraxial focus, at marginal focus and midway between the two. So far as defocusing was concerned, his results did not go beyond Lommel's. His computations were later extended by A. Buxton (**10**) and L. C. Martin (**11**).

The next substantial contributions to the theory were made in 1925 by Picht (**12**) and by Steward (**13**). Both considered the effects of Seidel aberrations on the light distribution in monochromatic diffraction images, and this subject has since been fairly extensively discussed during the past 25 years. However, apart from the computed figure of Zernike and Nijboer already mentioned, the only work published during this period which has an immediate bearing on the topic of star images in visual telescopes is Steward's investigation, in the paper just referred to, of the effect on the images of a central obstruction of the telescope aperture.

In the present paper we take up once more the old question of star images in visual refracting telescopes and develop the theory to the point where a quantitative estimate can be obtained of the light lost from the central part of the image by the combined effects of diffraction and of the secondary spectrum. Some comparison results for reflectors are also obtained. A preliminary survey of the problem showed that to carry out this programme on the basis of the existing mathematical literature would involve a very large amount of computational labour, and the attempt was therefore postponed until an extension of Lommel's and Struve's analysis by one of us (Wolf (**14**)) had made the work easier.

The part played by atmospheric tremor is very different in the visual and in the photographic use of telescopes. In the former, the rare moments of best "seeing" are seized upon by the eye, and eye and memory work together to build up a picture from what has been glimpsed. In the latter, the photographic plate records indiscriminately whatever reaches it during the exposure time and consequently it is the tremor disk—or rather its average over the long exposure time—which is recorded on the plate.

It follows that a study of the effect of atmospheric tremor is an essential part of any adequate theory of the photographic star images formed by large astronomical telescopes, while a theory of visual star images *as glimpsed during moments of nearly perfect seeing* may, and indeed should, be developed without taking account of the effects of tremor. Accordingly, we have not attempted to incorporate a theory of tremor disks into the present analysis, although we do include some results which could be used to obtain a rough estimate of the space-penetrating power of large refractors and reflectors under conditions of average seeing.

2. *Mathematical Preliminaries*

We begin with a brief account of some known results (Lommel (**3**), H. Struve (**5**), Wolf (**14**)) on monochromatic light distribution in space near the focus of converging spherical waves issuing from a circular aperture. The formulae derived in (**3**) and (**5**) concern intensity distribution; those in (**14**) the total illumination within an arbitrarily given circle about the origin in the receiving plane. The intensity formulae form the basis of the later work and because the handling of the approximations and error terms by Lommel and Struve was not quite precise enough for the purposes of the present investigation, they are rederived here by a more accurate discussion.

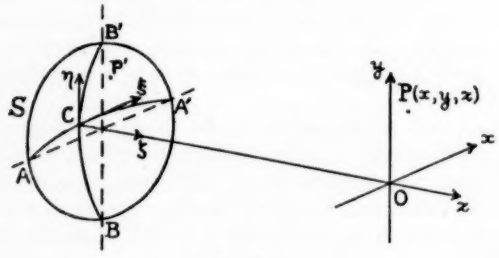

FIG. 1.

In Fig. 1, ABA′B′ represents a circular aperture through which issues a train of converging spherical waves of wave-length λ. $2a = AA'$ is the diameter of this aperture, C the pole of the wave surface S which momentarily fills it, O the centre of curvature of S. We call CO the axis of the wave train and set $CO = f$.

Ox, Oy, Oz are axes of Cartesian coordinates (x, y, z) in the space near O; Cξ, Cη, Cζ axes of Cartesian coordinates (ξ, η, ζ) in the space near C. It is assumed throughout that $a/f \ll 1$.

By Huygens' principle, the complex displacement at $P(x, y, z)$, near O which results from waves of unit amplitude on S is

$$D_\lambda(P) = \frac{i}{\lambda} e^{ikf} \iint_S \frac{e^{-iks}}{s}\, dS, \tag{2.1}$$

where s denotes the distance of P from the element dS located at $P'(\xi, \eta, \zeta)$, on the wave front filling the aperture and $k = 2\pi/\lambda$. Write

$$\left.\begin{aligned} \xi &= a\rho\cos\phi, & x &= r\cos\psi, \\ \eta &= a\rho\sin\phi, & y &= r\sin\psi. \end{aligned}\right\} \tag{2.2}$$

Then

$$dS = a^2\rho\, d\rho\, d\phi, \tag{2.3}$$

with an error which in the case of an $f/15$ telescope nowhere exceeds one part in 1000, and hence

$$D_\lambda(\mathrm{P}) = \frac{ia^2}{\lambda} e^{ikf} \int_0^1 \int_0^{2\pi} \frac{e^{-iks}}{s} \rho \, d\rho \, d\phi. \tag{2.4}$$

Now on the surface S

$$\zeta = f - \sqrt{(f^2 - a^2\rho^2)} = f - f\left\{1 - \frac{1}{2}\frac{a^2\rho^2}{f^2} - \frac{1}{8}\frac{a^4\rho^4}{f^4} - \ldots.\right\}$$
$$= \frac{a^2\rho^2}{2f} + \frac{a^4\rho^4}{8f^3} + \ldots.. \tag{2.5}$$

Therefore

$$s^2 = \mathrm{PP}'^2 = (x-\xi)^2 + (y-\eta)^2 + (z-\zeta+f)^2$$
$$= (x^2+y^2+z^2) + (\xi^2+\eta^2+\zeta^2) - 2(x\xi + y\eta + z\zeta) + 2f(z-\zeta) + f^2$$
$$= [(f+z)^2 + r^2] + [(f-\zeta)^2 + a^2\rho^2] - f^2 - 2ar\rho\cos(\phi-\psi) - 2z\zeta$$
$$= \mathrm{CP}^2 + \mathrm{OP}'^2 - f^2 - 2ar\rho\cos(\phi-\psi) - 2z\zeta$$
$$= R'^2 - 2ar\rho\cos(\phi-\psi) - 2z\zeta \tag{2.6}$$

(where R' is written for CP)

$$= R'^2 - 2ar\rho\cos(\phi-\psi) - z\left(\frac{a^2\rho^2}{f} + \frac{a^4\rho^4}{4f^3} + \ldots.\right). \tag{2.7}$$

When $a/f = \frac{1}{30}$ (as it is in an $f/15$ refracting telescope), the error in replacing the last term of (2.7) by $za^2\rho^2/f$ does not exceed $\frac{1}{3600}$ of $za^2\rho^2/f$.

If P is only a "finite number" $O(1)$ of fringes away from focus laterally*, then $ar\rho/f = O(\lambda)$. If P is only a "finite number" $O(1)$ of fringes away from focus longitudinally, then $az \,.\, a\rho/2f^2 = O(\lambda)$. Both these conditions are satisfied in the region we wish to investigate. Therefore in this region

$$2ar\rho/f = O(\lambda), \qquad \tfrac{1}{2}za^2\rho^2/f^2 = O(\lambda), \tag{2.8}$$

where O means "less than a moderate multiple of", say 5 or 10.

From (2.7), (2.8)

$$s = R'\left[1 - \frac{2ar\rho}{R'^2}\cos(\phi-\psi) - \frac{z}{R'^2}\left(\frac{a^2\rho^2}{f} + \frac{a^4\rho^4}{4f^3} + \ldots.\right)\right]^{1/2}$$
$$= R' - \frac{ar\rho}{R'}\cos(\phi-\psi) - \frac{za^2\rho^2}{2fR'} + O\left(\lambda\frac{a^2}{f^2}\right) + O\left(\frac{\lambda^2}{f}\right). \tag{2.9}$$

The term $O(\lambda^2/f)$ is negligible since $\lambda \simeq 2 \times 10^{-5}$ inch and f is not small. The term $O(\lambda a^2/f^2)$ is $O(\lambda/900)$ in an $f/15$ pencil and so is negligible in a refracting telescope when P is only $O(1)$ fringes away from focus.

Therefore in investigating the value of (2.4) in the present problem we may set

$$s = R' - \frac{ar\rho}{R'}\cos(\phi-\psi) - \frac{za^2\rho^2}{2fR'},$$
$$ks = kR' - f/R'[v\rho\cos(\phi-\psi) + \tfrac{1}{2}u\rho^2],$$

where the new variables u, v are defined by the equations

$$u = \frac{ka^2z}{f^2}, \qquad v = \frac{kar}{f}. \tag{2.10}$$

In physical terms, $u/4\pi$ is the number of fringes of defocusing and v/π the number of fringes of lateral displacement of P relative to O. We note that $|v/u| \lesssim 1$

* That is to say, if the displacement of P from O would correspond to the appearance of only a "finite number" $O(1)$ of fringes on the surface S seen under test in an interferometer. $ar/f = \lambda/2$ gives "one fringe of lateral displacement"; $za^2/f^2 = 2\lambda$ gives "one fringe of defocusing".

according as P lies in the geometrical cone of rays or in the geometrical shadows. From (2.4), on substituting for ks and noting that $R'=f+O(\lambda)$ in the region where $u/4\pi$, v/π are both $O(1)$, we now obtain the approximate formula

$$D_\lambda(\mathrm{P})=\frac{ia^2}{\lambda f}\exp[ik(f-R')]\int_0^1\int_0^{2\pi}\exp\{i[\tfrac{1}{2}u\rho^2+v\rho\cos(\phi-\psi)]\}\rho\,d\rho\,d\phi$$
$$=\frac{2\pi ia^2}{\lambda f}\exp[ik(f-R')]\int_0^1\exp(\tfrac{1}{2}iu\rho^2)J_0(v\rho)\rho\,d\rho. \tag{2.11}$$

The integral on the right of (2.11) can be evaluated in terms of the functions

$$U_n(u,v)=\sum_{m=0}^{\infty}(-1)^m\left(\frac{u}{v}\right)^{n+2m}J_{n+2m}(v) \tag{2.12}$$

introduced by Lommel for this purpose; in fact (see Watson, "Bessel Functions", p. 541)

$$2\int_0^1 J_0(v\rho)\exp(\tfrac{1}{2}iu\rho^2)\rho\,d\rho=C(u,v)+iS(u,v), \tag{2.13}$$

where

$$\left.\begin{aligned}C(u,v)&=\frac{\cos\frac{1}{2}u}{\frac{1}{2}u}U_1(u,v)+\frac{\sin\frac{1}{2}u}{\frac{1}{2}u}U_2(u,v),\\ S(u,v)&=\frac{\sin\frac{1}{2}u}{\frac{1}{2}u}U_1(u,v)-\frac{\cos\frac{1}{2}u}{\frac{1}{2}u}U_2(u,v).\end{aligned}\right\} \tag{2.14}$$

(2.11) therefore gives

$$D_\lambda(\mathrm{P})=\frac{\pi a^2}{\lambda f}\exp\left\{ik\left[(f-R')+\chi(u,v)+\frac{\pi}{2}\right]\right\}\sqrt{(C^2+S^2)}, \tag{2.15}$$

where C, S are written for $C(u,v)$, $S(u,v)$ respectively,

$$\cos\chi=\frac{C}{\sqrt{(C^2+S^2)}},\qquad \sin\chi=\frac{S}{\sqrt{(C^2+S^2)}} \tag{2.16}$$

and

$$\sqrt{(C^2+S^2)}=\frac{2}{u}\sqrt{\{U_1^2(u,v)+U_2^2(u,v)\}}. \tag{2.17}$$

The intensity $I_\lambda(z,r)=I(u,v)$ at P is then given by the equation

$$\begin{aligned}I_\lambda(z,r)&=|D_\lambda(\mathrm{P})|^2\\ &=\frac{4\pi^2a^4}{\lambda^2f^2}(C^2+S^2)\\ &=\frac{4\pi^2a^4}{\lambda^2f^2}\,\frac{1}{u^2}[U_1^2(u,v)+U_2^2(u,v)].\end{aligned} \tag{2.18}$$

(2.18) is valid, subject to the limitations already imposed by our approximations, for all u, v; but it is only convenient for computation when $|v/u|>1$. When $|v/u|<1$ it may, as Lommel showed, be replaced with advantage by the equivalent formula*

$$I_\lambda(z,r)=\frac{4\pi^2a^4}{\lambda^2f^2}\,\frac{1}{u^2}\left[1+V_0^2(u,v)+V_1^2(u,v)\right.$$
$$\left.-2V_0(u,v)\cos\left\{\frac{1}{2}\left(u+\frac{v^2}{u}\right)\right\}-2V_1(u,v)\sin\left\{\frac{1}{2}\left(u+\frac{v^2}{u}\right)\right\}\right], \tag{2.19}$$

* When $|v/u|=1$, (2.18) and (2.19) reduce to

$$I_\lambda(z,r)=\frac{\pi^2a^4}{\lambda^2f^2}\,\frac{1}{u^2}[J_0^2(u)-2J_0(u)\cos u+1].$$

where

$$V_n(u,v)=\sum_{m=0}^{\infty}(-1)^m\left(\frac{v}{u}\right)^{n+2m}J_{n+2m}(v). \tag{2.20}$$

Lommel used in his argument slightly different approximations from those made in the above modernized version; for example, his parameters specifying the position of P are not strictly identical with ours. But the final formulae (2.18), (2.19) are the same.

In the geometrical focal plane, $u=0$ and (2.18) reduces to

$$I_\lambda(0,r)=\frac{4\pi^2a^4}{\lambda^2f^2}\left(\frac{2J_1(v)}{v}\right)^2, \tag{2.21}$$

in agreement with Airy (**1**). On the axis, $v=0$ and (2.19) gives

$$I_\lambda(z,0)=\frac{4\pi^2a^4}{\lambda^2f^2}\left(\frac{\sin\frac{1}{4}u}{\frac{1}{4}u}\right)^2. \tag{2.22}$$

Lommel's equations (2.18), (2.19) for the intensity distribution in space near focus formed the starting point for the derivation by one of us (Wolf (**14**)) of expressions, needed below, for the fraction of the total illumination L which falls inside a given small circle about the (x,y)-origin in the receiving plane $z=$ constant. We define

$$L_\lambda(z,r_0)=\frac{1}{\pi a^2}\int_0^{r_0}\int_0^{2\pi}I_\lambda(z,r)r\,dr\,d\phi. \tag{2.23}$$

To the order of accuracy here in question, $L_\lambda(z,r_0)$ measures the fraction of the total energy issuing from the aperture which reaches the circle $r\leqq r_0$ in the given receiving plane. Then

$$\begin{aligned}L_\lambda(z,r)=&\left(\frac{v}{u}\right)^2\left[1+\sum_{s=0}^{\infty}\frac{(-1)^s}{2s+1}\left(\frac{v}{u}\right)^{2s}Q_{2s}(v)\right]\\&-\frac{4}{u}\left[Y_1(u,v)\cos\left\{\frac{1}{2}\left(u+\frac{v^2}{u}\right)\right\}+Y_2(u,v)\sin\left\{\frac{1}{2}\left(u+\frac{v^2}{u}\right)\right\}\right]\qquad(|v/u|\leqq 1)\end{aligned} \tag{2.24}$$

$$=1-\sum_{s=0}^{\infty}\frac{(-1)^s}{2s+1}\left(\frac{u}{v}\right)^{2s}Q_{2s}(v),\qquad(|v/u|\geqq 1), \tag{2.25}$$

where

$$Y_n(u,v)=\sum_{s=0}^{\infty}(-1)^s(n+2s)\left(\frac{v}{u}\right)^{n+2s}J_{n+2s}(v), \tag{2.26}$$

$$Q_{2s}(v)=\sum_{i=0}^{2s}(-1)^i[J_i(v)J_{2s-i}(v)+J_{i+1}(v)J_{2s+1-i}(v)]. \tag{2.27}$$

When $u=0$, (2.25) reduces to Rayleigh's formula

$$L_\lambda(0,r)=1-Q_0(v)=1-J_0^2(v)-J_1^2(v). \tag{2.28}$$

When $|v/u|=1$, (2.24) and (2.25) reduce to $L_\lambda(z,r)=1-J_0(u)\cos u-J_1(u)\sin u$. Figs. 2 and 3 show the distribution of $I_\lambda(z,r)$ and $L_\lambda(z,r)$ near focus in each meridional plane. In Fig. 3 the curves $L_\lambda(z,r)=$ const., or $L(u,v)=$ const. can be regarded as analogues in a certain sense of the rays of the geometrical theory. Their form near the geometrical focus $(u,v)=(0,0)$ agrees well with that postulated by Dennis Taylor (**8**) on experimental grounds for the "cone" of light near focus. The comparison is rather rough and ready, since Taylor's

observations were made in polychromatic light. Nevertheless, his value of just below $\pm 0{\cdot}2$ mm for the permissible focal tolerance of an $f/15$ pencil is in good accordance with Figs. 2 and 3.

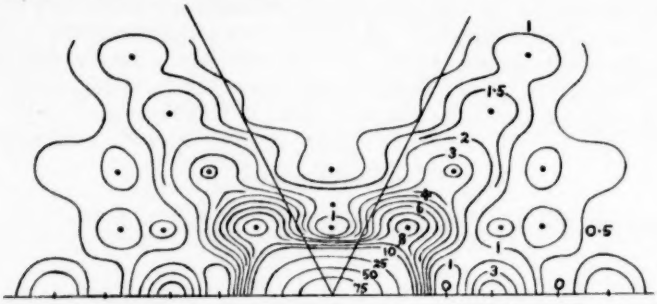

FIG. 2.—*Isophotes of an aberration-free pencil near focus. (Contour lines of* $I(u, v) = I_\lambda(z, r)$.*) The figure covers approximately the region* $-35 \leq u \leq 35$, $0 \leq v \leq 15$. *The straight lines show the boundary of the geometrical shadow. The numbers give intensities as a percentage of the intensity at focus. Axial maxima and minima are indicated by short strokes; others by small circles. (After Zernike and Nijboer.)*

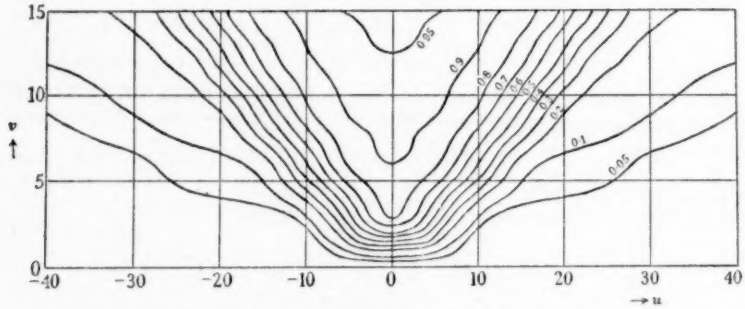

FIG. 3.—*Contour lines of* $I(u, v) = I_\lambda(z, r)$, *the fraction of the total illumination inside circles* $r = \text{const.}$ *in receiving planes* $z = \text{const.}$ *near focus, expressed in terms of the scale-normalized co-ordinates* $u = \dfrac{2\pi a^2 z}{\lambda f^2}$, $v = \dfrac{2\pi a r}{\lambda f}$. *(After Wolf.)*

3. *Star images formed by telescope objectives*

3.1. The results of the last section can be used to analyse the structure of star images formed by refracting and reflecting telescopes at the centre of their field of view and to draw conclusions about the relative efficiency of the two types of instruments under conditions of perfect "seeing".

In a refracting telescope with a well-figured doublet objective achromatized for visual use, the only appreciable optical error affecting the axial images is the secondary spectrum, the effect of which is to bring the light of each separate wave-length to a separate focus.

This focal spread leads to a rather serious loss of light in the central diffraction disks of star images formed by large refractors; Dennis Taylor (**8**) estimated the loss as high as 42 per cent in a 24-inch refractor of 30 feet focal length. But this estimate rested on too primitive a theoretical foundation to be quantitatively reliable, and an ingenious attempt two years later by the same author

(**15**) to investigate the problem experimentally likewise failed to give more than a very rough estimate of the light loss.

To obtain a quantitative description of the image, we need to analyse, in terms of wave-length and intensity, the light distribution in space near focus which results from the superposition of the three-dimensional diffraction images formed in light of all the relevant wave-lengths. Each of these images can be taken to be similar to the "aberration-free diffraction image" represented in Fig. 2, but their size and brightness vary with the wave-length and their centres are distributed along the axis in accordance with the colour curve of the objective.

To make the problem sufficiently precise for numerical calculation, we must introduce some assumptions about the colour curve of the objective and its focal ratio, the energy distribution in the spectrum of the star whose image is being investigated, and the relative sensitivity of the eye in different regions of the visual spectrum. The product of the last two quantities gives the effective visual brightness distribution of the starlight as a function of wave-length.

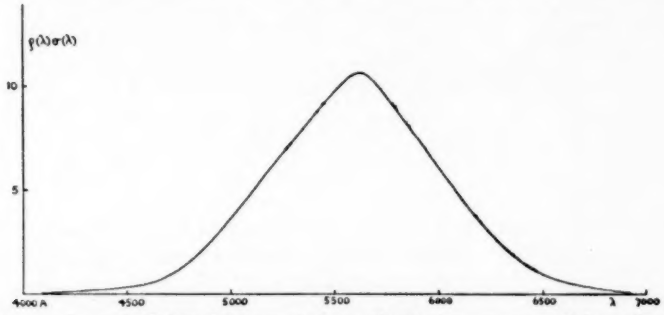

FIG. 4.—*Assumed effective brightness function $\rho(\lambda)\sigma(\lambda)$ for average starlight. $\rho(\lambda)$ is taken from the Planck curve for $T=6000$ deg. K; $\sigma(\lambda)$ from the visibility curve of the average human eye for light of ordinary brilliance.*

Fig. 4 shows the distribution assumed. It is derived by multiplying Planck's ideal energy distribution function $\rho(\lambda)$ corresponding to a temperature $T=6000$ deg. K and the visibility function $\sigma(\lambda)$ of the average human eye* for light of ordinary brilliance. This choice of $\rho(\lambda)$, which corresponds to the "smoothed" G-type stars, is intended to represent a special case of practical importance. It is one rather favourable to the refractor, since it is one in which the visually brightest part of the spectrum comes near to the turning point of the colour curve of an ordinary visual doublet objective. For a considerable range of colour temperatures it is the σ-function, with its maximum at about 5500 A, which dominates the results and in this range our numerical findings continue to give a fairly accurate picture of the situation. But when used on a blue or on a red star, a visual refractor of normal design would not perform as well as on the yellow stars considered in the remainder of this paper.

We make two different assumptions about the colour curve of the objective, corresponding respectively to the cases of a large visual refractor of about 24 inches aperture and 30 feet focal length and of a medium-sized visual refractor of the same design but of one-third the linear dimensions. These cases seem useful ones to examine, since experience shows that, for refractors working at about the

* Taken from Strong, *Procedures in Experimental Physics*, New York, p. 449, 1936.

usual focal ratio $f/15$, the colour correction is satisfactory to the eye in an 8-inch objective and far from satisfactory in a 24-inch, even though the angular colour aberrations in the two systems may be identical.

More precisely, we consider the following cases of practical interest:

Case A. (The Newall telescope at Cambridge.) A refractor of $24\frac{7}{8}$ inches aperture and 29 feet focal length, with a colour curve shown in Fig. 5. The minimum focus is in light of wave-length $\lambda_m = 5660$ A. We take this as a typical large visual refractor.

Case B. A refractor of one-third the linear dimensions of the Newall telescope; that is, one of aperture $8\frac{7}{24}$ inches and focal length $9\frac{2}{3}$ feet, whose colour curve is obtained from Fig. 5 on reducing the ordinates in the ratio 1:3. This is near to the dimension and colour curve of the Thorrowgood refractor at Cambridge and of many other excellent 8-inch refractors made by Messrs Cooke and Sons in the early part of this century.

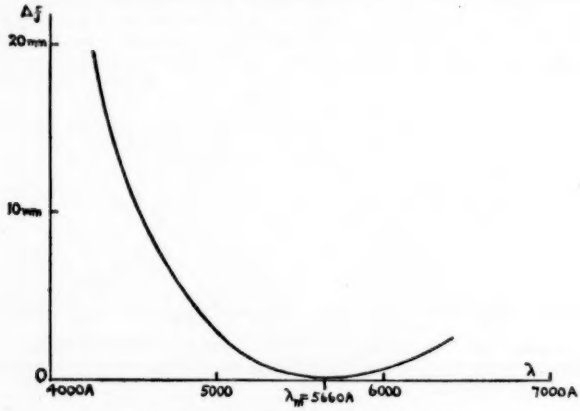

FIG. 5.—*Colour curve of the Newall telescope.*

We also consider, for comparison purposes, the hypothetical Case R of a reflecting telescope of the same focal ratio as the Newall telescope and as the refractor in Case B. (The image formed by a reflector working in polychromatic light depends, in all respects except brightness, on its focal ratio and not on its linear dimensions.)

Case R probably does not correspond to any existing telescope, since one must go back to Herschel's time to find examples of reflectors working, without central obstruction, at focal ratios as long as $f/15$. But from Case R may be derived at once the corresponding results for a Herschelian reflector working at any other focal ratio, since the polychromatic diffraction images at different focal ratios differ only by a simple linear transformation.

3.2. *The "summed visual intensity" and the "summed visual illumination".*—Fig. 6 represents a pencil of light of wave-length λ issuing from the circular exit pupil of a telescope objective and converging towards the corresponding geometrical focal point F_λ on the axis of the telescope. Let λ_m denote the value of λ for which the geometrical focal length of the objective is a minimum. We take the corresponding focal point F_{λ_m} as the origin O of Cartesian coordinates (x, y, z), the axis Oz being along the principal ray of the pencil. In these coordinates

F_λ is the point $(0, 0, \delta(\lambda))$, where the value of $\delta(\lambda) = F_{\lambda_m} F_\lambda$ can be read off from the colour curve of the objective. In the selected special Cases A and B, $\lambda_m = 5660$ A; in Case A, $\delta(\lambda)$ is the quantity Δf of Fig. 5; in Case B, $\delta(\lambda)$ is one-third of this quantity. Case R is covered by setting $\delta(\lambda) = 0$ for all values of λ.

Denoting $\sqrt{(x^2+y^2)}$ by r, we can then define the "summed visual intensity" $I^*(z, r)$ at the point $P(x, y, z)$ of the polychromatic diffraction image by the equation

$$I^*(z, r) = \frac{\int I_\lambda(z - \delta(\lambda), r)\sigma(\lambda)\rho(\lambda)\, d\lambda}{\int \sigma(\lambda)\rho(\lambda)\, d\lambda}; \tag{3.1}$$

here $\rho(\lambda)$ measures the energy distribution in the starlight as a function of wave-length and $\sigma(\lambda)$ the colour sensitivity of the eye, while I_λ is the intensity function of (2.18) and (2.19).

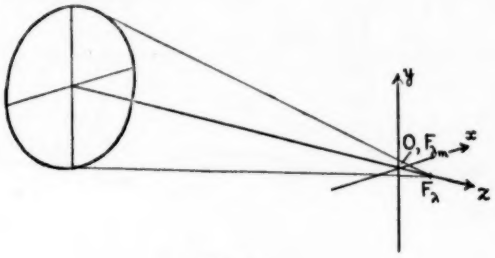

FIG. 6.

The definition can be extended very easily to cover monochromatic light, or spectra with bright lines, by substituting for (3.1) the equation

$$I^*(z, r) = \frac{\int_\lambda I(z - \delta(\lambda), r)\sigma(\lambda)\, dP(\lambda)}{\int \sigma(\lambda)\, dP(\lambda)}, \tag{3.2}$$

in which $P(\lambda)$ measures the total energy of the received starlight in the wave-length range $(0, \lambda)$.

We can also define the "summed visual illumination" $L^*(z, r_0)$ contained in a circle of radius r_0, centred on Oz, in the receiving plane specified by the parameter z, by the equation

$$L^*(z, r_0) = \frac{\int L_\lambda(z - \delta(\lambda), r_0)\sigma(\lambda)\, dP(\lambda)}{\int \sigma(\lambda)\, dP(\lambda)}, \tag{3.3}$$

which reduces to the form

$$L^*(z, r_0) = \frac{\int L_\lambda(z - \delta(\lambda), r_0)\sigma(\lambda)\rho(\lambda)\, d\lambda}{\int \sigma(\lambda)\rho(\lambda)\, d\lambda} \tag{3.4}$$

in the case of a continuous spectrum. It follows at once from (2.23), (3.2) and (3.4) that

$$\begin{aligned} L^*(z, r_0) &= \frac{1}{\pi a^2} \int_0^{r_0} \int_0^{2\pi} I^*(z - \delta(\lambda), r) r\, dr\, d\theta \\ &= \frac{2}{a^2} \int_0^{r_0} I^*(z - \delta(\lambda), r) r\, dr. \end{aligned} \tag{3.5}$$

3.3. *Choice of receiving plane.*—In attempting a definition of best focus which shall correspond reasonably well with practical requirements, two obvious procedures suggest themselves. One is to define the best focal setting as that position of the receiving plane for which the visual brightness at the centre of

the image is greatest. The other is to define it as the position for which as much visual illumination as possible is contained in a circle of suitable radius lying in the receiving plane and centred on the principal ray.

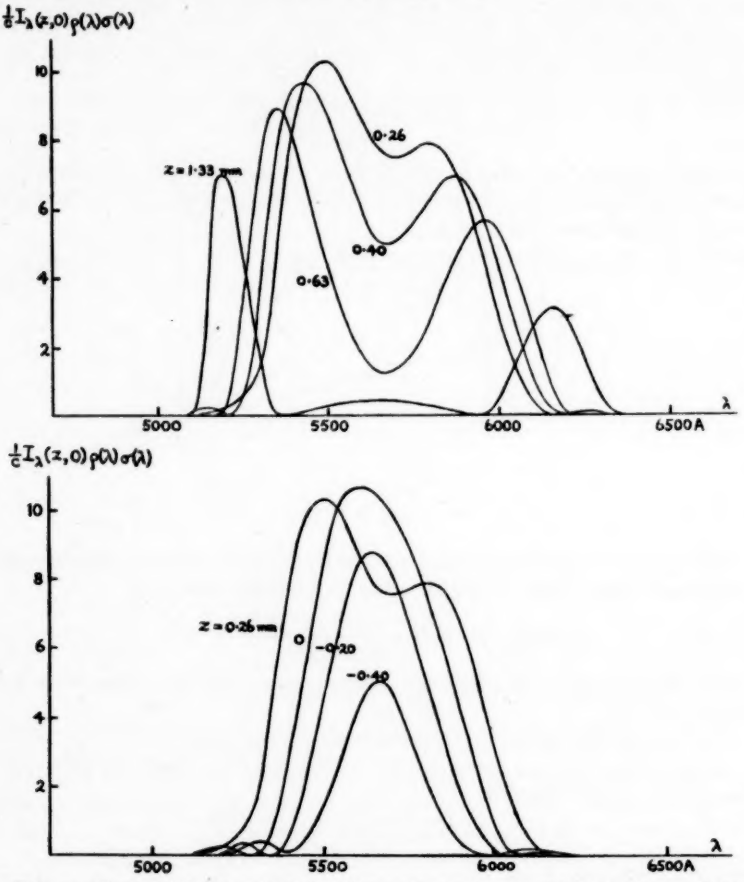

FIG. 7.—*Case A (Newall telescope). Chromatic structure of axial intensity in different receiving planes. The "condensation factor"* $c = \frac{4\pi^2 a^4}{\lambda_m^2 f^2} = 1{\cdot}56 \times 10^{10}$ *measures the ratio of the intensity of the light of wave-length* λ_m *at geometrical focus to its intensity in the entering beam.*

In Case R (or in the case of any aberration-free image formed by a reflector) the best focal setting according to either of these definitions agrees with that according to geometrical optics. In Cases A and B the determination of best focus on either definition involves a fairly detailed examination of the chromatic structure of the image.

Figs. 7 and 12 give the required information about the visual intensities along the axis of the image in Cases A and B respectively. Figs. 8 and 13 give the corresponding information about the total visual illumination in a small circle drawn about the centre of the image in each of a selected set of receiving

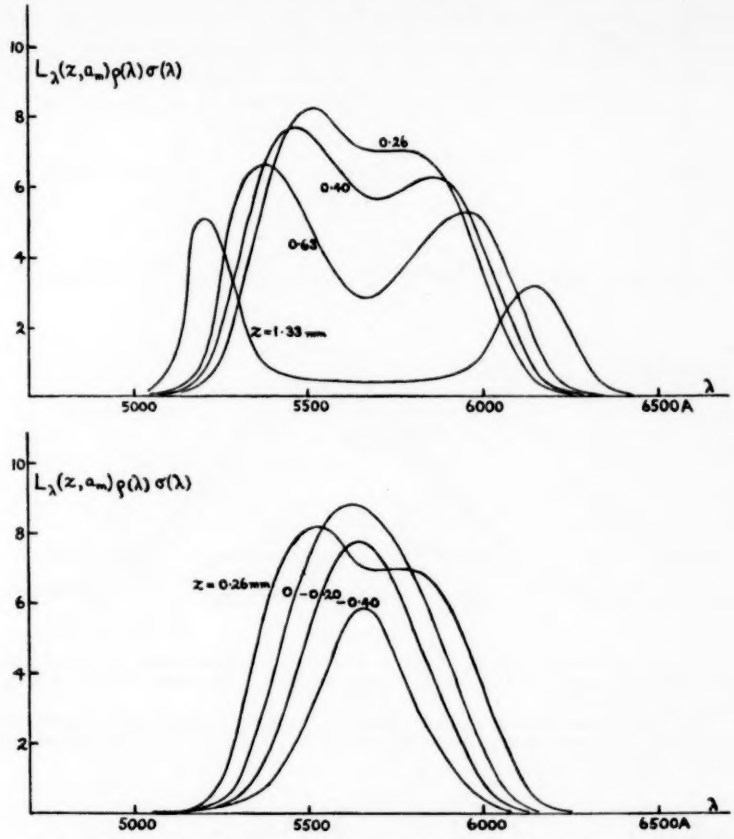

FIG. 8.—*Case A (Newall telescope). Chromatic structure in different receiving planes of the visual illumination inside a circle of radius a_m, equal to the first Airy dark ring for $\lambda=\lambda_m=5660$ A.*

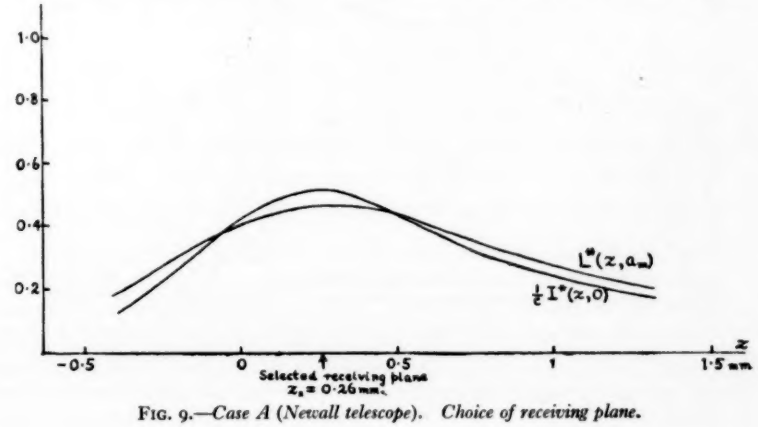

FIG. 9.—*Case A (Newall telescope). Choice of receiving plane.*

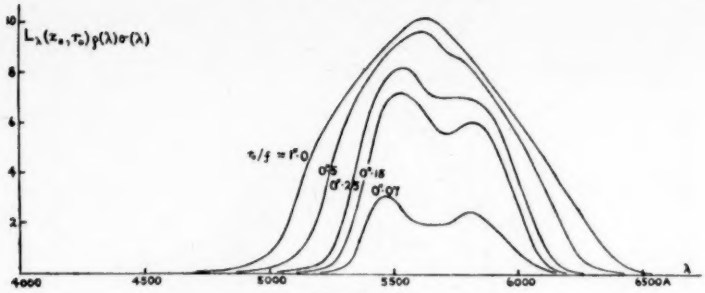

FIG. 10 (*a*).

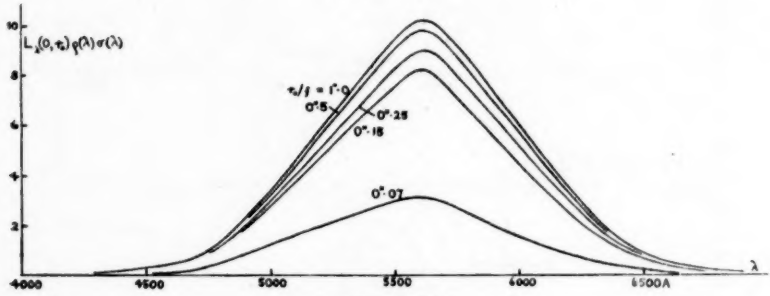

FIG. 10 (*b*).

FIG. 10.—(*a*) *Case A (Newall telescope.) Chromatic structure of image in selected receiving plane* ($x_s = 0{\cdot}26$ mm); (*b*) *Case R (Comparison reflector). Chromatic structure of image in geometrical focal plane.*

Each curve shows the total visual illumination, classified according to wave-length, inside a circle of angular radius r_0/f *about the origin in the selected focal plane. The angular radius of the first Airy dark ring* ($\lambda = 5660$ A) *is* $a_m/f = 0''{\cdot}23$.

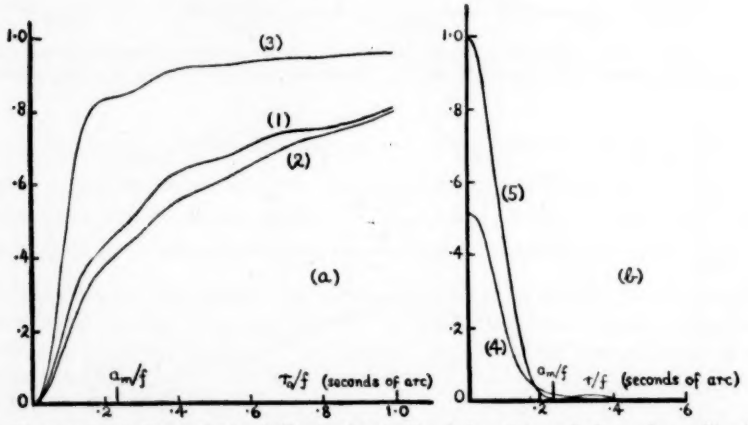

FIG. 11.—(*a*) *Summed visual illumination inside circles of prescribed angular radii* r_0/f. *Curve 1 : Case A (Newall telescope) at selected focus; Curve 2 : Newall telescope at minimum geometrical focus; Curve 3 : Comparison reflector at geometrical focus.* (*b*) *Summed visual intensity at prescribed angular distances* r/f *from the centre of the image. Curve 4 : Newall telescope at selected focus; Curve 5 : Comparison reflector at geometrical focus.*

planes near focus; the radius r_0 of this circle is in each case taken equal to the radius a_m of the Airy disk at the wave-length $\lambda_m = 5660$ A. This wave-length corresponds to the minimum geometrical focal length of the two objectives and also, fairly closely, to the brightest part of the visual spectrum (see Fig. 4).

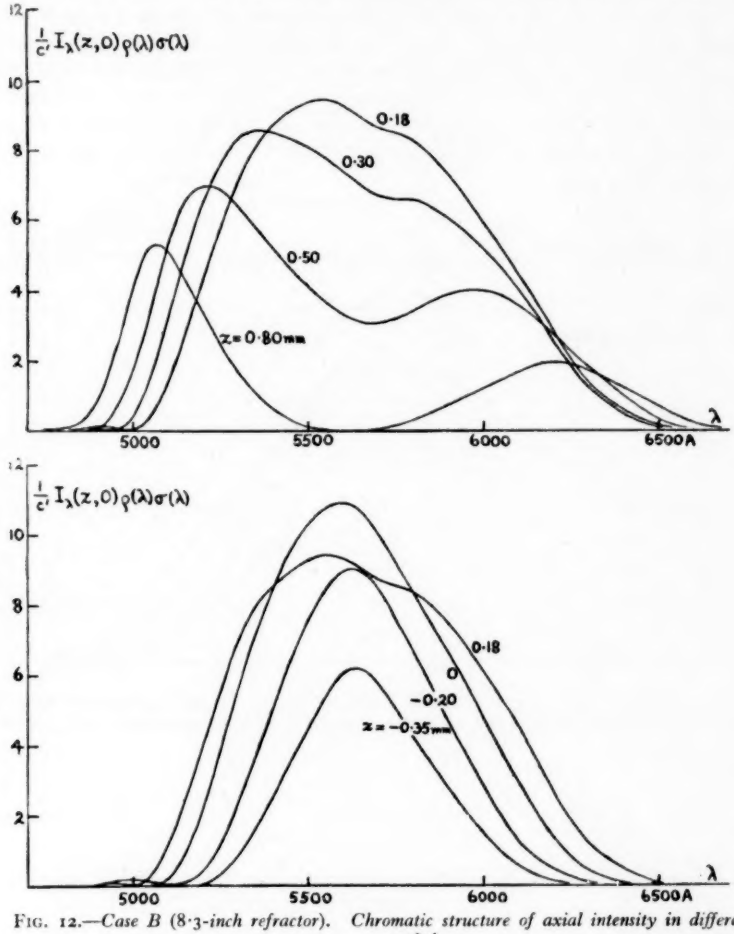

FIG. 12.—*Case B (8·3-inch refractor). Chromatic structure of axial intensity in different receiving planes. The "condensation factor"* $c' = \frac{4\pi^2 a^4}{\lambda_m^2 f^2} = 1{\cdot}73 \times 10^8$ *measures the ratio of the intensity of the light of wave-length* λ_m *at geometrical focus to its intensity in the entering beam.*

From Figs. 7, 8, 12 and 13 the summed visual axial intensity $I^*(z, 0)$ and the summed visual illumination $L^*(z, r_0)$ in Cases A and B can be obtained with sufficient accuracy with a planimeter. They are represented, with the appropriate normalizing coefficients, in Fig. 9 (Case A) and Fig. 14 (Case B). The point of greatest axial intensity $I^*(z, 0)$ corresponds to the best focal setting according to the first definition; that of greatest visual illumination $L^*(z, a_m)$ to the best focal setting according to the second.

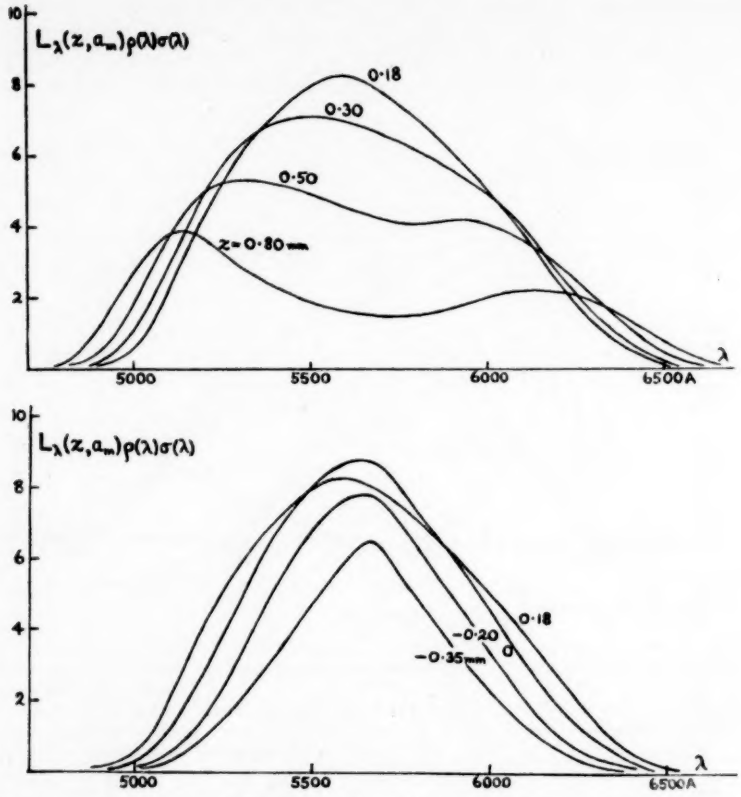

FIG. 13.—*Case B (8·3-inch refractor). Chromatic structure in different receiving planes of the visual illumination inside a circle of radius a_m, equal to the first Airy dark ring for $\lambda=\lambda_m=5660\,A$.*

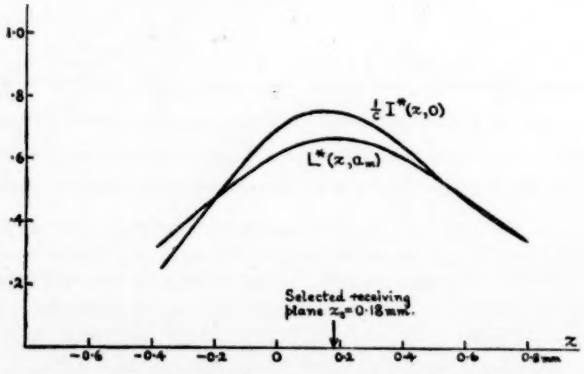

FIG. 14.—*Case B (8·3-inch refractor). Choice of receiving plane.*

It appears from Figs. 9 and 14 that, in the two cases considered, both the adopted definitions lead to substantially the same choice of best focal setting, about 0·26 mm outside minimum focus in Case A and about 0·18 mm in Case B.

3.4. *Structure of the image at best focus.*—Fig. 10 shows the structure of the star image formed in the best focal plane in Case A (25-inch refractor) and compares it with that formed by the corresponding reflector (Case R). Each curve in Fig. 10*a* shows the total illumination, classified according to wave-length, contained in a circle of specified angular radius r_0/f. The five selected values of r_0/f range from 0·07 seconds of arc (about one-third of the angular radius of the full Airy disk at the brightest part of the spectrum) to one second of arc (about four Airy disk radii). Fig. 10*b* shows the corresponding curves for the reflector.

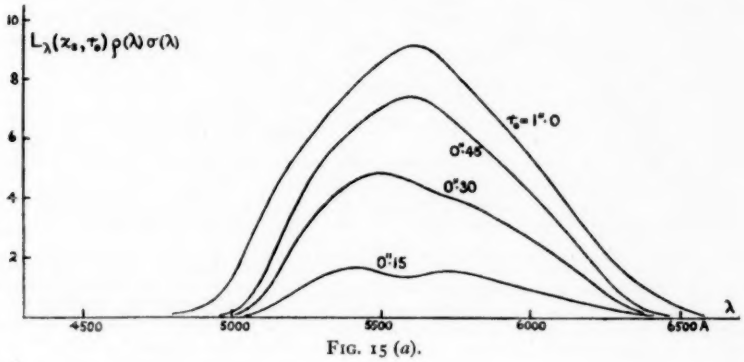

FIG. 15 (*a*).

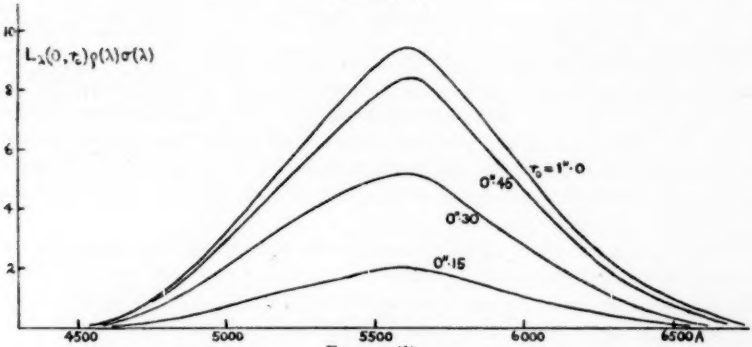

FIG. 15 (*b*).

FIG. 15.— (*a*) *Case B (8·3-inch refractor). Chromatic structure of image in selected receiving plane* (z_s=0·18 *mm*); (*b*) *Case R (Comparison reflector). Chromatic structure of image in geometrical focal plane.*

Each curve shows the total visual illumination, classified according to wave-length, inside a circle of angular radius r_0/f *about the origin in the selected focal plane. The angular radius of the first Airy dark ring* (λ=5660 *A*) *is* a_m/f=0".68.

Comparison of the Case A curves with the Case R curves for r_0/f=0".07, 0".15 and 0".25 shows in detail how the central core of the star image in the refractor is robbed of light by the residual chromatism. Inside the circle r_0/f=0".25, roughly equal in size to the yellow Airy disk, is found hardly any light outside the wave-length range 5000–6200 A. Light outside this range,

that is to say from both ends of the visual spectrum, therefore makes no appreciable contribution to the penetrating power of the telescope; it provides the violet or purple halo which is such a disagreeable accompaniment to the star images formed by every large visual doublet objective. Fig. 4 shows that this purple light contains an appreciable fraction of the whole visual illumination, and comparison of the curves for $r_0/f = 1''{\cdot}0$ in Figs. 10 *a* and 10 *b*, shows that the colour error sends only a small part of it outside a circle two seconds of arc in diameter.

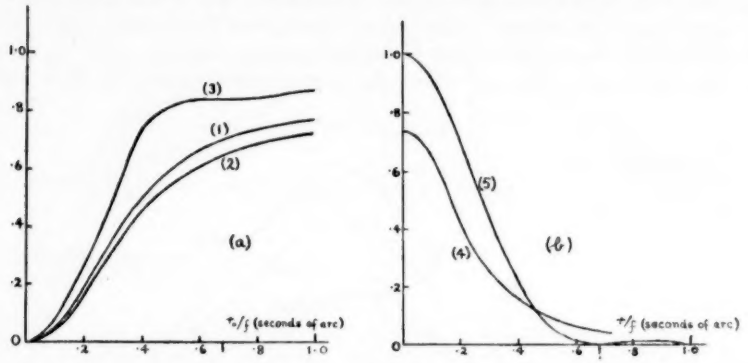

FIG. 16.—(*a*) *Summed visual illumination inside circles of prescribed angular radius* r_0/f. *Curve* 1 : *Case B* (8·3*-inch refractor) at selected focus; Curve* 2 : 8·3*-inch refractor at minimum geometrical focus; Curve* 3 : *comparison reflector at geometrical focus.* (*b*) *Summed visual intensity at prescribed angular distances* r/f *from the centre of the image. Curve* 4 : 8·3*-inch refractor at selected focus; Curve* 5 : *comparison reflector at geometrical focus.*

Abscissae: a_m/f.

Fig. 15 *a* gives the corresponding information about image structure in the smaller refractor (Case B) and its comparison reflector. Comparison of Fig 15 *a* with Fig. 10 *a* allows us to see how much smaller is the disturbance of the central core of the diffraction image by residual chromatism in Case B than in Case A. For example, in Case B the chromatism reduces the total visual illumination inside a circle of half the diameter of the (yellow) Airy disk* by about 30 per cent; in Case A by about 50 per cent.

Figs. 11 and 16 follow up this point in more detail. In Fig. 11 *a* is shown the "summed visual illumination" (defined in Section 3.2) inside circles of different angular radii r_0/f about the centre of the image. Curve 1 refers to Case A in the selected focal plane, curve 2 to Case A in the minimal focal plane and curve 3 to the monochromatic image ($\lambda = \lambda_m = 5660$ A) in the plane through F_{λ_m}. Curve 3 may also stand for Case R in the geometrical focal plane, since the difference between the curves for Case R and for the monochromatic case turns out to be inappreciable.

(The last result explains why the images in a reflector appear free from spurious colour, although they are formed by the superposition of coloured diffraction images of different sizes.)

Fig. 16 *a* gives the corresponding curves with Case B in place of Case A. For the same reason as before, curve 3 may be taken as referring either to the

* M. Verdet (**16**) estimates the apparent diameter of the visible bright nucleus of a star image under nearly perfect seeing conditions at about half the diameter of the first Airy dark ring.

monochromatic image ($\lambda = \lambda_m = 5660$ A) received on the plane through F_{λ_m}, or to the polychromatic image in Case R, received on the geometrical focal plane.

Figs. 11*b*, 16*b* show the corresponding "summed visual intensities" at different distances r/f from the centre of the image. Curve 4 in the figures gives the summed visual intensity distributions in the selected focal plane in Cases A, B respectively; curve 5 those at geometrical focus in the monochromatic case or, equally well, in Case R. The axial intensities in curves 4 were found from Figs. 9, 14; their values are probably more accurate than those of the intensities at other points on these two curves, which were derived by graphical methods from curve 1 in Figs. 11*a*, 16*a* respectively.

The Observatories,
Cambridge:
1951 *December* 4.

The University,
Edinburgh.

References

(1) G. B. Airy, *Camb. Phil. Trans.*, **5**, 283, 1835.
(2) Rayleigh, *Scientific Papers*, Vol. I, 415.
(3) E. v. Lommel, *Abh. der Bayerischen Akad.*, **53**, 233, 1885.
(4) K. Schwarzschild, *Sitzber. der Kgl. Bayerischen Akad. der Wiss.*, **28**, 271, 1898.
(5) H. Struve, *Mém. de l'Acad. de St. Petersbourg* (7), **34**, No. 5, 1, 1886.
(6) M. Berek, *Z. Phys.*, **40**, 421, 1926.
(7) F. Zernike and B. R. A. Nijboer, Contribution in *Théorie des Images Optiques*, Paris, p. 227, 1949.
(8) H. Dennis Taylor, *M.N.*, **54**, 67, 1894.
(9) A. E. Conrady, *M.N.*, **79**, 575, 1919.
(10) A. Buxton, *M.N.*, **81**, 547, 1921.
(11) L. C. Martin, *M.N.*, **82**, 310, 1922.
(12) J. Picht, *Ann. Phys.*, Leipzig, **77**, 685, 1925; *ibid.*, **80**, 491, 1926.
(13) G. C. Steward, *Phil. Trans. Roy. Soc.* A, **225**, 131, 1925; *Trans. Camb. Phil. Soc.*, **23**, 235, 1926.
(14) E. Wolf, *Proc. Roy. Soc.* A, **204**, 533, 1951.
(15) H. Dennis Taylor, *Mem. R.A.S.*, **51**, 77, 1894.
(16) M. Verdet, *Leçons d'Optique Physique*, t. I, 309.

OCCULTATIONS OF STARS BY THE MOON OBSERVED AT THE NIZAMIAH OBSERVATORY, HYDERABAD, DURING THE YEAR 1951

(Communicated by the Director)

(Received 1952 February 4)

TABLE I

No.	Star N.Z.C. No.	Mag.	Phase	Date 1951	U.T. h m s
1	166	6·9	D	January 14	14 47 3·1
2	173	6·6	D	,, 14	17 6 56·8
3	399	5·7	D	,, 16	16 8 57·4
4	603	7·5	D	February 14	17 9 13·2
5	1308	4·7	D	,, 19	22 12 42·7
6	2383	2·9	D	March 1	0 29 19·3
7	538	5·6	D	,, 13	15 47 30·8
8	996	6·8	D	,, 16	18 23 3·6
9	1108	6·9	D	,, 17	15 20 31·5
10	2108	6·4	D	June 16	16 36 27·6
11	2109	6·1	D	,, 16	17 18 49·7
12	2644	6·3	D	November 3	12 44 40·9
13	2660	6·1	D	,, 3	14 38 40·2
14	2991	6·2	D	,, 5	15 50 11·2
15	3267	7·2	D	,, 7	14 33 17·7
16	3222	7·1	D	December 4	13 43 8·9
17	3502	7·4	D	,, 6	18 14 15·8

All the observations were made by the Senior Observer, Mahomed Ghouse.

The instrument used throughout was the 15-inch Grubb refractor. The corrections to the standard clock were determined from B.B.C. time signals weekly. The reductions were carried out by S. Aravamudhan assisted by M. M. Ramanathan in accordance with the formulae given in the Supplement to the *Nautical Almanac* for 1938.

A correction of $-0^{h}\cdot00076$ was applied to the observed time, to allow for the error of $-1''\cdot5$ in the mean longitude of the Moon.

TABLE II

No.	$\sigma'-\sigma$	$\cos(\rho-\psi)$	$\sin(\rho-\psi)$	No.	$\sigma'-\sigma$	$\cos(\rho-\psi)$	$\sin(\rho-\psi)$
	"				"		
1	−0·9	+0·97	−0·25	10	−1·1	+0·81	+0·58
2	+0·9	+0·83	−0·56	11	+0·1	+0·85	+0·52
3	+0·5	+0·68	−0·74	12	[−3·0]	+0·36	+0·93
4	−1·0	+0·94	+0·34	13	−0·9	+0·82	−0·58
5	−0·3	+0·96	+0·28	14	+0·9	+0·65	−0·76
6	+0·9	+0·61	−0·79	15	−1·0	+0·99	+0·12
7	−0·4	+0·72	−0·70	16	−0·6	+0·97	+0·25
8	−0·6	+0·97	+0·25	17	−0·3	+0·53	−0·85
9	−0·8	+0·72	−0·69				

Nizamiah Observatory,
Hyderabad,
Deccan, India:
1952 *January* 24.

A SUGGESTED EXPLANATION OF THE PRESENT VALUE OF THE VELOCITY OF ROTATION OF THE EARTH*

E. R. R. Holmberg

(Communicated by E. C. Bullard, F.R.S.)

(Received 1952 March 29)

Summary

It is suggested that the coincidence of the period of rotation of the Earth and a natural period of vibration of the atmosphere is not fortuitous but due to the Earth being driven at a constant rate in synchronism with the vibration. An observation by Kelvin that the gravitational couple on the atmospheric tides accelerates the Earth's rotation is recalled, and the production of mechanical energy to balance the dissipation of the oceanic tides is discussed. The astronomical evidence supporting the current view that the rotation is being steadily retarded is reviewed and found to contain contradictions, and it is claimed that the high value of the angular momentum of the Earth–Moon orbit supports the hypothesis of equilibrium.

* The full text of this paper is published in *M.N., Geophys. Suppl.*, **6**, No. 6, 1952.

CONTENTS

PAGE

Meeting of 1952 March 14:
- Fellows elected ... 359
- Junior Members elected ... 359
- Presents announced ... 359
- George Darwin Lecture announced ... 359

Meeting of 1952 April 9:
- Death of Dr Bernard Lyot ... 359
- Fellows elected ... 359
- Associates elected ... 360
- Presents announced ... 360

V. C. A. Ferraro and D. J. Memory, Oscillations of a star in its own magnetic field: an illustrative problem ... 361

K. N. Dodd, The unsteady accretion problem ... 374

R. A. Buckingham, S. Reid and R. Spence, Continuous absorption by the hydrogen molecular ion ... 382

R. J. Tayler, Radiative solutions of the stellar equations ... 387

J. A. Clegg, The velocity distribution of sporadic meteors. III. Calculation of the theoretical distributions ... 399

H. H. Plaskett, Motions in the Sun at the photospheric level. I. Methods ... 414

T. D. Kinman, Motions in the Sun at the photospheric level. II. The Evershed effect in Sunspot Mt. Wilson No. 9987 ... 425

P. B. Fellgett and F. B. Schmeidler, On the sharpening of observational data with special application to the darkening of the solar limb ... 445

E. H. Linfoot and E. Wolf, On telescopic star images ... 452

Nizamiah Observatory, Hyderabad, Occultations of stars by the Moon observed at the Nizamiah Observatory, Hyderabad, during the year 1951 ... 470

Summary of paper published in the *Geophysical Supplement:*

E. R. R. Holmberg, A suggested explanation of the present value of the velocity of rotation of the Earth ... 471

Printed in London by Taylor & Francis, Ltd., 1952 December